Shin-ichi Uchida

# High Temperature Superconductivity

The Road to Higher Critical Temperature



#### **Springer Series in Materials Science**

#### Volume 213

#### **Series editors**

Robert Hull, Charlottesville, USA Chennupati Jagadish, Canberra, Australia Richard M. Osgood, New York, USA Jürgen Parisi, Oldenburg, Germany Tae-Yeon Seong, Seoul, Korea, Republic of (South Korea) Shin-ichi Uchida, Tokyo, Japan Zhiming M. Wang, Chengdu, China The Springer Series in Materials Science covers the complete spectrum of materials physics, including fundamental principles, physical properties, materials theory and design. Recognizing the increasing importance of materials science in future device technologies, the book titles in this series reflect the state-of-the-art in understanding and controlling the structure and properties of all important classes of materials.

More information about this series at http://www.springer.com/series/856

#### Shin-ichi Uchida

# High Temperature Superconductivity

The Road to Higher Critical Temperature



Shin-ichi Uchida Department of Physics, Graduate School of Science The University of Tokyo Tokyo Japan

ISSN 0933-033X ISSN 2196-2812 (electronic)
ISBN 978-4-431-55299-4 ISBN 978-4-431-55300-7 (eBook)
DOI 10.1007/978-4-431-55300-7
Springer Tokyo Heidelberg New York Dordrecht London

Library of Congress Control Number: 2014952900

#### © Springer Japan 2015

This work is subject to copyright. All rights are reserved by the Publisher, whether the whole or part of the material is concerned, specifically the rights of translation, reprinting, reuse of illustrations, recitation, broadcasting, reproduction on microfilms or in any other physical way, and transmission or information storage and retrieval, electronic adaptation, computer software, or by similar or dissimilar methodology now known or hereafter developed. Exempted from this legal reservation are brief excerpts in connection with reviews or scholarly analysis or material supplied specifically for the purpose of being entered and executed on a computer system, for exclusive use by the purchaser of the work. Duplication of this publication or parts thereof is permitted only under the provisions of the Copyright Law of the Publisher's location, in its current version, and permission for use must always be obtained from Springer. Permissions for use may be obtained through RightsLink at the Copyright Clearance Center. Violations are liable to prosecution under the respective Copyright Law.

The use of general descriptive names, registered names, trademarks, service marks, etc. in this publication does not imply, even in the absence of a specific statement, that such names are exempt from the relevant protective laws and regulations and therefore free for general use.

While the advice and information in this book are believed to be true and accurate at the date of publication, neither the authors nor the editors nor the publisher can accept any legal responsibility for any errors or omissions that may be made. The publisher makes no warranty, express or implied, with respect to the material contained herein.

Printed on acid-free paper

Springer is part of Springer Science+Business Media (www.springer.com)

#### **Preface**

At the time of writing this book, in the summer 2014, the highest superconducting transition temperature  $T_{\rm c}$  remains 135 K which was recorded in 1993 for one of the copper oxide compounds. The "silence" period over 20 years is the longest since the recorded history of superconductivity started from 1911. The second longest silence was between 1973 and 1986, the period between the discovery of Nb<sub>3</sub>Ge with  $T_{\rm c}$  = 23 K and the discovery of high- $T_{\rm c}$  superconductivity in copper oxides. During this period between 1973 and 1986, researchers of superconductivity were pessimistic for further rising  $T_{\rm c}$ , and superconductivity at liquid nitrogen temperature was only a dream, as it was believed that superconductivity was a very low-temperature phenomenon. However, in the present silence period, researchers are no longer pessimistic, since they know that high- $T_{\rm c}$  superconductivity is real and that there is no reason that  $T_{\rm c}$  does not increase beyond 135 K. So, it is a realistic challenge in material sciences to search for new superconducting materials with higher  $T_{\rm c}$  and/or to enhance  $T_{\rm c}$  of the known superconducting materials.

In contrast to the long silence in  $T_{\rm c}$ , several material families have successively been found to show superconductivity at temperature higher than the old record 23 K such as  ${\rm MgB_2}$  and iron arsenides. Like copper oxides, most of them were not expected to be superconductors before their discovery. Notably, these superconductors are from completely different material families than copper oxides, encouraging researchers to search for new high- $T_{\rm c}$  superconductors in materials yet to be investigated.

To unravel the mechanism of high- $T_{\rm c}$  superconductivity in copper oxides remains a challenging problem of physics. Nevertheless, there has been well advanced understanding of their unusual physical properties, various ordering phenomena other than superconductivity, and in particular of the electronic and structural parameters that influence  $T_{\rm c}$ . We now understand why  $T_{\rm c}$  of one copper oxide is higher than  $T_{\rm c}$  of another one.  $T_{\rm c}$  of conventional superconductors is rather a trivial problem. It is basically understandable in the framework of the Migdal-Eliashberg theory developed from the original Bardeen-Cooper-Schrieffer (BCS) theory, even though the theoretical calculations do not necessarily reproduce  $T_{\rm c}$  of real material precisely. On the other hand,  $T_{\rm c}$ 's of most of the high- $T_{\rm c}$  superconductors show a broad distribution within each family due to unusual sensitivity to electron concentration,

vi Preface

lattice disorder in the lattice, and so on. This, in turn, will give an experiment-based strategy for enhancing  $T_{\rm c}$  in the known high- $T_{\rm c}$  families. Also, we have learned from various different high- $T_{\rm c}$  families what the common ingredients are among these families, which will provide a guide for searching out new high- $T_{\rm c}$  superconductors. Thus, it is now possible to develop a new approach to the problem of  $T_{\rm c}$  on the basis of the results from the long and extensive study of the copper oxides and the lessons learned from a plethora of different high- $T_{\rm c}$  families. This is a main objective of this book.

This book has been written aiming to provide non-specialist readers with an indepth overview of the past, present, and future of high-temperature superconductivity. Specialist readers will be given up-dated information on the research forefront of the study of various high- $T_{\rm c}$  families and some hints on the possibility of enhancing  $T_{\rm c}$  and on finding new high- $T_{\rm c}$  materials. A message that the author would like to pass to researchers of the younger generation and graduate-course students is not to give up the challenges to the problems of high-temperature superconductivity.

Tokyo Shin-ichi Uchida

#### Acknowledgements

The author of this book started his research of superconductivity in 1984 motivated by the unusual oxide superconductor  $\operatorname{BaPb}_x\operatorname{Bi}_{1-x}O_3$ . Since 1986, the high- $T_c$  copper oxides have continued to be the main subject of his laboratory, and from 2008 iron arsenides/selenides were added as a research target. He was involved in the discovery of some copper oxide superconductors and borocarbides. Many parts of this book are based on the experimental results that are due to the dedicated persistent efforts by the former students, H. Sato, T. Ito, T. Ido, S. Ishibashi, Y. Nakamura, K. Takenaka, K. Tamasaku, T. Noda, K. Fujita, M. Ishikado, H. Hobou, Y. Hirata, S. Ishida, M. Nakajima, T. Liang, L. Liu and many others. In particular, the author would like to acknowledge long-standing experimental collaboration with J.C. Seamus Davis, H. Eisaki, A. Fujimori, C.-Q. Jin, K.M. Kojima, Z.-X. Shen, S. Tajima, H. Takagi, Y. Tokura, J.M. Tranquada, and Y.J. Uemura. He has been inspired also by the discussions with many theorists, particularly, with T.P. Devereaux, D.-H. Lee, S. Maekawa, and N. Nagaosa.

#### **Contents**

1		oduction			
2	Overview of Superconducting Materials with $T_c$ Higher than 23 K				
	2.1	Introduction			
	2.2	Materials with Phonon-Mediated Pairing			
	2.3	High-T <sub>c</sub> Superconductivity in MgB <sub>2</sub>			
	2.4	Other Electron-Phonon Superconductors with Fairly High $T_c$			
		2.4.1 Doped Bismuthate $Ba_{1-x}K_xBiO_3$			
		2.4.2 Elemental Superconductors at High Pressures			
		2.4.3 Borocarbide YPd <sub>2</sub> B <sub>2</sub> C			
		2.4.4 Electron Doped β-HfNCl			
		2.4.5 Doped Fullerides ( $C_{60}$ ) and Polycyclic-			
		Aromatic-Hydrocarbons			
	2.5	Materials with Unconventional Pairing			
	2.6	Possibility of Higher $T_c$ in Electron-Phonon Superconductors			
	Refe	erences			
3		opper Oxide Superconductors			
	3.1	Introduction			
	3.2	A brief history of high- $T_c$ cuprates			
	3.3	Uniqueness of the Cuprates			
		3.3.1 Characteristics of the CuO <sub>2</sub> Plane			
		3.3.2 Necessary Ingredients for High $T_c$			
	3.4	Temperature-Doping Phase Diagram			
		3.4.1 Unconventional Superconductivity			
		3.4.2 Phase Diagram and Pseudogap Regime			
		3.4.3 Quantum Critical Points and "Strange" Metal			
	3.5	Material Dependence of $T_c$ and Factors that Influence $T_c$			
		3.5.1 Doping Effect			
		3.5.2 Disorder Effect			

x Contents

		3.5.3	Multilayer Effect	43		
		3.5.4	Lattice Effect	47		
	3.6	Possib	oility of Enhancing T <sub>c</sub>	48		
		3.6.1		48		
		3.6.2	Optimizing Multilayer Structure	53		
	References					
4	Iron-Based Superconductors					
	4.1		uction			
	4.2	Mater	ial Dependence of $T_c$ and Parameters that Influence $T_c$			
		4.2.1	Material Dependence of $T_c$	62		
		4.2.2	Parameters that Influence $T_c$	64		
	4.3	Uniqu	eness of Iron Arsenides/Selenides	66		
		4.3.1	Unique Fe-As(Se) Combination			
		4.3.2	Unique Electronic State			
	4.4	Phase	Diagram and Competing Order			
		4.4.1	Temperature-Doping Phase Diagram			
		4.4.2	Nature of the Competing Order	70		
		4.4.3	Unconventional Superconductivity	74		
	4.5	Role o	of Doping and Electronic Correlations	75		
		4.5.1	Role of Doping	76		
		4.5.2	Electronic Correlations.	79 82		
	4.6	6 Possibility of Enhancing T <sub>c</sub>				
	References					
5	Summary and Perspectives 8					
	5.1					
	5.2					
	References 92					

# Chapter 1 Introduction

**Abstract** Triggered by the discovery of high-transition-temperature (high- $T_c$ ) superconducting copper oxides in 1986, seven different material families have been found to show superconductivity at temperatures higher than 23 K, the record high- $T_c$  value before 1986. Six of them have  $T_c$ 's not reaching 40 K, but the copper oxides and the iron compounds are distinct from others in their outstandingly high  $T_c$  values, 135 K and 55 K, respectively and unconventional Cooper pairs. Most of them do not obey the Matthias rules which gave a guiding principle for finding new superconducting materials with high  $T_c$ . Instead, several features emerge in common with most of the high- $T_c$  families. In this chapter, are raised basic questions; what makes  $T_c$  high in each family and why copper oxides and iron compounds are so special with central concern on a possibility of enhancing  $T_c$ .

The discovery of high temperature superconducting copper oxides by Bednorz and Müller [1] in 1986 opened up a new era of superconductivity. Since then, eight (nine) different families of materials have continually been discovered and joined the group of high temperature superconductors (HTSCs) with their superconducting critical temperature (T<sub>c</sub>) exceeding 23 K recorded in 1973 for A15 intermetallic compound Nb<sub>3</sub>Ge [2]. The HTSC families are in the order of the discovery year indicated in parentheses; (1) layered copper oxides built up of the CuO, planes (discovered in 1986), (2) bismuth oxides, Ba<sub>1-x</sub>K<sub>x</sub>BiO<sub>3</sub>, with perovskite structure (1988) [3], (3) fullerides composed of  $C_{60}$  molecules (1991) [4], (4) borocarbides, YPd<sub>2</sub>B<sub>2</sub>C (1994) [5], (5) transition-metal chloronitrides, HfNCl (1998) [6], (6) magnesium diborides, MgB, (2001) [7], (7) elemental calcium (Ca) metal under high pressure (2006) [8], (8) iron arsenides/selenides (2008) [9]. The  $T_c$ -histogram is shown in Fig. 1.1 for these eight families. Picene  $(C_{22}H_{14})$ , a member of the polycyclic aromatic hydrocarbons, was found to show superconductivity at 18 K in 2009 [10]. Afterward,  $T_c \sim 30$  K was reported for its relative, but superconductivity has not been fully confirmed yet. From heavy fermions, a representative family of strongly interacting electrons, PuCoGa<sub>5</sub> achieved  $T_c$  = 18 K [11]. These are from surprisingly different families of materials, so high temperature superconductivity is now ubiquitous and possibility of finding a new HTSC in a different family of 2 1 Introduction

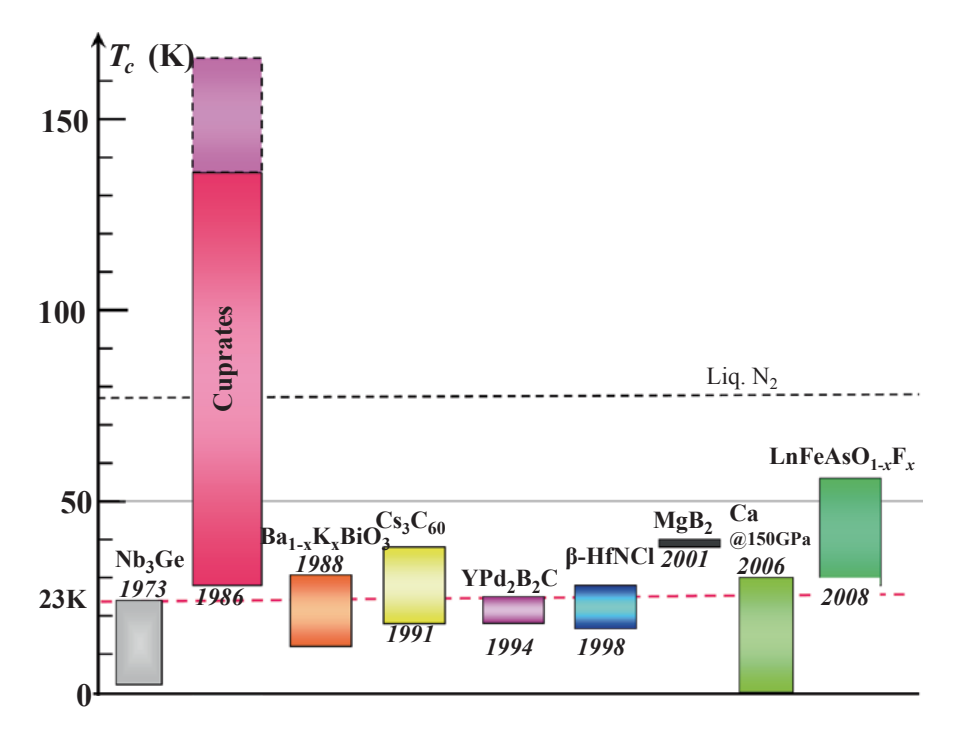


Fig. 1.1  $T_{\rm c}$  histograms. Distribution of  $T_{\rm c}$  and the maximum value of  $T_{\rm c}$  for each family of high- $T_{\rm c}$  superconducting materials discovered since 1986. Representative material and the year of discovery are indicated

materials is high. Ubiquitous high- $T_{\rm c}$  superconductivity has changed a landscape of physics and chemistry of superconductivity.

Before 1986 a guiding principle for finding new superconducting materials with high  $T_c$  was the so-called Matthias rules [12] such as

#1: find cubic crystals,

#2: find d-electron metals,

#3: find metals with the average number of valence electrons, preferably odd numbers 3, 5, and 7,

#4: exclude metals showing or in close vicinity of magnetism,

#5: exclude metals near a metal-insulator transition such as oxide materials.

These rules successfully lead to the finding of the A15-Nb<sub>3</sub>Ge. The Matthias rules apply to metals with high electron density or high electron density of state at the Fermi level which are favorable for high  $T_{\rm c}$  in the framework of the Bardeen-Cooper-Schrieffer (BCS)—Migdal-Eliashberg theory. Interestingly, the newly discovered high- $T_{\rm c}$  materials are in most cases completely outside the Matthias rules.

Despite the discovery of a number of HTSCs in the past 28 years, the rise of  $T_c$  has stopped for over 20 years, since the highest  $T_c$  value of 135 K at ambient pressure [13] (164 K at pressure of 30 GPa [14]) was recorded for the Hg-based copper oxide in 1993. The period of this "silence" is longest in the history of superconductivity

Introduction 3

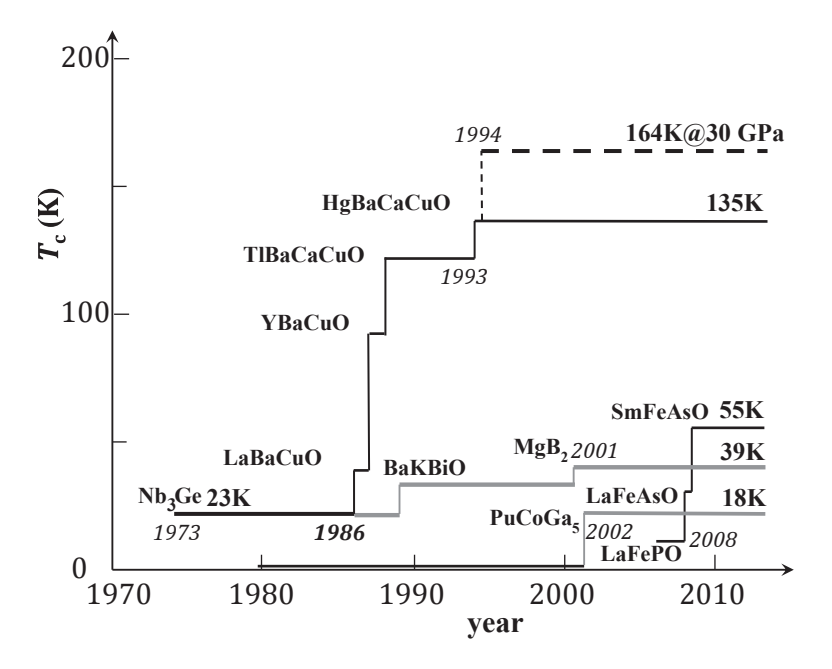


Fig. 1.2 History of  $T_{\rm c}$  ( $T_{\rm c}$  vs year) for four representative classes of superconductors, cuprates, iron-based compounds, superconductors with phonon-mediated pairing, and heavy-fermion superconductors

(see the curves  $T_{\rm c}$ —year shown in Fig. 1.2). The second longest silence was 13 years from 1973, the year of the discovery of Nb<sub>3</sub>Ge, to 1986. Therefore, to break the silence and to find a material with higher  $T_{\rm c}$  is one of the most challenging problems in material sciences.

Among eight (nine) families of HTSCs so far discovered, six (seven) are superconductors with  $T_{\rm c}^{\rm max}$  lower than 40 K. In most of them the electron-electron attractive interaction mediated by phonons is thought to be a major pairing interaction. In particular, MgB<sub>2</sub> with the highest  $T_{\rm c}$  (=39 K) among the six (seven) is obviously a phonon-mediated superconductor as conventional superconductors, and its high  $T_{\rm c}$  value is understood in the framework of the (BCS) Migdal-Eliashberg theory. For others, a usual application of the Migdal-Eliashberg theory is difficult to explain high  $T_{\rm c}$  values and additional effects, such as electronic correlations, which may enhance the electron-phonon coupling seems to be at work.

The copper oxides and the iron compounds are distinct from others in their outstandingly high  $T_{\rm c}$  values,  $T_{\rm c}^{\rm max} = 135\,\rm K$  for the former and 55 K for the latter [15], and unique in their material diversity. In both families  $T_{\rm c}$  is material dependent despite having the common structural units. Also, common with these two systems is superconductivity with unconventional pairing symmetry and emergent by doping into parent compounds showing an antiferromagnetic order. Both evidence an important role of repulsive electron-electron interaction (electronic correlation) in

4 1 Introduction

the formation of Cooper pairs. Although the mechanisms of Cooper pair formation in both systems are still under hot debate, the understanding of the two systems have well advanced thanks to the intense and persistent experimental and theoretical efforts. Also, on the basis of more than 28 years accumulation of a huge number of experimental data and improvement of the crystal quality we can specify factors (material parameters) that influence  $T_{\rm c}$  and hence are sources of diverse  $T_{\rm c}$  values in each family. Now it is ready to address the basic questions on the high- $T_{\rm c}$  values in these families;

- i. Why the two families are distinct from others,
- ii. Which factors are most influential on  $T_c$ ,
- iii. How each factor affects the electronic state in the normal state and the superconducting properties,
- iv. Whether or how one can find a possibility to enhance  $T_c$ .

The Matthias rules no more apply to the new HTSCs. Many of them have *layer* structures. Most are in close vicinity of metal-insulator phase transition boundary, thereby having *low carrier density* and *low superfluid density*. In addition, most families contain *light elements* (B, C, N, or O) which take part in *strong chemical bond*. Notably, *strong electronic correlations* play a dominant role in the formation of Cooper pairs in the copper oxides and the iron compounds with the highest  $T_c$ 's among all. Electronic correlations also play a role in enhancing electron-phonon interaction and hence  $T_c$  in many of the families. Certainly, these features constitute a new paradigm in the physics and chemistry of superconductivity and provide an experiment-based strategy for finding new high- $T_c$  superconducting materials.

This book presents "physics of  $T_c$ " of new high- $T_c$  superconductors. Starting from an overview of HTSCs with possible phonon-mediated superconductivity in Chap. 2, major emphases are put on the factors which influence  $T_c$  and give rise to diverse  $T_c$  values for the two unconventional high- $T_c$  superconducting materials, the copper oxides (Chap. 3) and for the iron-based high- $T_c$  superconductors (Chapter 4). In each chapter, a possibility of enhancing  $T_c$  or a possible route toward higher  $T_c$  are discussed. In Chap. 5 are summarized necessary ingredients for high- $T_c$  superconductivity learned by the lessons from the study of variety of HTSCs. Finally, with a particular emphasis on the role of electronic correlations played in HTSC, is proposed new possible high- $T_c$  superconducting materials that would hopefully follow the cuprates and iron-based compounds.

#### References

- Bednorz JG, Müller KA (1986) Possible high T<sub>c</sub> superconductivity in the Ba-La-Cu-O system. Z Phys B 64:189–193
- Testardi LR, Wernik JH, Reyer WA (1974) Superconductivity with onset above 23 K in Nb-Ge sputtered films. Solid State Commun 15:1–4
- Cava RJ et al (1988) Superconductivity near 30 K without copper. Nature 332:814–815. doi:10.1038/332814a0

References 5

4. Hebard AF et al (1991) Superconductivity at 18 K in potassium-doped fullerene ( $C_{60}$ ). Nature 350:600–601. doi:10.1038/350600a0

- Cava RJ et al (1994) Superconductivity at 23 K in yttrium palladium boride carbide. Nature 367:146–148. doi:10.1038/367146a0
- Yamanaka S, Hotehama KI, Kawaji H (1998) Superconductivity at 25.5 K in electron-doped layered hafnium nitride. Nature 392:580–582. doi:10.1038/33362
- Nagamatsu J, Nakagawa N, Muranaka T, Akimitsu J (2001) Superconductivity at 39 K in magnesium diboride. Nature 410:63–65. doi:10.1038/35065039
- 8. Yabuuchi T, Matsuoka T, Nakamoto Y, Shimizu K (2006) Superconductivity of Ca exceeding 25 K at megabar pressures. J Phys Soc Jpn 75:083703. doi:10.1143/JPSJ.75.083703
- 9. Kamihara Y, Watanebe T, Hirano M, Hosono H (2008) Iron-based layered superconductor La[O<sub>1-x</sub>F<sub>x</sub>]FeAs with T<sub>c</sub>=26 K. J Am Chem Soc 130:3296–3297. doi:10.1021/ja800073m
- Mitsuhashi R et al (2010) Superconductivity in alkali-metal-doped picene. Nature 464:76–79. doi:10.1038/nature08859
- 11. Serrao JL et al (2002) Plutonium-based superconductivity with a transition temperature above 18 K. Nature 420:297–299. doi:10.1038/nature01212
- 12. Matthias BT (1955) Empirical relation between superconductivity and the number of valence electrons per atom. Phys Rev 97:74–76
- Schilling A, Cantoni M, Ott HR (1993) Superconductivity above 130 K in the Hg-Ba-Ca-Cu-O system. Nature 363:56–58. doi:10.1038/363056a0
- 14. Gao L et al (1994) Superconductivity up to  $164 \,\mathrm{K}$  in HgBa<sub>2</sub>Ca<sub>n-1</sub>Cu<sub>n</sub>O<sub> $2m+2+\delta$ </sub> (m=1, 2, and 3) under quasihydrostatic pressures. Phys Rev B 50:4260-4263
- Ren ZA et al (2008) Superconductivity at 55 K in iron-based F-doped layered quaternary compound Sm[O<sub>1.x</sub>F<sub>.</sub>]FeAs. Chin Phys Lett 25:2215–2216. doi:10.1088/0256-307X/25/6/080

# Chapter 2 Overview of Superconducting Materials with $T_c$ Higher than 23 K

**Abstract** Among the eight families of high- $T_c$  superconductors, magnesium diboride (MgB<sub>2</sub>), borocarbide (YPd<sub>2</sub>B<sub>2</sub>C), and calcium (Ca) at high pressures are thought to be conventional superconductors with phonon-mediated pairing.  $T_c = 39$  K for a simple metal MgB<sub>2</sub> is surprising in view of the old-known ceiling of 30 K of the electron-phonon mechanism. Several circumstances in MgB, appear to optimize the phonon-mediated pairing and to up-shift the old ceiling of  $T_c$ . These give a hint on further optimization or further enhancement of  $T_c$ . In doped bismuthates (BaBiO<sub>3</sub>), fullerides (C60), and chloronitrides (HfNCl), dominant pairing interaction is also supposed to be electron-phonon coupling. These superconductors are proximate to insulating phases. Because of this, the electron (carrier) density is significantly low as compared to that in simple metals, suggestive of contribution from electronelectron interactions which may act to strengthen electron-phonon coupling. One other family, from organic compounds, is going to join the latter group. Copper oxides and iron arsenides/selenides, as well as heavy fermions compounds, are distinct from others, and obviously belong to unconventional superconductors with dominant electron-electron interactions.

#### 2.1 Introduction

Among the eight families of high- $T_c$  superconductors (HTSCs), superconductivity in PdY<sub>2</sub>B<sub>2</sub>C, MgB<sub>2</sub>, and elemental Ca in the high-pressure phase is discussed in the context of superconductivity with the phonon-mediated pairing interaction. Superconductivity in Ba<sub>1-x</sub>K<sub>x</sub>BiO<sub>3</sub> (BKBO), doped C<sub>60</sub> and  $\beta$ -HfNCl are also supposed to be phonon-mediated, but the estimated  $T_c$  values are significantly lower than those of real materials. As these three are in proximity to some insulating phases, it is plausible that contributions from electron-electron interactions (electronic correlations) enhance the electron-phonon coupling. A possible high- $T_c$  organic superconductor, doped polycyclic-aromatic-hydrocarbon, might join the second group. All these families, except Ca, have light elements, B, C, N, or O and strong covalent bonds, so that large energy prefactor  $\Omega_0$  (phonon frequency) and strong electron-phonon coupling  $\lambda$  in a simplified formula,  $k_B T_c \sim \hbar \Omega_0 \, \mathrm{e}^{-1/\lambda}$ , are presumably important factors for high  $T_c$ 's.

Although there is uncertainty in evaluating the parameter for screened/renormalized Coulomb interaction, usually parameterized by  $\mu^*$ , the calculation of  $T_{\rm c}$  in the framework of the Migdal-Eliashberg theory successfully reproduces  $T_{\rm c}$ =39 K of MgB<sub>2</sub>, the highest  $T_{\rm c}$  so far achieved in obviously weakly correlated systems.  $T_{\rm c}$ =39 K for a simple metal MgB<sub>2</sub> is surprising in view of the old-known ceiling of 30 K of the electron-phonon mechanism. Several circumstances appear to be optimized in MgB<sub>2</sub> to allow for very strong electron-phonon coupling without inducing lattice instability.

Copper oxides and iron arsenides/selenides, as well as  $PuCoGa_5$  with  $T_c=18$  K derived from heavy fermions compounds, are distinct from others, and obviously belong to unconventional superconductors with dominant electronic correlations.

#### 2.2 Materials with Phonon-Mediated Pairing

For superconductors with phonons as pairing glue,  $T_{\rm c}$  is understood or the  $T_{\rm c}$  value is calculated in the well-established framework of the Migdal-Elishaberg theory. Two important parameters that determine  $T_{\rm c}$  are the electron-phonon coupling strength  $\lambda$  and the phonon frequency  $\Omega_0$ . Large  $\Omega_0$  and strong  $\lambda$  are favorable for high  $T_{\rm c}$ , while the phonon energy  $\hbar\Omega_0$  needs to be considerably smaller than the Fermi energy  $E_{\rm F}$  of the electronic system,  $\hbar\Omega_0$   $\phi$   $E_{\rm F}$  (the Migdal (retardation) condition). The Migdal condition is necessary for the bare Coulomb repulsive interactions ( $\mu$ ) between electrons to be significantly renormalized (decreased);

$$\mu^* = \mu / [1 + \mu \ln (E_F / \hbar \Omega_0)].$$

The coupling strength  $\lambda$  is usually expressed by

$$\lambda = N(E_{\rm F})\langle I^2 \rangle / M \langle \omega^2 \rangle = N(E_{\rm F})V_{ph},$$

with  $\langle I^2 \rangle$  being the mean-square electron-phonon matrix element averaged over the Fermi surface,  $N(E_{\rm F})$  the electron density of states at the Fermi energy, M the ion mass,  $\langle \omega^2 \rangle$  the averaged square phonon frequency, and  $V_{ph}$ , the effective electron-phonon interaction. In a crude approximation, that is a guide for extracting important parameters for  $T_{\rm c}$ ,  $\langle \omega^2 \rangle \sim K/M$  (K, stiffness of the lattice) and  $T_{\rm c}$  is approximated by the McMillan formula,  $k_{\rm B} T_{\rm c} \sim \hbar \Omega_0$  e<sup>-1/( $\lambda - \mu^*$ )</sup>. More rigorously,  $T_{\rm c}$  is expressed by the McMillan-Allen-Dynes formula [1]. In the strong coupling limit (large  $\lambda$ ), the formula has an asymptotic form,  $T_{\rm c} \sim \lambda^{1/2}$ , and  $T_{\rm c}$  continues to increase, if other parameters are kept unchanged.

These equations suggest that larger  $N(E_{\rm F})$ ,  $\langle I^2 \rangle$ , and  $\Omega_0$  are favorable for higher  $T_{\rm c}$  values. Some of the old Matthias rules, #1: cubic crystals #2: d-electron metals, and #3: special average number of valence electrons, are guides to a search for materials with larger  $N(E_{\rm F})$ . Also, metals composed of light elements (small M) with stiff lattice (large K), hence large  $\Omega_0$ , were candidates for high- $T_{\rm c}$  SC. Since  $V_{ph}$  is

independent of M and  $\Omega_0 \sim 1/M^{1/2}$ , it was expected that materials composed of light elements would have a large  $\Omega_0$  and a substantial  $\lambda$ . Metallic hydrogen (H) was supposed to be the limiting case as predicted in 1968 [2], but realization of HTSC in metallic hydrogen remains challenging.

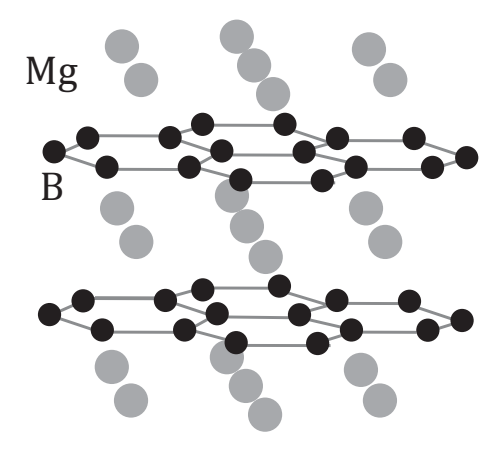
However, there were discussions on the  $T_{\rm c}$  ceiling for SC with phonon mediated pairing:

- 1. The magnitude of  $T_c$  is bound by the inequalities,  $k_B T_c \ll \hbar \Omega_0 \ll E_F$ , so it was thought that  $T_c$  could not be high.
- 2. Large  $N(E_{\rm F})$  is a characteristic of narrow band metals which implies a small  $E_{\rm F}$ . This tends to make the renormalization of repulsive interaction weaker. Materials with a pronounced peak in N(E) at  $E_{\rm F}$  which was expected by the Matthias rule #3, have tendency for electronic and structural instabilities and their  $T_{\rm c}$  would be sensitive to disorder or impurities.
- 3. The old idea, which is not necessarily correct, is that  $\Omega_0$  and  $\lambda$  are not independent parameter; when  $\Omega_0$  is large,  $\lambda$  cannot be large, since the formula for  $\lambda$  contains  $\Omega_0^2$  in its denominator.
- 4.  $T_{\rm c}$  for SC in the strong coupling regime is thought to monotonically increase following the Allen-Dynes formula,  $T_{\rm c} \sim \lambda^{1/2}$  However, even so, too strong electron-phonon coupling induces a structural instability which gives a ceiling.

#### 2.3 High- $T_c$ Superconductivity in MgB<sub>2</sub>

In this regard, MgB<sub>2</sub> with  $T_c$ =39 K is a surprising material [3]. As shown in Fig. 2.1, the crystal structure consists of a stack of hexagonal honeycomb Mg layer sandwiched by hexagonal B layers above and below. It is a sort of fully intercalated graphite structure. The B-B bond is a strong covalent bond arising from the  $sp^2$  hybridization, and hence the corresponding bond-stretching phonon modes have high frequencies ( $\Omega_0 \sim 1000 \text{ cm}^{-1}$ ) [4]. MgB<sub>2</sub> is obviously a simple metal in the normal

**Fig. 2.1** Crystal structure of MgB<sub>2</sub>



state and phonon-mediated SC is evidenced, for example, by the boron isotope effect (for  $^{10}\text{B} \Rightarrow ^{11}\text{B}$  isotope substitution  $T_{\rm c}$  decreases by 1 K [5]). MgB<sub>2</sub> is basically a weakly correlated (s)p-band metal with large Fermi energy  $E_{\rm F}\sim$  several eV which is much larger than the highest energy phonon ( $\sim$ 0.1 eV), so that SC is understood within the framework of the Migdal-Eliashberg theory. Indeed, the calculation of  $T_{\rm c}$  based on the density-functional theory (DFT) and linear-response theory (LRT) in the local-density approximation (LDA) successfully reproduces  $T_{\rm c}$ =40 K [6], though the renormalized Coulomb repulsion  $\mu^*$  is adjusted to  $\mu^*$ =0.09–0.13 which are used for conventional superconductors.

The crucial ingredients for the high- $T_{\rm c}$  value in MgB<sub>2</sub> are thought to be the followings:

- 1. Layer structure:  $N(E_{\rm F})$  maintains a substantial magnitude even when  $E_{\rm F}$  is located near the band edge, since the electronic density of states is nearly constant against energy in two dimensions.
- 2. Strong  $sp^2$  bonding: Layer structure favors  $sp^2$  hybridization/bonding. The  $sp^2$  bond is much stronger than d-d bond, and even stronger than  $sp^3$ .
- 3. Light element B: Combined with the strong  $sp^2$  bond leads to very large  $\Omega_0$ .
- 4. Very strong electron-phonon coupling without instability: There is a cylindrical FS (so-called G-FS) with character of strong bonding orbitals ( $E_{\rm F}$  crosses the  $sp^2$  hybridized bands) which couples strongly to the B-B bond stretching phonon modes. The calculated deformation potential  $\Sigma_D$ , a change of electronic band energy due to lattice distortion by a unit length (Å) corresponding to a specific phonon mode, is  $\Sigma_D = 13 \, {\rm eV} / \, {\rm A} \left( \langle I^2 \rangle \propto \Sigma_D^2 \right)$ . If the electronic system very strongly couples with a particular phonon mode at momentum Q, the frequency of this phonon is strongly renormalized and softened, and the lattice becomes unstable. In the case of MgB<sub>2</sub> the relevant FS is circular associated with 2D parabolic bands, so there is no nesting Fermi surface nor a special Q. The electronphonon coupling is very strong ( $\lambda \sim 0.82$ ) for phonons in the two bond-stretching branches. This gives rise to nearly constant Q-renormalization over a range of Q's with Q remaining large, and thereby the material avoids a structural instability.
- 5. Band degeneracy  $n_B = 2$ : MgB<sub>2</sub> is a multiband/multiple FS system. There are two almost identical but separated  $\sigma$ -FSs which are relevant to the strong coupling with phonons in the two bond-stretching mode branches exist in the 1st BZ. In this case  $\lambda$  is further enhanced by a factor of  $n_B^2 = 4$  [7]. These seem to conspire to optimize the phonon-mediated superconductivity in MgB<sub>2</sub>.

# 2.4 Other Electron-Phonon Superconductors with Fairly High $T_c$

#### 2.4.1 Doped Bismuthate $Ba_{1-x}K_xBiO_3$

 $Ba_{1-x}K_xBiO_3$  (BKBO) shows superconductivity at  $T_c \sim 30$  K [8, 9]. The parent compound  $BaBiO_3$  is a distorted perovskite oxide (see Fig. 2.2a), and a three-

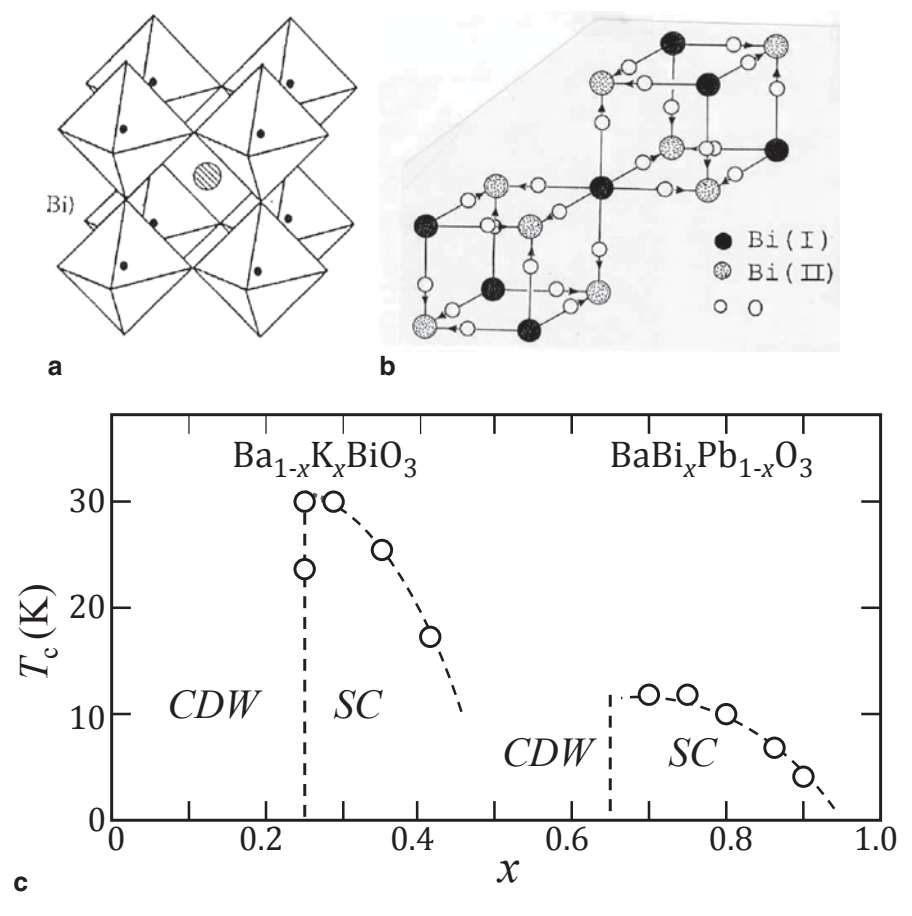


**Fig. 2.2** a Idealized perovskite structure of  $BaBiO_3$ . Actual structure is distorted due to breathing-mode distortion and rigid rotation of  $BiO_6$  octahedra. **b** Breathing-mode distortions in the CDW state of  $BaBiO_3$  which make the compound insulating with inequivalent neighboring Bi atoms [10]. **c** Temperature (T)-doping (x) phase diagram of doped  $BaBiO_3$ ,  $Ba_{1-x}K_xBiO_3$  and  $BaPb_xBi_{1-x}O_3$ . The superconducting region is bounded by a half-dome in both cases. Most of the remaining region is CDW state which is so robust that the CDW transition temperature is too high to be chased

dimensional charge-density-wave (CDW) insulator with a CDW gap of 2 eV [10]. CDW is supposedly an array of alternating Bi<sup>3+</sup> ( $6s^2$ -lone pair) and Bi<sup>5+</sup> (closed shell ion). In reality, only little charge difference on the Bi sites is observed, but the oxygen sites are distorted, the breathing-mode distortion—the O atoms expanding around a Bi atom and shrinking around the neighboring Bi atom as sketched in Fig. 2.2b. The CDW order is quite stable and never melts up to temperature 1000 K. It melts by substituting (doping) K for Ba ( $x \sim 0.3$ ) or Pb for Bi (BaPb<sub>x</sub>Bi<sub>1-x</sub>O<sub>3</sub>,  $x \sim 0.6$ ), giving way to superconductivity. The phase diagram is displayed in

Fig. 2.2c. The CDW order occupies a wide region of the phase diagram and is quite stable. As a consequence of the robust CDW, strong CDW fluctuations either static or dynamical, remain viable even in the SC regime [11].

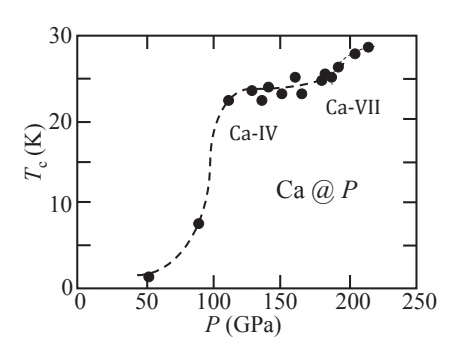
The electron-phonon coupling estimated by the DFT and LRT in the local-density approximation (LDA) is  $\lambda$ =0.34 [12] which is well below the value required to account for SC with  $T_{\rm c}\sim$ 30 K. This failure indicates some correlations beyond LDA need to be incorporated, since the LDA tends to underestimate  $\lambda$  due to overscreening. This is particularly the case with materials in the vicinity of a metal-insulator transition. SC in the doped bismuthates is realized in the metallic side of the CDW insulator-metal transition and  $T_{\rm c}$  is high in close vicinity of the transition. An attempt to go beyond LDA shows that  $\lambda$  is enhanced by a factor of 3 by taking into account of nonlocal electronic correlation effect arising from a poor screening [13]. The value of  $\mu$ \* $\sim$ 0.1 is estimated by first-principle calculations. Using the enhanced  $\lambda$ , the renormalized  $\Omega$ , and  $\mu$ \*,  $T_{\rm c}$  is calculated to be 30 K from the modified McMillan equation.

#### 2.4.2 Elemental Superconductors at High Pressures

In the last 15 years a number of elements have been found to be SC with fairly high  $T_c$  values under pressures (P) of 30–50 GPa or higher. These include sulphur (S) ( $T_c$ =17 K) [14], lithium (Li) ( $T_c$ =20 K) [15], yttrium (Y)( $T_c$ =20 K) [16], and calcium (Ca) ( $T_c$ =29 K) [17, 18]. As in the case of MgB<sub>2</sub>, for these elemental SCs the LDA-based calculations appear to be successful in deriving large  $\lambda$  and estimating high  $T_c$ . Li is an s-electron metal and is not expected to have large electron-phonon coupling  $\lambda$  despite its light atomic mass. In fact,  $T_c$  of Li at ambient pressure is only 100  $\mu$ K. The enormous increase of  $T_c$  at high pressures is ascribed to the transformation from an s-band metal to an s-p metal [7] in which the covalent character is possibly added to the bonding and thus Li may possess necessary ingredients for high  $T_c$  in common with MgB<sub>2</sub>.

Ca in the high-P phases have distinctly higher  $T_{\rm c}$  and joins the group of HTS. As plotted in Fig. 2.3,  $T_{\rm c}$  rapidly rises in the P range between 50 and 100 GPa, reaching

Fig. 2.3  $T_c$  of calcium plotted as a function of pressure (the data points are from [17, 18])



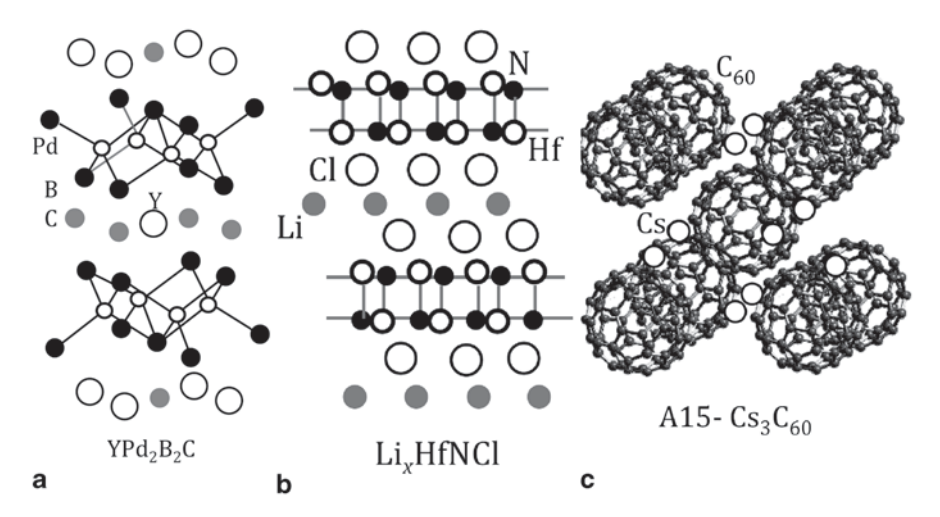


**Fig. 2.4 a** Crystal structure of YPd<sub>2</sub>B<sub>2</sub>C. **b** Crystal structure of β-HfNCl. It becomes a superconductor at  $T_c$ =26 K upon electron doping. **c** A15 type crystal structure of Cs<sub>3</sub>C<sub>60</sub>.  $T_c$ =38 K is achieved upon applying pressure [29]

25 K at P=160 GPa in the Ca IV structural phase [17]. With further increase of P,  $T_{\rm c}$  gradually rises to 29 K at P=220 GPa [18] where Ca is in the distinct Ca VII phase with so-called "host-guest" structure [19]. It is surprising that Ca is not a light mass element. It is unlikely that Ca under pressure is a strongly correlated electronic system with some magnetic state nearby because of its proximity to the 3d transition-metal elements. Instead, as the Ca IV and VII phases are structures with high-density of Ca atoms which is by a factor of 4–5 higher than that at ambient pressure, hardened phonons and/or a 3d orbitals mixing may strengthen electronic correlations and enhance the electron-phonon coupling as in the case of the doped bismuthates.

#### 2.4.3 Borocarbide YPd,B,C

Among the family of borocarbides,  $YPd_2B_2C$  has the highest  $T_c$ =23 K [20]. Since single crystals are not available, its physical properties and material parameters have not been studied yet. Instead, most extensively studied compounds are the Ni borocarbides, representatively  $YNi_2B_2C$  ( $T_c$ =15 K). The basic building block of the layer structure, displayed in Fig. 2.4a, is a B-C-B trimer (double dumbbell) linked to  $YNi_2$  layers. The Ni-B configuration is the same as that of Fe-As (Se) in the Fe-based high- $T_c$  superconductors (see Chap. 4). The strong B-C-B bonds and light masses give rise to high-frequency optical phonon modes (~1000 cm<sup>-1</sup>) well separated from the low-lying phonons. The high-frequency phonons are considered

to provide a majority of electron-phonon coupling strength as in the case of  $\mathrm{MgB}_2$  [21]. However, some low-frequency modes show a marked change, either softening or line-broadening, upon cooling down to above  $T_{\rm c}$  [22], which is a signature of strong electron-phonon coupling, not arising from FS nesting nor from phonon anharmonicity. Nevertheless, given that there is no insulating phase nearby and that 4d-Pd compound has higher  $T_{\rm c}$  than 3d-Ni compound, superconductivity of this family is understood most likely by the type of phonon-mediated pairing without need for electronic pairing interactions nor correlation-induced enhancement of the electron-phonon coupling.

#### 2.4.4 Electron Doped β-HfNCl

Transition-metal chloronitrides MNX (M=Ti, Zr, and Hf, N=nitrogen, X=Cl, Br, and I) form a fairly large family of superconductors. These materials are basically insulating, but electron doping makes them superconductors.  $T_c$  is 16 K for electron doped ZrNCl ( $\beta$ -Li<sub>x</sub>ZrNCl) [23] and the highest  $T_c$ =26 K was recorded in 1998 for  $\beta$ -Li<sub>x</sub>(THF)<sub>y</sub>HfNCl (THF stands for tetrahydrofrun) [24]. The crystal structure, shown in Fig. 2.4b, consists of (grapheme-like) honeycomb double sheets of alternating Hf and N. Each Hf (N) atom is bonded with three N (Hf) atoms within a layer. Layers of Cl on either side of this double sheet form an insulating block with charge neutral (HfNCl)<sub>2</sub> units. The neutral (HfNCl)<sub>2</sub> blocks are coupled each other via a weak van der Waals force along the c axis.

The chloronitrides have some features in common with MgB<sub>2</sub>, such as layer structure and light element N. However, the LDA-based calculation yield the electron-phonon coupling  $\lambda \sim 0.5$  and  $\omega_{ln} \left( \sim \sqrt{\langle \omega^2 \rangle} \right) \sim 36$  meV, giving  $T_c \sim 6$  K for the electron doped ZrNCl assuming  $\mu^* = 0.1$  [25]. The calculated low  $T_c$  indicates either that an electronic pairing mechanism may be in operation or that electronic correlations (beyond LDA) may enhance the electron-phonon coupling as suggested for doped bismuthates. In fact, the doped MNCls are metals with low carrier density in the normal state, and thus the screening effect is expected to be weak. An ab initio analysis using a DFT for SC non-empirically calculates both electron-phonon ( $\lambda$ ) and electron-electron ( $\mu^*$ ) interactions. The calculated  $\lambda$  is larger than 0.5 obtained by the LDA based calculation, but the screened/renormalized Coulomb interaction parameter  $\mu^*$  is found to be larger by a factor of about 2 than the commonly used empirical values (0.09–0.13). Because of the large  $\mu^*$ values, the resulting  $T_c$  values are low, below 10 K both for doped ZrNCl and HfNCl [26]. On the other hand, the calculations beyond LDA as is adapted to the doped bismuthates yield correlation-enhanced electron-phonon coupling  $\lambda \sim 1$ , giving T's comparable with the experimental values, but they assume  $\mu^*=0.1$ [13]. The discrepancy between experiment and theory may be a signature for unconventional superconductivity. This remains open for future experiments and theories.

# 2.4.5 Doped Fullerides ( $C_{60}$ ) and Polycyclic-Aromatic-Hydrocarbons

Superconductivity of doped (alkaline ions (A) intercalated) fullerides ( $A_3C_{60}$ ) was discovered in 1991 [27]. Within a year  $T_c$  rose from 18 to 33 K by using larger alkaline ions as dopants [28]. In these fullerides  $C_{60}$  molecules build up a cubic fcc lattice. Since Cs has largest ionic radius,  $T_c$  for  $Cs_3C_{60}$  was expected to be higher. In fact, superconducting  $Cs_3C_{60}$  with  $T_c$ =38 K was synthesized in 2008 [29]. However, its crystal structure is not fcc but A15, a bcc packing of  $C_{60}$  with Cs-Cs pairs on the faces of the cubes (see Fig. 2.4c), and it is insulating at ambient pressure. Application of hydrostatic pressure transforms A15-Cs $_3C_{60}$  from insulator to superconductor at  $P\sim4$  kbar. The maximum  $T_c$ =38 K is achieved at  $P\sim7$  kbar.

Organic molecular SCs are one of the oldest "exotic" superconductors. The first discovered in 1980 was the one-dimensional (TMTSF)PF<sub>6</sub> showing SC with  $T_c$ =0.9 K under pressure of 12 kbar [30]. After several years  $T_c$  of organic SCs increased in the class of the organic charge transfer solids up to 13 K for the  $\kappa$ -(ET)<sub>2</sub>Cu[N(CN)<sub>2</sub>]Cl salt under pressure [31], but its increase stopped for more than 10 years before jumping up to 18 K in 2009. The newly discovered SC is a picene ( $C_{22}H_{14}$ ) which shows superconductivity at  $T_c$ =18 K at ambient pressure when doped (intercalated) with potassium [32]. The picene is composed of a hydrocarbon molecule with *five* benzene rings arranged in an "armchair" form and a member of a family of polycyclic aromatic hydrocarbons (PAH) (see Fig. 2.5). The K-doped phenanthrene ( $C_{14}H_{10}$ ) with *three* benzene rings is also a superconductor with  $T_c$ =5 K [33]. It is natural to expect a higher  $T_c$  for PAH with *seven* benzene rings. Recently,  $T_c \sim 30$  K has been reported for K-doped dibenzopentacene ( $C_{30}H_{18}$ ) [34]. However, the zero-resistance has not been confirmed yet.

A15-Cs $_3$ C $_{60}$  as well as doped PAHs is narrow band metals. High electronic density of state at the Fermi energy  $N(E_{\rm F})$  and high phonon frequencies involving light C and H atoms may favor high  $T_{\rm c}$ . Moreover, since they are in the proximity to an insulator-metal transition, the correlation-induced enhancement of the electron-phonon coupling may also be at work. On the other hand,  $E_{\rm F}$  should be small and comparable with phonon energy  $\hbar\Omega_0$ , so they might be in the regime outside the Migdal-Eliashberg theory. A15-Cs $_3$ C $_{60}$  is also an insulator at ambient pressure. The large inter  $C_{60}$  separation results in a reduction of the overlap between neighboring  $C_{60}$  molecules which produces a narrow band. The insulating states of both A15-Cs $_3$ C $_{60}$  and undoped PAHs are likely Mott insulators due to electronic correlation U larger than the bandwidth W. The application of pressure would drive an insulator-metal transition by increasing the bandwidth. In this regard, superconductivity in doped  $C_{60}$  and PAH systems are marginal between phonon-mediated and electronic pairing.

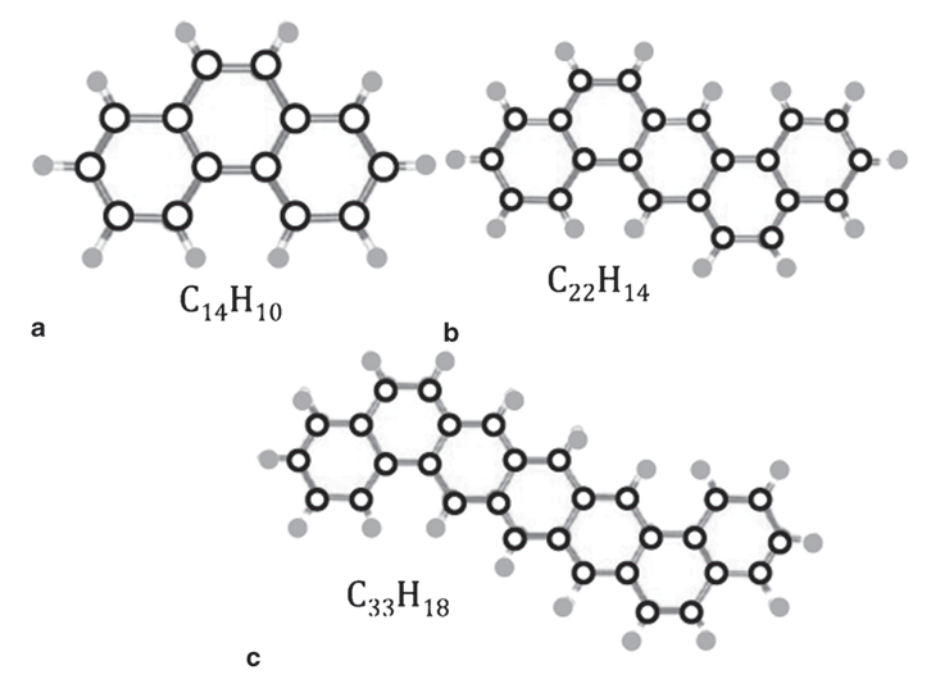


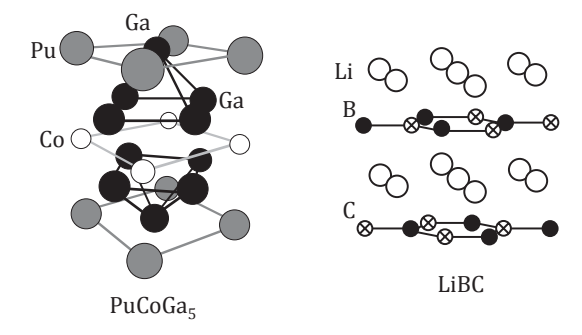
**Fig. 2.5** Structural units of polycyclic aromatic hydrocarbons with 3 ( $C_{14}H_{10}$ ), 5 ( $C_{22}H_{14}$ ), and 7 ( $C_{30}H_{18}$ ) benzene rings. Picene with 5 rings becomes a superconductor with  $T_c$  = 18 K upon electron doping [32]

#### 2.5 Materials with Unconventional Pairing

Dominant pairing interaction, either electron-phonon or electron-electron, is yet to be determined for  $\beta$ -HfNCl,  $A_3C_{60}$ , and doped picene. On the other hand, the cuprates, heavy fermions compounds, iron pnictides/chalcogenides, and possibly some class of the organic superconductors are obviously superconductors with Cooper pairs formed by electronic pairing interactions derived from purely repulsive Coulomb interactions. This is evidenced by the unconventional SC pairing with sign-changing/anisotropic order parameter (SC gap). The *d*-wave gap is established for the cuprates with the maximum  $T_c^{\text{max}}$ =135 K at ambient pressure, and the gap symmetry for most of iron-based superconductors with  $T_c^{\text{max}}$ =55 K is either  $s_+$  or nodal s (or d-wave) depending on the material and doping level.  $T_c$ 's and their physics will be discussed in details in the next two Chapters.

The heavy-fermions (HF) superconductors, first discovered for  $CeCu_2Si_2$  in 1980 [35], are one of the representative strongly correlated electron systems. Their  $T_c$ 's are basically very low,  $T_c < 1$  K. Exceptionally, one of the HF families, the 115 family (CeMIn<sub>5</sub> and PuMGa<sub>5</sub> where M=Co, Ir, or Rh), show unusually high  $T_c$ .

**Fig. 2.6** a Crystal structure of PuCoGa<sub>5</sub>. **b** Crystal structure of LiBC with potential higher *T*<sub>2</sub> than MgB<sub>2</sub> [41]



 $T_{\rm c}$ =18 K was recorded for PuCoGa<sub>5</sub> in 2002 [36]. A schematic crystal structure of 115 is shown in Fig. 2.6a. The 115 materials are remarkably similar to the cuprates in the layer structure and the d-wave pairing symmetry or the SC gap with nodes [37]. In particular, the nearest-neighbor spin-spin interaction J for PuCoGa<sub>5</sub> is as large as ~400 K [38], distinctly larger than J ~70 K for CeCoIn<sub>5</sub> with  $T_{\rm c}$ =2.6 K and orders of magnitude larger than J of other HFs. Note that the corresponding spin superexchange interaction J in the cuprates is typically ~1500 K. In view of typical  $T_{\rm c}$  ~90 K, it seems that  $T_{\rm c}$  scales with J as expected from the spin-fluctuation theory in which the energy scale of spin fluctuation J plays a role of  $\Omega_0$  in the phonon-mediated SCs. From this fact, a guide for discovering higher  $T_{\rm c}$  in strongly correlated systems is proposed [38]:

- Antiferromagnetic materials which can be metallic by tuning doping and/or pressure
- The normal-state is characterized by two-dimensional spin and charge dynamics.
- Containing local spin moments whose nearest neighbor interaction *J* is comparable to or larger than *J* in the cuprates.

However, the spin fluctuation mechanism is not a unique one to explain the  $T_{\rm c}$  of PuCoGa<sub>5</sub>. In fact, the electrons in PuCoGa<sub>5</sub> are no more heavy with the electronic specific heat coefficient  $\gamma \sim 77~{\rm mJ/mol.K^2}$  by an order of magnitude smaller than  $\gamma \sim 1000~{\rm mJ/mol.K^2}$  of CeCoIn<sub>5</sub>. Small  $\gamma$  value is linked to the large exchange interaction J. On the other hand, Pu is a valence-skipping element like Bi and Tl, so the mechanism of valence (charge) fluctuation is also possible [39]. Note that even for the cupartes,  $T_{\rm c}$  does not necessarily scale with J. Despite the large variation of  $T_{\rm c}$  across the cuprate family, 25–135 K, the value of J changes only between 1100 and 1500 K.  $T_{\rm c}^{\rm max}$  is known to even anticorrelate with J in the LnBa<sub>2</sub>Cu<sub>3</sub>O<sub>7</sub> (Ln, rare earth element) family [40]. As will be shown and discussed in the next chapter, the cuprate- $T_{\rm c}$  is influenced by many factors.

## 2.6 Possibility of Higher $T_c$ in Electron-Phonon Superconductors

Elemental superconductors at high pressures continue to be a candidate for achieving higher  $T_{\rm c}$ . Metallic hydrogen, supposed to be realized at very high pressure of ~1000 GPa, is the limiting case. It would be a high- $T_{\rm c}$  superconductor with possible  $T_{\rm c}$  value of 100 K or even higher [2]. At present, hydrogen at pressure of ~600 GPa is not metallic due to a strong tendency for dimerization (H<sub>2</sub>), but the prediction remains unretract.

Though fully confirmed yet,  $T_c$  of the K-doped PAH is rising with increase of the number (N) of benzene rings;  $T_c$ =5 K for N=3 (phenanthrene), 18 K for N=5 (picene), and possibly 30 K for N=7 (dibenzopentacene). If  $T_c$  continues to rise with N, then higher  $T_c$  may be realized in doped PAHs with N=9 and more.

Given that  $T_{\rm c}$  was raised to the level of 40 K in MgB<sub>2</sub>, there is no theoretical reasoning that  $T_{\rm c}$  will never exceed 40 K in the phonon-SCs. Since  $T_{\rm c}$  of MgB<sub>2</sub> is well explained by the calculation based on the DFT (LRT) in LDA within the framework of the Migdal-Eliashberg theory, a practical approach toward higher  $T_{\rm c}$  is to search for or to design materials having similar features to those of MgB<sub>2</sub> and having the electronic and phonon parameters more favorable for the  $T_{\rm c}$ - enhancement. As was discussed in 2.3, the following circumstances appear to optimize the phonon-mechanism of superconductivity in MgB<sub>2</sub>, (i) layer structure, (ii) light elements with strong covalent bonds between them, (iii) high frequency phonon modes corresponding to the modulations of the bond length between light elements (bond stretching mode), (iv) FS with character of strong bonding orbitals ( $\sigma$ -FS), and (v) band degeneracy.

To further optimize the circumstances in MgB<sub>2</sub>, candidate higher  $T_{\rm c}$  compounds should have much stronger electron-phonon coupling  $\lambda$  and higher bond stretching mode frequency  $\Omega_0$  than those of MgB<sub>2</sub>. Note that stronger electron-phonon coupling  $\lambda$  tends to decrease  $\Omega_0$ , but it is possible that the larger value of  $\lambda$  more than compensates the decrease in  $\Omega_0$ . An experimental attempt along this guideline was the elemental substitution for MgB<sub>2</sub>. All substitution for Mg results in a decrease in  $T_{\rm c}$ , and Be for Mg leads to collapse of the MgB<sub>2</sub> structure. Substitution of monovalent atoms for Mg is theoretically expected to increase  $T_{\rm c}$ , but it has been unsuccessful to date.

A theoretically predicted higher  $T_c$  compound is Li<sub>x</sub>BC [41]. As is shown in Fig. 2.6b, LiBC has a hexagonal lattice structure with alternating Li and B-C layers. It is derived from MgB<sub>2</sub> by substituting Li for Mg and BC for B<sub>2</sub>. In a hexagonal BC layer each hexagon is composed of alternating three B and three C atoms, and the layers are B-C alternating also along the stacking direction. LiBC is isovalent to MgB<sub>2</sub>—one less valence electron Li substituted for Mg is compensated by one more electron C substitution for B. Since the nearest neighbor B-C bonds are strongly covalent ( $sp^2$ ) and Li is also a light element, the frequencies of the most phonon branches are very high.

References 19

LiBC is, however, insulating because of the alternating array of B and C in a layer [42]. It can be made metallic by reducing the Li content, Li<sub>x</sub>BC (x<1). The reduction of the Li content corresponds to "hole" doping, and results in the appearance of the  $\sigma$ -FS. As in the case of MgB<sub>2</sub>, the electrons on the  $\sigma$ -FS are strongly coupled to the B-C bond-stretching mode. The calculations of the electronic yield the corresponding deformation potential  $\Sigma_D$ =18.5 eV/Å, considerably larger than 13 eV/Å in MgB<sub>2</sub>. The calculated frequency of the B-C bond-stretching mode is also higher by about 20% than the corresponding B-B stretching mode frequency in MgB<sub>2</sub> due to the shorter in-plane lattice constant. These results indicate that  $T_c$  of Li<sub>x</sub>BC could be significantly higher than 40 K. A crude and overoptimistic estimate of  $T_c$  gives a value close to 100 K. Unfortunately, attempts to realize this high  $T_c$  have been unsuccessful due to difficulty in reducing the Li content [43].

#### References

- Allen PB, Dynes RC (1975) Transition temperature of strong-coupled superconductors reanalyzed. Phys Rev B 12:905–922
- Ashcroft NW (1968) Metallic hydrogen: a high temperature superconductor? Phys Rev Lett 21:1748–1749
- Nagamatsu J, Nakagawa N, Muranaka T, Akimitsu J (2001) Superconductivity at 39 K in magnesium diboride. Nature 410:63–65. doi:10.1038/35065039
- Baron AQR, Uchiyama H, Tajima S, Ishikawa T (2004) Kohn anomaly in MgB<sub>2</sub> by Inelastic X-Ray Scattering. Phys Rev Lett 92: 197004. doi:10.1103/PhysRevLett.92.197004
- Bud'ko SL, Lapertot G, Petrovic C, Cunningham CE, Anderson N, Canfield PC (2001) Boron isotope effect in superconducting MgB<sub>2</sub>. Phys Rev Lett 86:1877–1880. doi:10.1103/PhysRevLett.86.4366
- An JM, Pickett WE (2001) Superconductivity in MgB<sub>2</sub>: covalent bond driven metallic. Phys Rev Lett 86:4366–4369. doi:10.1103/PhysRevLett.86.4366
- Pickett WE (2008) The next breakthrough in phonon-mediated superconductivity. Physica C 468:126–135. doi:10.1016/j.physc.2007.08.018
- Mattheiss LF, Gyorgy EM, Johnson DW (1988) Superconductivity above 20 K in the Ba-K-Bi-O system. Phys Rev B 37: 3745–3746
- Cava RJ et al (1988) Superconductivity near 30 K without copper. Nature 332:814–815. doi:10.1038/332814a0
- Uchida S, Kitazawa K, Tanaka S (1987) Superconductivity and metal-semiconductor transition in BaPb<sub>1-x</sub>Bi<sub>x</sub>O<sub>3</sub>. Phase Transit 8:95–128. doi:10.1080/01411598708209371
- Tajima S, Uchida S, Masaki A, Takagi H, Kitazawa K, Tanaka S, Katsui A (1985) Optical study of the metal-semiconductor transition in BaPb<sub>1-x</sub>Bi<sub>x</sub>O<sub>3</sub>. Phys Rev B 32:6302–6311. doi:10.1103/PhysRevB.32.6302
- Maregalli V, Savrasov SY (1998) Electron-phonon coupling and properties of doped BaBiO<sub>3</sub>. Phys Rev B 57:14453–14469
- Yin ZP, Kutepov A, Kotliar G (2013) Correlation-enhanced electron-phonon coupling: application of GW and screened hybrid functional to bismuthates, chloronitrides, and other high-T<sub>c</sub> superconductors. Phys Rev X 3:021011. doi:10.1103/PhysRevX.3.021011
- Struzhkin VV, Hemley RJ, Mao HK, Timofeev YA (1997) Superconductivity at 10–17 K in compressed sulphur. Nature 390:382–384. doi:10.1038/37074
- Shimizu K, Ishikawa H, Takao D, Yagi T, Amaya K (2002) Superconductivity in compressed lithium at 20 K. Nature 419:597–599. doi:10.1038/nature01098

- Hamlin JJ, Tissen VG, Schilling JS (2006) Superconductivity at 17 K in yttrium metal under nearly hydrostatic pressure up to 89 GPa. Phys Rev B 73:094522. doi:10.1103/Phys-RevB73.094522
- 17. Yabuuchi T, Matsuoka T, Nakamoto Y, Shimizu K (2006) Superconductivity of Ca exceeding 25 K at megabar pressures. J Phys Soc Jpn 75:083703. doi:10.1143/JPSJ.75.083703
- Sakata M, Nakamoto Y, Shimizu K, Matsuoka T, Ohishi Y (2011) Superconducting state of Ca-VII below a critical temperature of 29 K at a pressure of 216 GPa. Phys Rev B 83:220512. doi:10.1103/PhysRevB.83.220512
- Fujihisa H et al (2013) A chain ordered host-guest structure of calcium above 210 GPa. Phys Rev Lett 110:235501. doi:10.1103/PhysRevLett.110.235501
- Cava RJ et al (1994) Superconductivity at 23 K in yttrium palladium boride carbide. Nature 367:146–148. doi:10.1038/367146a0
- Pickett WE, Singh DJ (1995) New class of intermetallic borocarbides superconductors: electron-phonon coupling and physical parameters. J Supercond 8:425–428
- Dervenagas P et al (1995) Soft phonon in superconducting LnNi<sub>2</sub>B<sub>2</sub>C. Phys Rev B 52:R9839– R9842
- Yamanaka S, Hotehama K, Kawaji H, Ohashi M (1996) A new layer-structured nitride superconductor. Lithium-intercalated b-zirconium nitride chloides, Li<sub>x</sub>ZrNCl. Adv Mater 8:771– 774. doi:10.1002/adma.19960080917
- Yamanaka S, Hotehama K, Kawaji H (1998) Superconductivity at 25.5 K in electron-doped layered hafnium nitride. Nature 392:580–582. doi:10.1038/33362
- 25. Heid R, Bohnen K-P (2005) *Ab Initio* lattice dynamics and electron-phonon coupling in Li,ZrNCl. Phys Rev B 72:134527. doi:10.1103/PhysRevB.72.134527
- 26. Akashi R, Nakamura K, Arita R, Imada M (2012) High temperature superconductivity in layered nitrides β-Li<sub>x</sub>MNCl (M = Ti, Zr, Hf): insight from density functional theory for superconductors. Phys Rev B 86:054513. doi:10.1103/PhysRevB.86.054513
- 27. Hebard AF et al (1991) Superconductivity at 18 K in potassium-doped fullerene ( $C_{60}$ ). Nature 350:600–601. doi:10.1038/350600a0
- 28. Tanigaki K et al (1991) Superconductivity at 33 K in cesium rubidium fulleride ( $Cs_xRb_yC_{60}$ ). Nature 352:222–223. doi:10.1038/352222a0
- Ganin AY, Takabayashi Y, Khimyak YZ, Margadonna S, Tamai A, Rosseinsky MJ, Prassides K (2008) Bulk superconductivity at 38 K in a molecular system. Nat Mater 7:367–371. doi:10.1038/nmat2179
- Jerome D, Mazaud A, Ribault M, Bechgaard K (1980) Superconductivity in a synthetic organic conductor (TMTSF),PF<sub>6</sub>. J Phys Lett 41:95–98
- 31. Williams JM et al (1990) From semiconductor-semiconductor transition to the highest-Tc organic superconductor, κ-(ET), Cu[N(CN],]Cl (T<sub>c</sub>=12.5 K). Inorg Chem 29:3272–3274
- Mitsuhashi R et al (2010) Superconductivity in alkali-metal-doped picene. Nature 464: 76– 79. doi:10.1038/nature08859
- 33. Wang X et al (2011) Superconductivity at 5 K in alkali-metal-doped phenanthrene. Nature Commun 2:507–513. doi:10.1038/ncomms1513
- Xue M et al (2012) Superconductivity above 30 K in alkali-metal-doped hydrocarbon. Sci Rep 2:389. doi:10.1038/srep00389
- 35. Schäfer H et al (1979) Superconductivity in the presence of strong Pauli paramagnetism. Phys Rev Lett 43:1892–1896
- 36. Serrao JL et al (2002) Plutonium-based superconductivity with a transition temperature above 18 K. Nature 420:297–299. doi:10.1038/nature01212
- Curro NJ et al (2005) Unconventional superconductivity in PuCoGa<sub>5</sub>. Nature 434:622–625. doi:10.1038/nature03428
- 38. Pines D (2013) Finding new superconductors: the spin-fluctuation gateway to high  $T_{\rm c}$  and possible room temperature superconductivity. J Phys Chem B 117:13145–13153. doi:10.1021/jp403088e
- 39. Shim JH, Haule K, Kotliar G (2007) Fluctuating valence in a correlated solids and the anomalous properties of δ-plutonium. Nature 446:513–516. doi:10.1038/nature05647

References 21

40. Tallon JL, Mallett B (2012)  $T_c$  is insensitive to magnetic interactions in high- $T_c$  superconductors. arXiv:1202.3078

- Rosner H, Kitaigorodsky A, Pickett WE (2002) Prediction of high-T<sub>c</sub> superconductivity in hole-doped LiBC. Phys Rev Lett 88:127001. doi:10.1103/PhysRevLett.88.127001
- Dewhurst JK, Sharma S, Ambrosch-Droxl C, Johansson B (2003) First-principles calculations of superconductivity in hole-doped LiBC: T<sub>c</sub>=65 K. Phys Rev B 68:020504. doi:10.1103/ PhysRevB.68.020504
- 43. Zhao L, Klavins P, Liu K (2003) Synthesis and properties of hole-doped  $L_{1-x}BC$ . J Appl Phys 93:8653. doi:10.1063/1.1556285

# **Chapter 3 Copper Oxide Superconductors**

**Abstract** The copper oxides (cuprates) stand out in their high  $T_c$  values, 135 K, and are only family that achieved  $T_c$  exceeding 100 K. Thanks to the enormous research efforts over 28 years, understanding of the cuprates has remarkably advanced, though some important issues remain under hot debate. A consensus which has been achieved is that primarily repulsive electron-electron interactions lead to superconductivity with such high  $T_c$  as well as to unconventional d-wave pairing. Superconductivity emerges upon doping into the Mott insulating CuO<sub>2</sub> planes. The temperature-doping phase diagram of the cuprates is extremely complex with several orders or incipient orders showing up. Among the known orders, the pseudogap order encompasses a wide doping-temperature region and appears to be home to the superconducting order and its fluctuation at very high temperatures. In contrast to these generic features,  $T_c$  values of the cuprates are strongly material dependent. A few parameters, such as disorder and multilayer, have been identified that control the wide-spread  $T_c$ .  $T_c$  is actually enhanced in some cuprates by reducing disorder in the crystal, and there is a possibility of  $T_c$  enhancement to 150 K or even higher by optimizing multilayer structure.

#### 3.1 Introduction

Among the eight families of high- $T_{\rm c}$  superconductors, the copper oxides (cuprates) stand out in their high  $T_{\rm c}$  values, and are only family that achieved  $T_{\rm c}$  well above the liquid nitrogen temperature. High- $T_{\rm c}$  superconductivity (HTS) in the cuprates was discovered by Bednorz and Müller in 1986 [1]. Even after intensive research efforts over 28 years unraveling the mechanism of HTS and searching for higher  $T_{\rm c}$  continue to be two grand challenges in condensed matter sciences. However, the understanding of the high- $T_{\rm c}$  cuprates has substantially advanced. A consensus that has been achieved is that primarily repulsive electron-electron interactions lead to superconductivity with unprecedentedly high  $T_{\rm c}$  as well as unconventional Cooper pairs. The common structural unit,  ${\rm CuO_2}$  plane, is an insulator driven by strong

electron-electron repulsive interaction (a Mott insulator). Unconventional superconductivity emerges upon doping into the insulating CuO<sub>2</sub> plane.

Another consensus is that characterization of the "normal" state, in particular, the pseudogap regime above  $T_{\rm c}$  and the "strange metal" regime at elevated temperatures in the phase diagram, is indispensable for unraveling the mechanism. Recent progress is the discovery of a "plethora of orders" with broken-symmetry and their fluctuations that manifest in the pseudogap regime. Also, by improvement in the crystal quality, a few important parameters that control  $T_{\rm c}$  are identified for the hole-doped cuprates, such as doping, disorder in the crystal, multilayer structure, and lattice parameters. In this chapter, starting from (1) a historical review, are discussed (2) necessary ingredients for high  $T_{\rm c}$  extracted from the unique features of the cuprates, (3) the current understanding of the doping-temperature phase diagram and relationship of various emergent orders with the superconducting order, (4) factors that influence  $T_{\rm c}$  values and thereby make  $T_{\rm c}$  strongly material dependent, and (5) possibility of enhancing  $T_{\rm c}$  and a few examples of  $T_{\rm c}$  enhancement by optimizing some of the influential factors.

#### 3.2 A brief history of high-T<sub>c</sub> cuprates

The cuprate high- $T_c$  superconductor was first discovered by Bednorz and Müller in early 1986. In December 1986, the structure and chemical composition were identified as La<sub>2-x</sub>Ba<sub>x</sub>CuO<sub>4</sub> (LBCO) with K<sub>2</sub>NiF<sub>4</sub> (layered perovskite or "214") structure shown in Fig. 3.1a [2].  $T_c^{\text{max}}$  of LBCO was 30 K, but by simply replacing Ba by Sr, La<sub>2-x</sub>Sr<sub>x</sub>CuO<sub>4</sub> (LSCO),  $T_c$  went up to ~40 K [3, 4]. Remarkable features of these cuprates were (i) the undoped (parent) compound La<sub>2</sub>CuO<sub>4</sub> is a Mott insulator due to strong inter-electron repulsive interactions [5] (the LDA band structure calculation predicted a metal with a half-filled conduction band), and (ii) superconductivity emerges by doping holes into this parent compound. Notably, these cuprates were not new materials but already known oxides by chemists. It was unlucky enough that the chemists who studied them did not measure resistivity below the liquid nitrogen temperature (77 K) [6].

Right after the identification of the structure and chemical compositions, many researchers tried to replace La by other rare earth elements.  $T_{\rm c}$  actually rose up to ~90 K for a compound composed of Y, Ba, Cu, and O during the period between December 1986 and January 1987 [7]. They aimed to apply chemical pressure by replacing La by Y with smaller ionic radius. This was really an epoch-making discovery of superconductor with  $T_{\rm c}$  exceeding the liquid nitrogen temperature. The crystal structure of this liquid-nitrogen superconductor was found to be really new [8], YBa<sub>2</sub>Cu<sub>3</sub>O<sub>7-y</sub> (YBCO) with so-called "123" structure, composed of double CuO<sub>2</sub> planes (CuO<sub>2</sub>-Y-CuO<sub>2</sub> unit), Ba<sub>2</sub>O<sub>2</sub> blocks, and incomplete CuO<sub>1-y</sub> chain blocks shown in Fig. 3.1b. The fully oxygen reduced compound YBa<sub>2</sub>Cu<sub>3</sub>O<sub>6</sub>

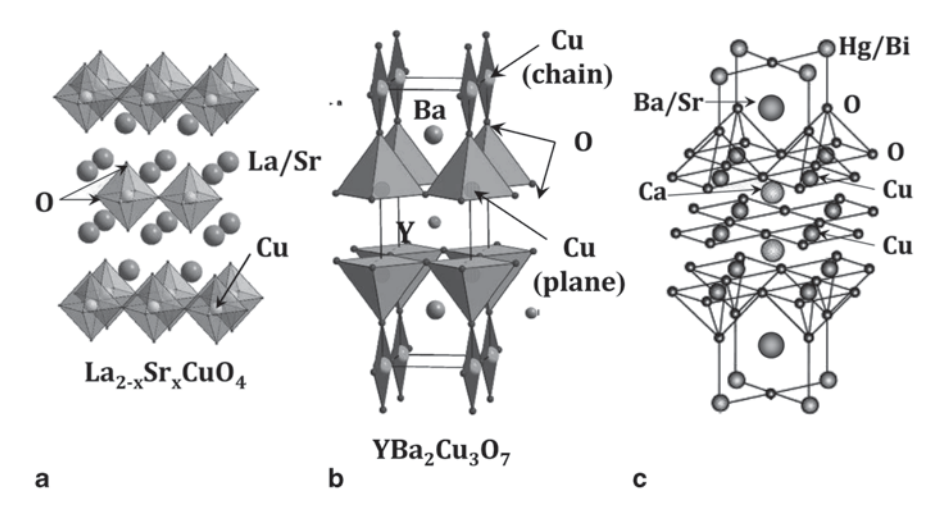


**Fig. 3.1** Crystal structures (schematic) of two representative high- $T_c$  cuprates, **a** La<sub>2,x</sub>Sr<sub>x</sub>CuO<sub>4</sub> and **b** YBa<sub>2</sub>Cu<sub>3</sub>O<sub>7</sub>. Structural unit for trilayer cuprates is shown in **c** which was first discovered for Bi<sub>2</sub>Sr<sub>2</sub>Ca<sub>2</sub>Cu<sub>3</sub>O<sub>10+δ</sub>, and the highest  $T_c$  value 135 K was recorded for HgBa<sub>2</sub>Ca<sub>2</sub>Cu<sub>3</sub>O<sub>8+δ</sub> with the same structural unit

is a Mott insulator, and hole doping is made by adding oxygen atoms to the CuO chains.

The third breakthrough was brought about in early 1988 [9].  $T_c$  exceeded 100 K in another new cuprate structure,  $\mathrm{Bi_2Sr_2Ca_2Cu_3O_{10+\delta}}(\mathrm{Bi2223})$ , with trilayer  $\mathrm{CuO_2-Ca-CuO_2}$  unit. In this compound  $\mathrm{Bi_2O_{2+\delta}}$  blocks are charge reservoir layers and excess oxygen atoms  $\mathrm{O_\delta}$  provide holes to the  $\mathrm{CuO_2}$  planes. The fundamental part of its crystal structure is displayed in Fig. 3.1c. The Bi-based cuprates are the first multilayer "homologous series", with chemical formula  $\mathrm{Bi_2Sr_2Ca_{n-1}Cu_nO_{2n+4+\delta}}$  [Bi22(n-1)n] including single layer (n=1)  $\mathrm{Bi_2Sr_2CuO_{6+\delta}}(\mathrm{Bi2201})$  and bilayer (n=2)  $\mathrm{Bi_2Sr_2CaCu_2O_{8+\delta}}(\mathrm{Bi2201})$  are its close relatives. Soon after this discovery, another homologous series  $\mathrm{Tl_2Ba_2Ca_{n-1}Cu_nO_{2n+4+\delta}}$  [Tl22(n-1)n] was discovered by replacing Bi and Sr by Tl and Ba, respectively [10].  $T_c^{\mathrm{max}} = 125$  K was achieved for Tl2223.

It was straightforward to find another homologous series by replacing Bi or TI by other heavy elements such as Pb or Hg. In 1993, Hg-homologous series, HgBa<sub>2</sub>Ca<sub>n-1</sub>Cu<sub>n</sub>O<sub>2n+2+δ</sub> [Hg12(n-1)n], was successfully synthesized. Again, the HgO<sub>δ</sub> blocks are charge reservoir and excess oxygen atoms (O<sub>δ</sub>) supply holes to the CuO<sub>2</sub> planes. HgBa<sub>2</sub>Ca<sub>2</sub>Cu<sub>3</sub>O<sub>8+δ</sub>(n=3) recorded the highest  $T_c$  value, 135 K, at ambient pressure [11].  $T_c$  of the same compound increased to 164 K at pressure higher than 20 GPa [12]. Striking feature of the Hg-based cuprate is that the multilayers up to n=8 or larger were synthesized [13, 14].  $T_c$  increases with n up to n=3 and then decreases for n larger than 4 which turned out to be generic for multilayer cuprates.

#### 3.3 Uniqueness of the Cuprates

#### 3.3.1 Characteristics of the CuO, Plane

High-temperature superconductivity with  $T_{\rm c}$  well exceeding the liquid-nitrogen temperature (77 K) is found only in a class of materials whose basic structural unit is the surprisingly simple  ${\rm CuO_2}$  plane, layers of Cu and O arranged in a square lattice (see Fig. 3.2a). The neighboring  ${\rm CuO_2}$  planes are separated by so-called "charge reservoir" layers/blocks. Representative charge reservoir blocks are seen in Fig. 3.1a–c. Roles of the charge reservoir layers are: (i) To supply carriers to the  ${\rm CuO_2}$  planes by chemical substitution and/or by adding or reducing oxygen atoms, (ii) to neutralize the negatively charged  ${\rm CuO_2}$  planes,  $[{\rm Cu}^2+{\rm O}^2\__2]^2-$  by forming an alternating stack with positively charged layers, and (iii) to stabilize the cuprate crystal structure by inserting layers consisting of cations with large ionic radii. Typical examples for (i) is the  ${\rm La_2}_{-x}{\rm Sr}_x{\rm O_2}$  layers in  ${\rm La_2}_{-x}{\rm Sr}_x{\rm CuO_4}$  (LSCO) and  ${\rm Bi}_2{\rm O}_{2+\delta}$  layers in  ${\rm Bi}_2{\rm Sr}_2{\rm Ca}$ - ${\rm Cu}_2{\rm O}_{8+\delta}$  (Bi2212).  ${\rm La}_2{\rm O}_2$  layers,  $[{\rm La}^3+_2{\rm O}^2-_2]^{2+}$ , play all the three roles in LSCO. Major role of the Y³+(Ca²+) layers in YBCO (Bi2212) is (ii) and that of the neutral  ${\rm Ba}_2{\rm O}_2$  (Sr<sub>2</sub>O<sub>2</sub>) layers is (iii).

The undoped CuO<sub>2</sub> plane is a "Mott" or charge transfer (CT) insulator due to the strong Coulomb repulsion ( $U \sim 6-8$  eV) between electrons on the 3d orbitals of Cu atoms. As schematically depicted in Fig. 3.2b, the energy gap is actually created between occupied O2p band and empty Cu3d band (the upper Hubbard band), so it is called as a charge-transfer (CT) gap  $E_{\rm CT}$ . A  ${\rm Cu}^{2+}$  ion has 9 electrons in the 3d orbitals and it is four-fold coordinated in a CuO<sub>2</sub> square lattice. As a consequence, the uppermost 3d orbital is  $3d_{x^2-v^2}$  and occupied by a single electron (hole) as depicted in Fig. 3.2c. This lone electron (hole) is localized on Cu due to strong Coulomb repulsion, leaving a magnetic moment associated with the S=1/2 spin quantum number. The Cu spins align antiferromagnetically on the CuO<sub>2</sub> plane in the undoped cuprate due to superexchange interaction J between neighboring Cu spins via an intervening O atom. The singly occupied Cu 3  $d_{x^2-y^2}$ level form a single band by the hybridization with the  $O2p_x$  and  $O2p_y$  states which would be half-full, if the Coulomb repulsion were not strong. Since Cu is at the end of the 3d transition metal series in the periodic table, the energies of Cu3d states are incidentally close to those of the O2p states as schematically shown in Fig. 3.3. This makes the CT energy gap small,  $E_{\rm CT}$ =1.5–2.0 eV, compared with that in other transition-metal oxide. In particular, the wavefunction of  $3d_{y^2-y^2}$  has large overlap with that of  $O2p_x$  and  $O2p_y$  (see Fig. 3.2b). The overlap integral or hopping matrix element  $t_{pd}$  (or t) is large, ~0.3–0.4 eV, leading to strong hybridization between the two.

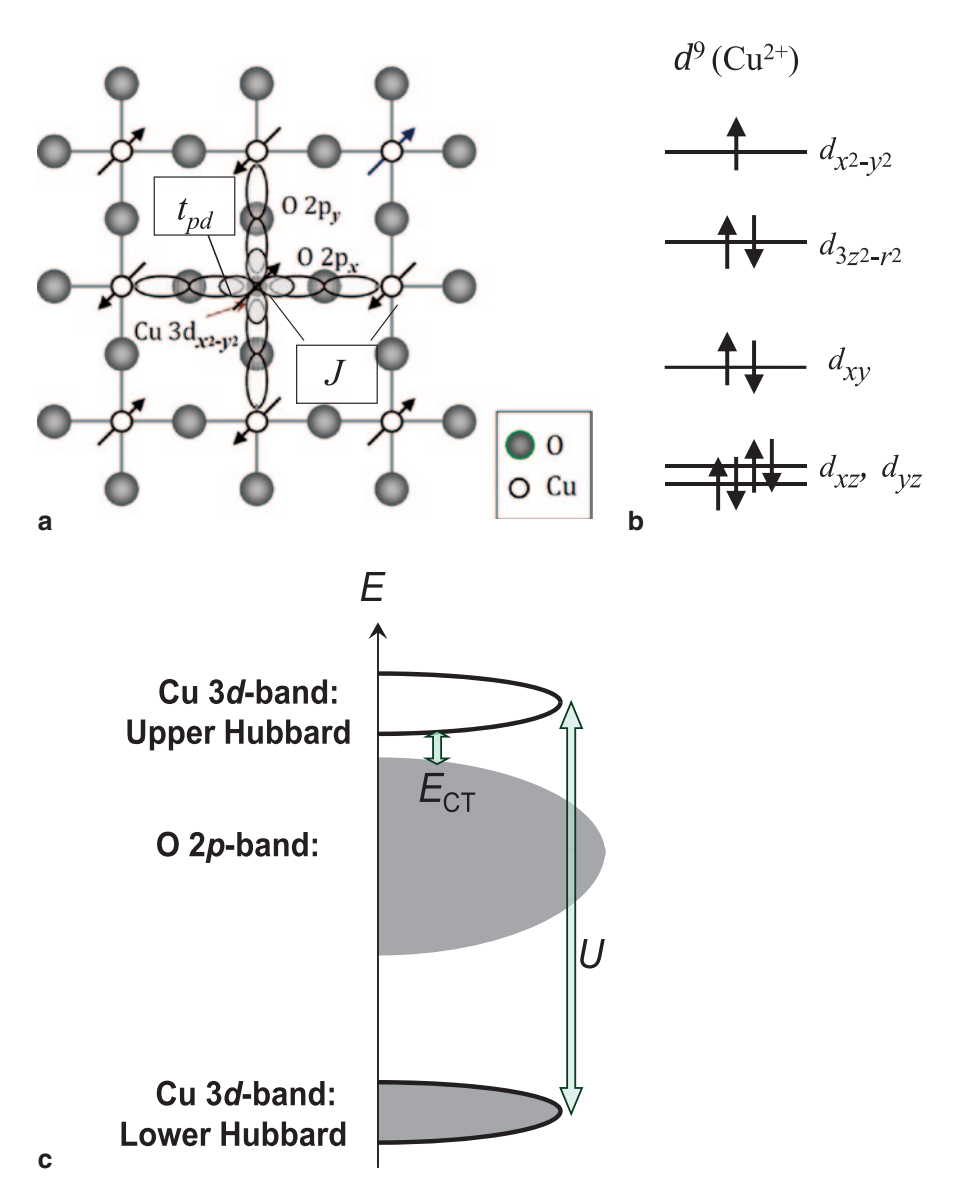
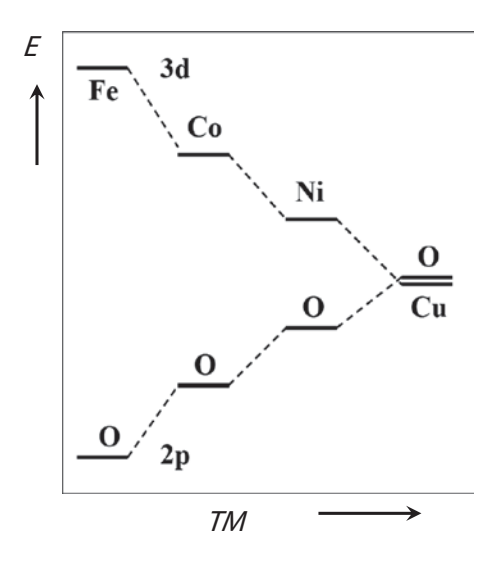


**Fig. 3.2** Basic structural and electronic structure of the cuprates: **a** Structure of  $\text{CuO}_2$  plane showing relevant  $\text{Cu}3d_{x^2-y^2}$  and  $\text{O2}p\sigma$  ( $\sigma$ =x or y) orbitals, both being strongly hybridized. **b** Electron filling of 3d orbitals of the  $\text{Cu}^{2+}(d^9)$  state. **c** Schematic energy scheme of the insulating undoped cuprate showing a strong electronic correlation (U) on a Cu atom and a charge-transfer (CT) energy gap between O2p and Cu3d upper Hubbard band

**Fig. 3.3** Schematic energy diagram of the energy level of transition-metal(TM)3*d* orbitals and that of O2*p* orbitals for various TM oxides in the order of the atomic number of TM element



#### 3.3.2 Necessary Ingredients for High T<sub>c</sub>

The unique features of the cuprates and widely anticipated necessary conditions for high  $T_c$  are thus summarized as

- 1. layer structure,
- 2. strong electronic correlations,
- 3. a single band,
- 4. S=1/2 spin state,
- 5. accidental degeneracy between Cu3d and O2p energies.

No other materials so far known have all these features simultaneously. The perovskite copper oxide, LaCuO<sub>3</sub> and the linear chain cuprate,  $Sr_2CuO_3$  shown in Fig. 3.4, satisfy (2)–(5), but the crystal structure is three-dimensional for the former and one-dimensional for the latter. In reality, LaCuO<sub>3</sub> is a non-superconducting metal.  $Sr_2CuO_3$  is a Mott/CT insulator and difficult to dope carriers, but the doped CuO chains in  $YBa_2Cu_3O_{7-y}$  (YBCO) do not show superconductivity by themselves. A counter-example is  $Sr_2VO_4$  which crystallizes in the same layered  $K_2NiF_4$  structure. In this compound the  $V^{4+}$  ion has only one electron in the 3d orbitals ( $3d^1$ ), so that the spin state is S=1/2. It is a Mott insulator due to strong electronic correlations. In this regard, it is an "electron" version of  $La_2CuO_4$  ( $3d^9$ ). Therefore, the conditions from (1), (2), and (4) are fulfilled in this compound. However, the lowest 3d levels,  $d_{xz}$  and  $d_{yz}$ , are degenerate in energy in a tetragonal lattice which makes the vanadate a multiband system. In addition, since V is near the other end of the 3d transition metal series, the V3d energy levels are significantly lower than the O2p levels. Probably because of these two differences, the vanadate remains insulating even when it is doped [15].

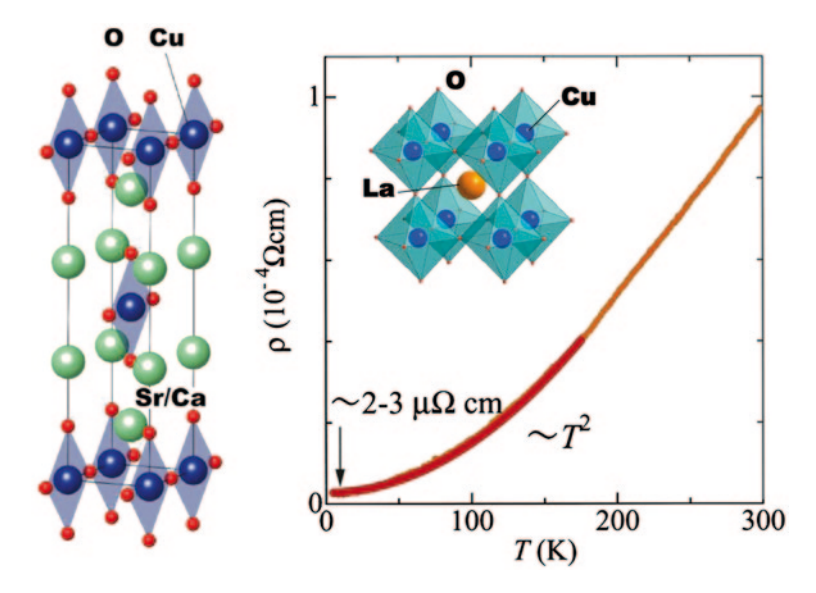


**Fig. 3.4** Crystal structure of the one-dimensional cuprate  $Sr_2CuO_3$  (a) and three-dimensional (perovskite)  $LaCuO_3$  (b).  $Sr_2CuO_3$  is a Mott (CT) insulator, whereas  $LaCuO_3$  is a good metal with low resistivity as shown in (c) measured for a polycrystalline sample

Another interesting case is  $\text{La}_{2-x} \text{Sr}_x \text{NiO}_4$  near x=1. This system has the same layer structure as that of LSCO. At x=1 the formal ionic state of Ni is Ni<sup>3+</sup> with  $3d^7$  filling. Ni<sup>3+</sup> state has two spin states, S=3/2 high-spin state and S=1/2 low-spin state. From the measurement of magnetic susceptibility the low-spin S=1/2 with localized spin only on the  $3d_{x^2-y^2}$  orbital is more likely in  $\text{LaSrNiO}_4$ . Moreover, the energy difference between Ni3d and O2p levels is very small in the Ni<sup>3+</sup> state in contrast to the Ni<sup>2+</sup> state where the 3d levels are significantly lower than the O2p levels. Then, it seems that  $\text{LaSrNiO}_4$  has all the features in common with the cuprates. Nevertheless, it does not show any signature of superconductivity, though metallic [16]. The reason might be that the condition (3), a single band, is not fully satisfied. The  $d^7$  configuration of Ni<sup>3+</sup> necessarily requires the energy band derived from the  $3d_{z^2}$  orbital involved in the electronic states near  $E_F$ .

Physical consequences of these features are two-fold:

The large overlap integral  $t_{pd}$  and the closeness of 3d and 2p levels, *i.e.*, small CT gap, give rise to strong covalent nature of the Cu-O bond as well as to the unusually large spin superexchange interaction  $J \sim t_{pd}^{-4}/E_{\rm CT}^{-3} \sim 0.15$  eV. The strong covalent bond makes the phonon frequency corresponding to the modulations of the Cu-O bond length (or bond angle) fairly high ( $\hbar\Omega_0\sim 0.07$  eV). The large energy scales of the charge ( $t_{pd}$ ), spin (J), and phonon ( $\Omega_0$ ) related excitations are probably sources of strong pairing interactions and hence high  $T_c$ .

The layer structure leads to their highly two-dimensional (2D) character of the electronic state, and S=1/2, the minimal spin quantum number, makes the spin fluctuation maximal. Because of these two, the otherwise very stable AF order (due to large

J) becomes fragile against doping and raising temperature. Finally, the strong correlations favor unconventional pairing with nodes in the superconducting (SC) gap.

## 3.4 Temperature-Doping Phase Diagram

A generic phase diagram of the hole doped cuprates is very complex. Multiple orders recently discovered by advanced spectroscopies are found to be superposed on the 'standard' phase diagram in which antiferromagnetic (AF), superconducting (SC), overdoped 'Fermi liquid' (FL), and pseudogap (PG) phases evolving with increasing the density of doped holes (*p*) and temperature (*T*).

It turns out that various ordering phenomena (broken symmetries) take place in the PG region, or more rigorously, in the PG region are observed various types of fluctuating orders including the SC fluctuations. At high temperatures, there is a "strange" metal regime in which the in-plane (current flowing along the  $\text{CuO}_2$  planes) resistivity continues to increase linearly with T without a tendency for saturation.

## 3.4.1 Unconventional Superconductivity

As regards the SC phase, there are many differences from conventional SCs:

- 1.  $T_{\rm c}$  is unprecedentedly high.
- 2. The SC gap (order parameter),  $\Delta(k)$ , has an unconventional d-wave symmetry [17], strongly momentum (k) dependent,  $2\Delta(k) = \Delta_0 \left[\cos(k_x a) \cos(k_y a)\right]$ , a being the in-plane lattice constant. It changes sign on the Fermi surface (FS) and hence vanishing at some k's (gap nodes). The gap nodes are along the Brillouin-zone diagonal, and the gap magnitude is maximum (called as "antinodes") at the zone edges,  $(\pm \pi, 0)$  and  $(0, \pm \pi)$  as schematically depicted in Fig. 3.5.
- 3. The SC transition temperature  $T_{\rm c}$  as a function of hole doping p,  $T_{\rm c}(p)$ , shows non-monotonic variation with p, consisting of a dome, starting to rise from  $p_{\rm min}$ , reaching a maximum at so-called "optimal" doping  $p^{\rm opt}$ , and then dropping to zero at  $p_{\rm max}$ . On the other hand, the amplitude of  $\Delta(k)$  is only weakly dependent on p (see Fig. 3.6a), so there appears no direct link between  $T_{\rm c}$  and  $\Delta_{0-}$  for conventional s-wave SC  $\Delta \sim 2k_{\rm B}T_{\rm c}$ .
- 4. The superfluid density or SC phase stiffness  $\rho_s$  ( $\sim n_s/m^*$ ,  $n_s$  and  $m^*$  being Cooper pair density and carrier effective mass, respectively) is by orders of magnitude smaller than that in conventional superconductors.  $T_c$  increases linearly with  $\rho_s$  in the underdoped region [18] (see Fig. 3.6b).
- 5. SC shows highly unusual response to disorder or impurities [19].

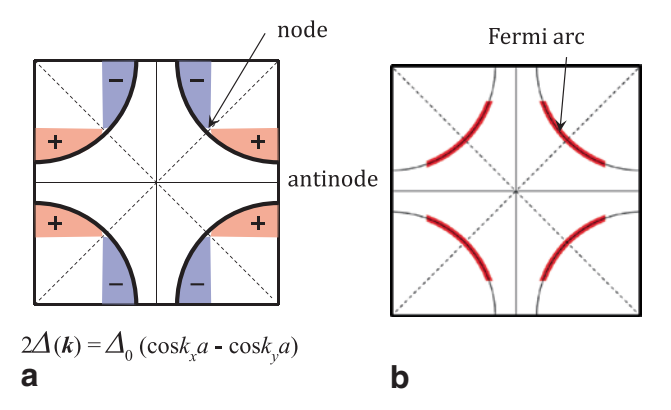


**Fig. 3.5 a** Fermi surface (schematic) in the first Brillouin zone for optimally doped cuprate. Superposed on the Fermi surface is shown the d-wave superconducting gap, both magnitude and sign. The gap nodes are along the zone-diagonal and the gap magnitude is maximal at the zone edges (antinodes). **b** The gapless region around the node defines the Fermi arc in the pseudogap regime above  $T_c$ . The arc appears to be reconstructed into electron pockets once charge order sets in, as revealed by quantum oscillation studies

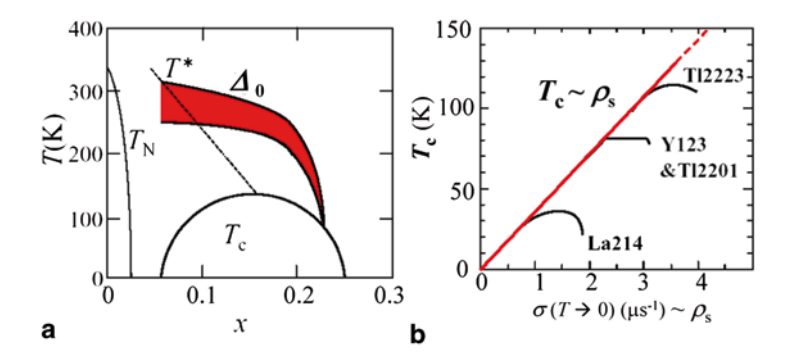


Fig. 3.6 Schematic doping dependence of **a** the superconducting gap magnitude  $\Delta_0$ . **b**  $T_c$  plotted against the superfluid density  $\rho_s$  which is proportional to the muon relaxation rate  $\sigma$  extrapolated to T=0 K and related to the magnetic penetration depth [18]. The large error bars in  $\Delta_0$  in the underdoped region id due to coexisting pseudogap in the gap excitation spectrum

## 3.4.2 Phase Diagram and Pseudogap Regime

The currently established temperature (T)—doping (p) phase diagram, sketched in Fig. 3.7, is very complicated and contains various orders (broken symmetries). The observed orders and the characteristic electronic feature in the six doping regions in the order of increasing hole density p:

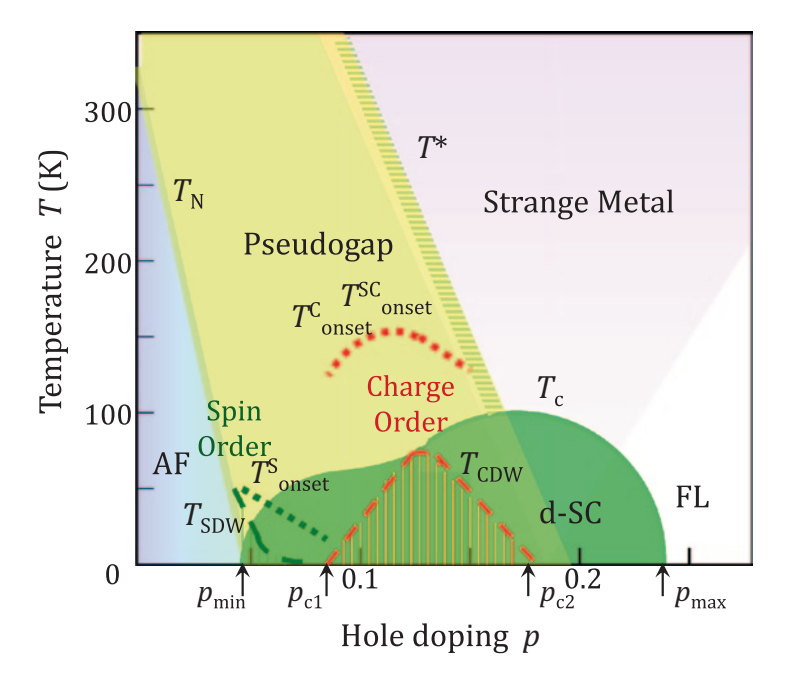


Fig. 3.7 Generic temperature (T) – doping (p) phase diagram of the cuprates. Various orders and their fluctuations are observed in the underdoped regime. "Onset" marks where precursor order or fluctuations become apparent

#### 3.4.2.1 Long-Range AF Order $(0 \le p < 0.02)$

Local S=1/2 spin magnetic moments on Cu atoms align antiferromagnetically in the CuO<sub>2</sub> plane (the Néel order with ordering wavevector  $\mathbf{Q} = (\pi, \pi)$  in the unit of 1/a) by the huge superexchange interaction J between neighboring Cu spins. The Néel order sets on at  $T=T_{\rm N}$  (~300 K for the parent compound) in a second order phase transition. This phase is essentially Mott insulating and the insulating gap is a Cu3d–O2p charge-transfer (CT) gap, not arising from the AF order. This phase does not allow for the presence of d-wave Cooper pairs or coexistence with the SC phase [20]

#### 3.4.2.2 Incommensurate Spin Order (0.02

This region is called as "heavily underdoped region". The long-range AF order is fragile against doping and temperature due to thermal and quantum mechanical fluctuations. After the commensurate Néel order collapses upon doping holes, spin order (SO) persists as an incommensurate spin order (or spin-density-wave (SDW) order). In contrast to the Néel order in the region (1), the incommensurate spin order freezes gradually with lowering temperature [21]. The onset temperature of the

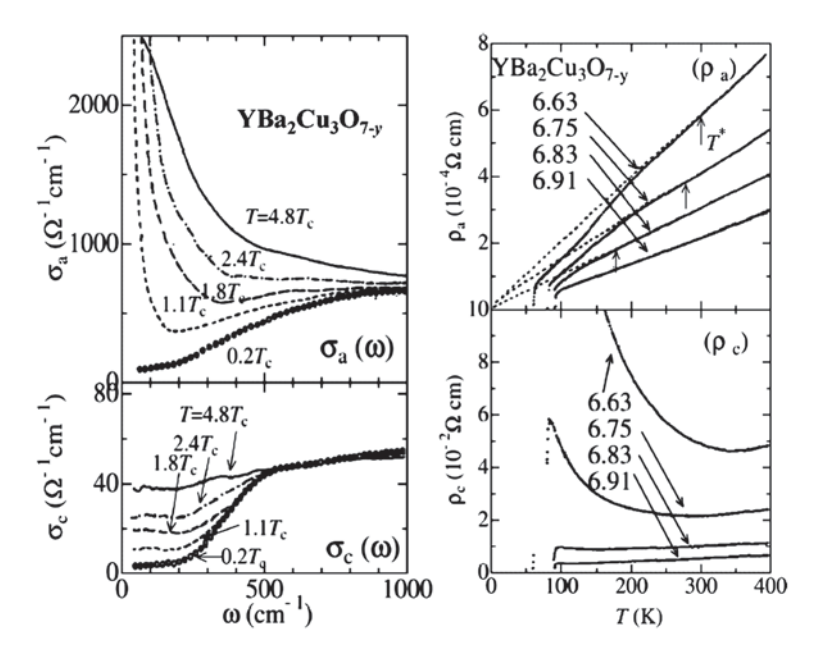


**Fig. 3.8** Doping evolution of the temperature dependent in-plane and c-axis resistivity measured for YBa<sub>2</sub>Cu<sub>3</sub>O<sub>7-y</sub>. Temperature evolution of optical conductivity spectra for polarization parallel and perpendicular to the planes is shown for a typical underdoped cuprate

incommensurate spin correlation is low  $T^{\rm S}_{\rm onset}$ < 50 K. The spin correlation length is short but finite at all temperatures showing slow dynamics with a wide distribution of the relaxation rates, characterized as a spin-glass.

In this phase some materials (e.g., LSCO) are insulating while others (e.g., YBCO) are superconducting. Probably, disorder effect would manifest in the former, and in either cases SC shows up or an insulator-superconductor transition takes place when the resistance of the  ${\rm CuO}_2$  sheet or  ${\rm CuO}_2$  bilayer sheet is near  $h/4e^2$ , the 2D universal resistance. Signatures of SC fluctuations such as the large Nernst effect are observed even for non-SC compounds. Notably, a large gap, a pseudogap (PG, see 3.4.2.4), opens in the *antinodal* region where the SC gap is maximal. Around the SC gap nodes (in the *nodal* region) gapless quasiparticles exist in a region of the Fermi surface centered at node—Fermi arcs—observed by the angle-resolved-photoemission-spectroscopy (ARPES) experiments. Obviously, the antinodal gap or pseudogap has nothing to do with the SDW order.

#### 3.4.2.3 Incommensurate Charge Order (0.08

This region, so-called "moderately underdoped region", has been identified recently and is characterized by charge order (CO). CO was first discovered in the La-based cuprates with the  $K_2NiF_4$  structure [22],  $La_{2-x-y}Nd_ySr_xCuO_4$  and  $La_{2-x}Ba_xCuO_4$  (LBCO) at  $x \sim 1/8$  as stripe order. As displayed in Fig. 3.8, various forms of charge

order or charge-density-wave (CDW) have been found depending on the degree of disorder and underlying lattice; checkerboard in YBCO (Hg1201) and Bi2201 [23–26], stripe (LBCO), disordered smectic electron liquid crystal (Bi2212) [27], and bond order with *d*-wave form factor [28]. The spin order disappears in YBCO, but coexists in La<sub>2-x</sub>Ba<sub>x</sub>CuO<sub>4</sub> (LBCO). The stripe charge order is a fairly longrange order, and is accompanied by the spin order in the La-based cuprates. To the contrary, in YBCO the spin order disappears in the doping range between  $p_{c1} \sim 0.08$  and  $p_{c2} \sim 0.16$  where the charge order is observed [29, 30]. Charge excitations in this regime continue to be gapless, while spin excitations are gapped. The x-ray scattering experiments find an onset of static and short-range CO (or CDW correlations) at  $T^{\rm C}_{\rm onset} = 100-160$  K, possibly due to the pinning of fluctuating CO by defects.

The CO is not destructive for d-wave superconductivity (d-SC), but is apparently "intertwined"—CO weakens below  $T_{\rm c}$ , but in turn its persistence weakens the interlayer SC phase coherence. Application of a high magnetic field ( $\sim$ 20 Tesla) weakens the d-SC order, and a field-induced transition to a long-range CO state is observed at  $T_{\rm CO}$  (<60 K) by NMR [31]. The doping dependence of  $T_{\rm CO}$  forms a subdome within the  $T_{\rm c}$ -dome terminating at  $p_{\rm c1}\sim$ 0.08 and  $p_{\rm c2}\sim$ 0.16–0.18 [32]. Notably, quantum oscillations associated with an *electron* Fermi surface pocket are observed when the magnetic field is intense enough to suppress the zero-resistance state [33]. A problem is how the *hole* Fermi arc at low fields is converted to the *electron* pockets at high fields. A scenario of Fermi surface reconstruction due to CO is proposed, as the doping region of CO coincides with that where the quantum oscillations are observed [34, 35].

#### 3.4.2.4 Pseudogap Regime ( $T < T^*$ and $\sim 0.02 )$

It is the most mysterious regime in the phase diagram, and the understanding its origin and nature is considered to be a key to resolve the high- $T_{\rm c}$  mechanism: The pseudogap (PG) regime covers a wide T-p area of the phase diagram in which various spectroscopies indicate a suppression of low energy electronic excitations below the pseudogap temperature  $T^*$ . There remains puzzles in this regime, but it is a playground for various types of "fluctuating" (short-range) order, SDW, CDW as well as d-SC fluctuations. As described above, the incommensurate spin and charge fluctuations/short-range order develop within the PG regime ( $T^{\rm S}_{\rm onset}$  and  $T^{\rm C}_{\rm onset}$  are significantly lower than the PG temperature  $T^*$ ). In other words, the PG state is unstable against these orders at low temperatures.

Other than the spectroscopic gap opening, various properties show a rather dramatic change at  $T^*$ . For example, as is shown in Fig. 3.9, the c-axis (directed perpendicular to the  $CuO_2$  planes) resistivity shows an upturn below  $T^*$  like an insulator, whereas the in-plane resistivity drops at  $T^*$  associated with a drop in the carrier scattering rate [36]. The ARPES revealed an anisotropic nature of PG in momentum space [37]. The magnitude of PG is maximal in the *antinodal* region (in the vicinity of the Brillouin-zone edges,  $k = (\pi, 0)$  and  $(0, \pi)$ ). On the other hand, gapless excitations are observed on a "Fermi arc" centered around the nodes (see

Fig. 3.9 T-p phase diagram (schematic) showing the regions of superconducting fluctuations and superconducting state in the overdoped region in the right-hand side of the T\*(p) line

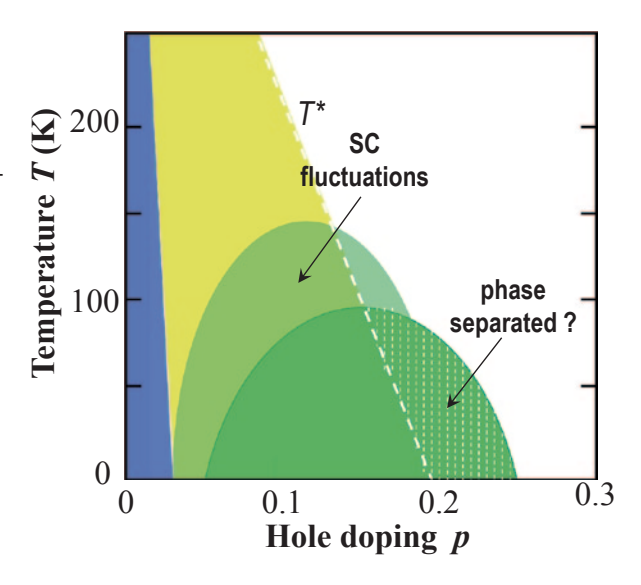


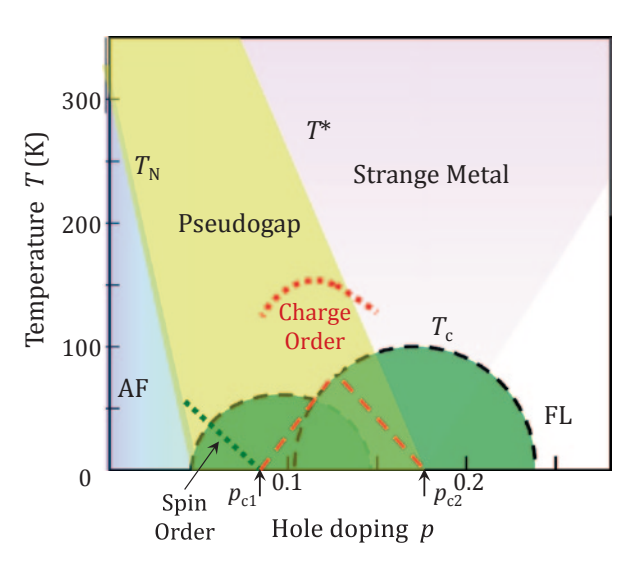
Fig. 3.5b). In this regard, PG has a d-wave-like anisotropy in the momentum space as the SC gap does. This anisotropy is reflected in the resistivity anisotropy; the inplane resistivity dominated by the nodal region of the FS, and the c-axis resistivity by the antinodal region.

Quasiparticles (QPs) in the antinodal region are completely incoherent—the spectral function does not show a discernible peak with a depletion of spectral weight at low energies. Nevertheless, the antinodal region is not only most important for pairing, but also is the place where the charge order (and possibly other orders) is supposed to get born [38].

PG and *d*-SC coexist in quite a non-trivial manner. Given that there is no evidence that the SC gap energy scale is diminished by the presence of PG, it is likely that PG is also home to the SC pairing correlation. In fact, for a range of temperature above  $T_{\rm c}$  up to  $T^{\rm SC}_{\rm onset}$  (< $T^*$ ) a fairly large diamagnetism and sizeable fluctuation conductivity are observed in the PG regime [39] (see Fig. 3.10). Another evidence for local phase coherence is that the interlayer Josephson plasma resonance within a bilayer in YBCO [40] persists up to  $T^{\rm SC}_{\rm onset}$  (see the discussion in 3.5.3 in this chapter).  $T^{\rm SC}_{\rm onset}$  is comparable with the onset temperature of the charge fluctuations,  $T^{\rm C}_{\rm onset}$ , and both show similar doping dependence. Hence, PG is not necessarily a competing order of *d*-SC, but appears to be home to various orders including SC. Note that the maximum  $T_{\rm c}$  value of 164 K achieved at high pressure is also comparable to these two temperature scales.

It continues to be a matter of debate whether the  $T^*$  line indicates a phase transition or a crossover. There are experimental observations that are suggestive of broken symmetries associated with the "PG phase". Spin-flip neutron scattering experiments on underdoped YBCO, HgBa<sub>2</sub>CuO<sub>4+8</sub>, Hg1201), and Bi2212 indicate intra-unit cell time-reversal symmetry breaking (q=0 antiferromagnetic order)

Fig. 3.10 Putative quantum critical points (QCPs),  $p_{\rm cl}$  and  $p_{\rm c2}$  inside the superconducting dome. In the case of YBa<sub>2</sub>Cu<sub>3</sub>O<sub>7-y</sub>, incommensurate spin order terminates and charge order appears at  $p_{\rm cl}$ . At  $p_{\rm c2}$  both charge order and the pseudogap  $T^*(p)$  line terminate. Two superconducting  $T_{\rm c}$  domes supposedly develop from these two QCPs



[41], supposedly arising from counter-circulating orbital current inside the unit cell [42]. Scanning Tunneling Spectroscopy (STS) also suggests a rotational symmetry breaking inside the unit cell (q=0 'nematic' order) [43]. This nematicity is ascribed to electronic inequivalence of the two oxygen atoms ( $O_x$  and  $O_y$ ) in the unit cell. Not only has the experimental indication of symmetry breaking, the ultrasound velocity also appeared to show a signature of a thermodynamic transition at  $T^*$  [44]. However, these experimental results and their interpretations have been a matter of debate. Furthermore, it appears difficult for the q=0 order to create such a large gap which might be rather linked to some local/fluctuating pairs. Thus, the origin of the PG has been identified yet.

## 3.4.2.5 Single *d*-wave Superconducting Phase ( $\sim 0.18 )$

In this "slightly overdoped region" CO and other orders are not seen, but SC survives maintaining fairly high  $T_{\rm c}$ . Existence of this region is based on the assumption that the PG- $T^*$  line terminates at ~0.18 inside the SC dome (see Fig. 3.9). The  $T^2$  component in the in-plane resistivity, characteristic of the heavily overdoped (non-SC) region, gradually dominates, and the SC gap magnitude gets smaller with increasing p in this region. Inelastic neutron scattering (INS) experiments indicate a dramatic suppression of spectral weight near the AF wavevector  $\mathbf{Q} = (\pi, \pi)$  [45]. In the context of the spin-fluctuation mediated pairing model, this implies a fading out of pairing glue leading to a decrease in  $T_{\rm c}$ . However, quite curiously the superfluid density also starts to decrease [46]. A hypothetical argument on the origin of the decreased superfluid density is that it arises from a mixing of non-SC phase spilled over from the FL phase far beyond  $p \sim 0.18$ . If this phase were not a single phase but spatially phase separated, then a single-phase uniform d-SC state might be unstable in the cuprates.

#### 3.4.2.6 'Fermi Liquid' Phase ( $\sim 0.25 < p$ )

In the "heavily overdoped region", a large FS, consistent with the result of band calculations, is observed by both ARPES and quantum oscillations measurements [47]. Most of the properties in this region are normal except for that the spin wave, characteristic of localized spins, is robustly present without changing its dispersion in the AF ordered phase [48].

## 3.4.3 Quantum Critical Points and "Strange" Metal

#### 3.4.3.1 Putative Quantum Critical Points Inside the $T_c$ Dome

As the correlation lengths of all these fluctuating orders in the PG regime get longer, it is reasonable to expect presence of one or more quantum critical points (QCPs) at which continuous phase transitions take place at zero-temperature. The two termination points in the  $T_c(p)$  "dome",  $p = p_{\min} \sim 0.05$  and  $p_{\max} \sim 0.25$  are possible QCPs. A two-dimensional superconductor to insulator transition appears to take place at  $p_{\min}$ , while it is debatable if  $p_{\max}$  is a real critical point as mentioned in 3.4.2.5. Both are too sensitive to disorder to explore the nature of transitions and associated changes of symmetry.

It is known that magnetic order, incommensurate SO/SDW order or spin-glass order, in the heavily underdoped region of YBCO disappears in the moderately underdoped region where magnetic excitations have a spin gap and no magnetic order is seen in most of the cuprates. This is suggestive of existence of some form of "magnetic QCP" at  $p_{\rm cl} \sim 0.08$  between  $p_{\rm min}$  and  $p^{\rm opt}$ ,  $p_{\rm min} < p_{\rm cl} < p^{\rm opt}$ , inside the superconducting dome. Further, the PG- $T^*(p)$  line seems to penetrate the  $T_c$  (p) dome and to extrapolate to another critical point  $p_{\rm c2} \sim 0.18$  with  $p^{\rm opt} < p_{\rm c2} < p_{\rm max}$ . Remember that  $p_{\rm cl}$  and  $p_{\rm c2}$  are close to the termination points of the long-range CO under strong magnetic field and/or zero-field CO correlations observable in the x-ray experiments. Then, the second QCP would be a "charge QCP" associated with the broken translational symmetry of the CO. It is also possible that, if PG is a phase associated with some broken symmetry, the nature of the second QCP would be tied up with the character of PG. However, experimental effort to unambiguously identify the presence of the two QCPs is limited by the onset of SC at fairly high temperature.

Supportive evidence for QCPs at  $p_{\rm c1}$  and  $p_{\rm c2}$  has recently been presented by quantum oscillation experiments on YBCO which show that observation of the quantum oscillations is confined to the range  $p_{\rm c1} , and that the effective mass, <math>m^*$ , deduced from the T dependence of the oscillations indicates that  $m^*$  tend to diverge as p approaches these limiting values [34, 35]. In fact, in the presence of a sufficiently high magnetic field, the superconducting dome appear to split into two domes—one centered at  $p \sim p_{\rm c1}$  and the second at  $p \sim p_{\rm c2}$  (the two-dome feature is reminiscent of the phase diagram for the stripe ordered LBCO in which  $T_{\rm c}$  is radically suppressed at around p=1/8 [49]). It is, however, possible that the QCPs detected in quantum

oscillations under high magnetic fields do not exist at low magnetic fields, that is, evolution of the phase diagram with magnetic field would be discontinuous, since it is difficult to imagine a continuous evolution from the Fermi arc at zero field to the Fermi surface pockets at high fields.

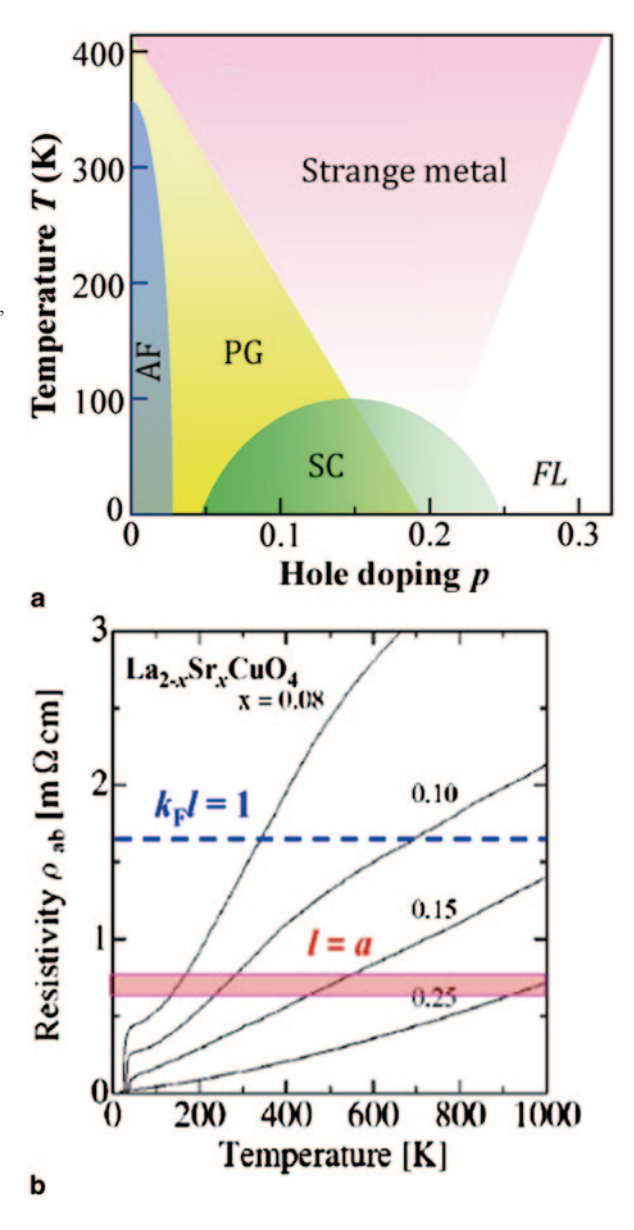
#### 3.4.3.2 "Strange" Metal Regime $(T>T^*)$

The cuprate near optimal doping are "bad metals" in which it is difficult to discern well-defined quasiparticles at high temperatures above  $T^*$ . Although the normal state resistivity shows a "metallic" T dependence (i.e., it increases with increasing temperature, typically linear in T), its magnitude is too large to be interpreted in terms of propagating quasiparticles—the Boltzmann transport theory. The large magnitude implies a quasi-particle mean-free path (1) comparable to or shorter than the de-Broglie wavelength,  $k_{\rm F} l < 1$  (de Broglie wavelength  $\lambda_{\rm F} = 1/k_{\rm F}$  where  $k_{\rm F}$  is the Fermi momentum) and the in-plane lattice constant a, l < a (this seems to violate the Heisenberg uncertainty principle  $\Delta x \Delta p > \hbar$ ). As is shown in Fig. 3.11a for LSCO, the T-linear resistivity persists from above  $T_c$  up to as high a temperature as measured without showing saturation of the resistivity [50] typically observed in the normal metallic state of A15 superconductors. In this temperature region, the coherent Drude spectral weight almost vanishes in the optical conductivity and the lowenergy spectral weight even decreases with elevating temperature which is found to be transferred to high-energy region comparable with the CT gap energy scale of the undoped cuprates [51]. The failure of the ordinary physics of good metals to account for this behavior has provided strong motivation for theoretical investigations. The origin of this behavior is, however, still a subject of much debate, but is of obvious importance since PG and/or FL appear to get born upon cooling from this regime.

In the QCP scenario, the strange metal regime, emphasized in Fig. 3.11b as well as the high- $T_{\rm c}$  superconductivity itself is controlled by the two or more QCPs discussed in 3.4.3.1. The strange metal would be a consequence of quantum critical fluctuations associated with the QCPs which might also serve as pairing glue for SC. Contrary to this "bottom up" scenario, a "top down" scenario has long been proposed [52] in which the strange metal regime is considered to be home to PG and overdoped FL and from PG various orders, including SC, emerges with lowering temperature.

A conclusion that can be inferred from the cuprate phase diagram is that the basic interactions between electrons are strong and repulsive. The repulsive nature of the interactions is inferred from the existence of AF phases in proximity to and even overlapping with the SC phase, and from the persistence of local spin magnetic moment over almost entire range of the phase diagram. The unconventional *d*-wave SC pairing arises also from dominant repulsive interactions. This is essentially different from the HTSCs discussed in the previous chapter, and is similar to the Fe-based superconductors as will be seen in the next chapter.

Fig. 3.11 a Schematic phase diagram emphasizing the strange metal regime at high temperatures. **b** Typical temperature dependent in-plane resistivity measured for La,\_ Sr, CuO, showing no resistivity saturation [51] in the strange metal regime. The resistivity continues to increase to high temperatures, even though its magnitude well exceeds the critical values,  $k_E l = 1$  and l = a, for conventional metallic charge transport



(\*) Footnote: Electron-doped cuprates Representative electron-doped cuprates are T'-Nd<sub>2-x</sub>Ce<sub>x</sub>CuO<sub>4</sub> ( $T_c^{max}$ =25 K) [53] and so-called infinite-layer Sr<sub>1-x</sub>La<sub>x</sub>-CuO<sub>2</sub> ( $T_c^{max}$ =40 K), both having no apical-O atoms [54]. The electron-doped cuprates appear to belong to a class different from the hole-doped cuprates with distinctly higher  $T_c$  values although the superconductivity is conceived to be unconventional in both cases. Because of its difficulty in controlling the chemical

compositions, in particular, the oxygen content, many things remain unclear yet. Even the phase diagram is currently under debate. In the old well-known phase diagram, the AF phase is robust, while the SC phase soon disappears with increasing doping. Recent finding is that the SC phase extends (the AF phase shrinks) toward the undoped point for oxygen controlled bulk crystals, and even the undoped (x=0) compound is metallic and superconducting below  $\sim$ 20 K for thin films [55]. We have at present no hint on whether the lower  $T_c$  is a property inherent to the electron-doped cuprates due to different mechanism of superconductivity or whether  $T_c$  could go up to the level of the hole-doped cuprates if, e.g., disorder in the charge reservoir block next to the CuO<sub>2</sub> plane is removed and/or if a new electron-doped cuprate were discovered with charge reservoir block distant from the CuO<sub>2</sub> plane.

## 3.5 Material Dependence of $T_c$ and Factors that Influence $T_c$

The maximum  $T_c$  so far attained at ambient pressure is 135 K for Hg-based trilayer cuprate HgBa<sub>2</sub>Ca<sub>2</sub>Cu<sub>3</sub>O<sub>8+δ</sub>, and  $T_c$  of the same compound goes up as high as 164 K under high pressure. The cuprate family consists of a large variety of materials with CuO<sub>2</sub> plane as an only common structural ingredient, but  $T_c$  is strongly material dependent, ranging from ~25 to 135 K at ambient pressure. After 28 years experimental and theoretical efforts, several important parameters that control  $T_c$  are identified for the hole-doped cuprates. these are, (a) doping level p, (b) number of CuO<sub>2</sub> planes (n) in a unit cell, (c) presence of competing orders, such as stripe and/or charge order, (d) disorder inside and outside the CuO<sub>2</sub> plane, (e) positions of apical-oxygen atoms, (f) ionic radius of cations, such as rare-earth (Ln), and (g) oxygen isotope substitution ( $^{16}O \rightarrow ^{18}O$ ).

## 3.5.1 Doping Effect

Quite distinct from conventional superconductors, doping, chemical substitution of constituent atoms or adding/removing oxygen atoms, is the primary parameter controlling  $T_{\rm c}$ . How the doping controls  $T_{\rm c}$  is now getting clear. Starting from optimal doping at which  $T_{\rm c}$  is maximum, underdoping (decreasing p) reduces the superfluid density ( $\rho_{\rm s}$ )—a measure of the phase stiffness of superconducting order parameter. Underdoping simultaneously weakens the interlayer Josephson coupling strength, making the SC state more two-dimensional, as indicated by the red-shift of the Josephson plasma frequency shown in Fig. 3.12a. Both small  $\rho_{\rm s}$  and weakened interlayer coupling result in strong superconducting phase fluctuations, and thereby  $T_{\rm c}$  is suppressed.

Possibly, these are connected to various ordering phenomena inherent to the underdoped regime. The competing order tends to reduce  $\rho_s$  as well as to decouple

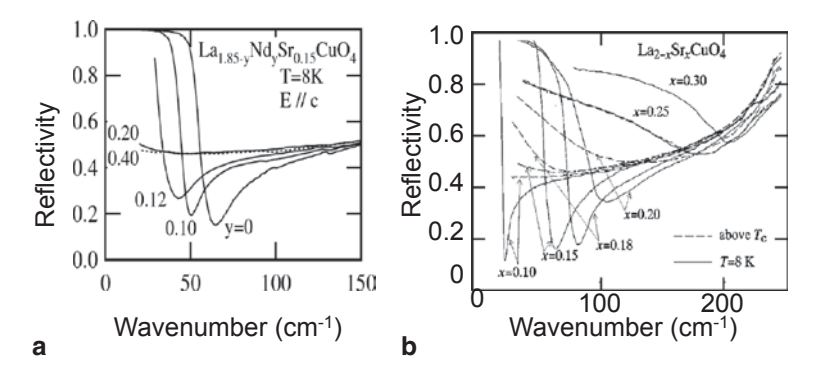


Fig. 3.12 Plasma edge in the *c*-axis reflectivity spectrum which emerges upon entering the superconducting state below  $T_c$  associated with Josephson coupling between  $CuO_2$  planes. The plasma edge—Josephson plasma—frequency shows a *red* shift with **a** decreasing Sr content in  $La_{2-x}Sr_xCuO_4$  [68] and **b** as the stripe order gets stronger with increase of Nd content in  $La_{1.85-y}Nd_sSr_{0.15}CuO_4$  [56], indicating an interlayer phase decoupling

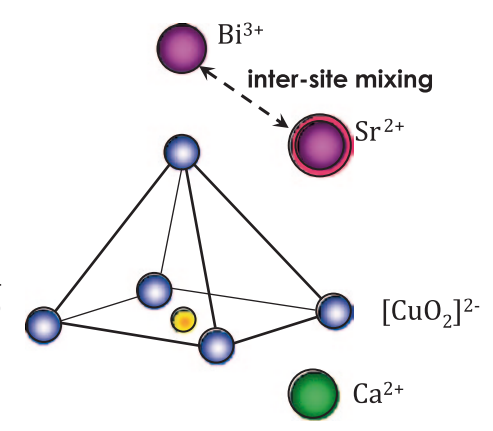
the planes making the superconducting state more two-dimensional and suppressing  $T_c$ , as is typically the case with the stripe order in  $\text{La}_{2-x-y}\text{Nd}_y\text{Sr}_x\text{CuO}_4$  [56] (see Fig. 3.12b) and in  $\text{La}_{2-x}\text{Ba}_x\text{CuO}_4$  [57]. On the other hand, there is evidence that overdoping (increasing p) weakens the pairing interaction supposedly mediated by antiferromagnetic fluctuations, although  $\rho_s$  also decreases with overdoping. It progressively turns out that a change of  $\rho_s$  and/or interlayer coupling is more or less related to a balance between superconducting and competing orders. This is radically different from that in conventional superconductors and seems to be difficult to understand in the framework of the Migdal–Eliashberg theory in which most relevant parameter controlling  $T_c$  is the superconducting gap magnitude or the electron-boson coupling strength  $\lambda$ .

The <sup>18</sup>O isotope substitution reduces  $T_{\rm c}$  in the underdoped regime. This appears to be the 'normal' isotope effect in conventional superconductors, since the <sup>18</sup>O substitution decreases the frequencies of the oxygen phonon modes. However, it turns out that the major isotope effect in the cuprates is to decrease  $\rho_{\rm s}$  and the reduction of  $T_{\rm c}$  appears to be a consequence of the decrease of  $\rho_{\rm s}$  in the underdoped regime [58]. The isotope substitution also decreases  $\rho_{\rm s}$  near optimal doping, but  $T_{\rm c}$  does not change at all (null isotope effect), as  $T_{\rm c}$  is almost independent of  $\rho_{\rm s}$  in this region (see Fig. 3.6b).

## 3.5.2 Disorder Effect

An important problem concerning  $T_c$  is what makes maximum value of  $T_c^{\text{opt}}$  so different (25–135 K) among different cuprate materials with optimal doping, despite that the normal state is a 'strange metal' showing universal linear in temperature (T) resistivity with almost the same carrier scattering rate. To the best of the current

Fig. 3.13 An example of disorder in the apical-oxygen block showing a Bi atom occupying the Sr site, Bi-Sr site mixing, in the Bi-based high- $T_c$  cuprates. This type of disorder, arising from substitution of cations with different ionic charge and ionic radius for the A-site cations neighboring the apical-O atoms, is most influential on  $T_c$  in any other cuprate



understanding, major causes of the diverse  $T_{\rm c}^{\rm opt}$  are the number of  ${\rm CuO_2}$  planes n (multilayer effect), disorder in the charge reservoir blocks, and the apical oxygen position/distance.

Disorder in the charge reservoir block, specifically that introduced by cation substitution with different ionic charge and radius in the layer (we call this as apical-O block as it contains apical oxygen atoms) next to the CuO<sub>2</sub> plane is found most influential—the disorder associated with substitution of Zn or Ni for the in-plane Cu is most detrimental for d-SC or  $T_c$ , if it is intentionally introduced. Such disorder is the most plausible reason for the distinctly lower  $T_{\rm c}^{\rm opt}$  values in many of the single-layer cuprates, such as  $La_{2-x}Sr_xCuO_4$  (LSCO,  $T_c^{opt}=40$  K),  ${\rm Bi}_{2+x}{\rm Sr}_{2-x}{\rm CuO}_{6+\delta}$  (Bi2201,  $T_{\rm c}^{\rm opt}=35$  K),  ${\rm Ca}_{2-x}{\rm Na}_x{\rm CuO}_2{\rm Cl}_2$  (CNCOC,  $T_{\rm c}^{\rm opt}=29$  K), and T\*-  ${\rm La}_{1-x}{\rm LnSr}_x{\rm CuO}_4$  ( $T_{\rm c}^{\rm opt}=25$  K) [59] as disordered layers exist on both sides, below and above a CuO, plane in the single-layer compounds [60]. These values should be compared with  $T_{\rm c}^{\rm opt}=98~{\rm K}$  for HgBa<sub>2</sub>CuO<sub>4+ $\delta$ </sub> (Hg1201) and  $T_{\rm c}^{\rm opt}\sim90~{\rm K}$  for Tl<sub>2</sub>Ba<sub>2</sub>CuO<sub>6+ $\delta$ </sub> (Tl2201) where disorder is in the charge reservoir layers well separated from the CuO, plane. Disorder effect is weaker (by a factor of two) in the bilayer cuprates, since the disordered apical-O block exists only in one side. It is further weakened in the trilayer systems because there is a plane (inner CuO, plane) isolated from the apical-O blocks. This is evidenced by the narrower distribution of  $T_c^{\text{opt}}$ ,  $T_c^{\text{opt}}$ =65–127 K across bilayer cuprates and  $T_c^{\text{opt}} = 115-135 \text{ K}$  across trilayer cuprates.

The crystals of Bi-based cuprates, which are most extensively studied by ARPES and STS owing their stable and clean surfaces, contain a large amount of disorder in the SrO blocks arising from Sr<sup>2+</sup>-Bi<sup>3+</sup> intersite mixing (shown in Fig. 3.13) which is difficult to remove completely. This disorder is a major source of the observed electronic inhomogeneity and substantially affects the *p-T* phase diagram [61].

The disorder in the charge reservoir block next to  $\text{CuO}_2$  plane results in a huge reduction in  $T_c^{\text{opt}}, \Delta T_c^{\text{opt}} \Delta T_c^{\text{opt}}$  appears as large as  $\sim 50$  K for single-layer cuprates estimated from the comparison between Bi2201 ( $T_c^{\text{opt}} \sim 35$  K) and isostructural Tl2201 ( $T_c^{\text{opt}} \sim 90$  K). For bilayer cuprates  $\Delta T_c^{\text{opt}} \sim 30$  K ( $\text{La}_{2-x} \text{Sr}_x \text{CaCuO}_6$  ( $T_c^{\text{opt}} \sim 60$  K) vs

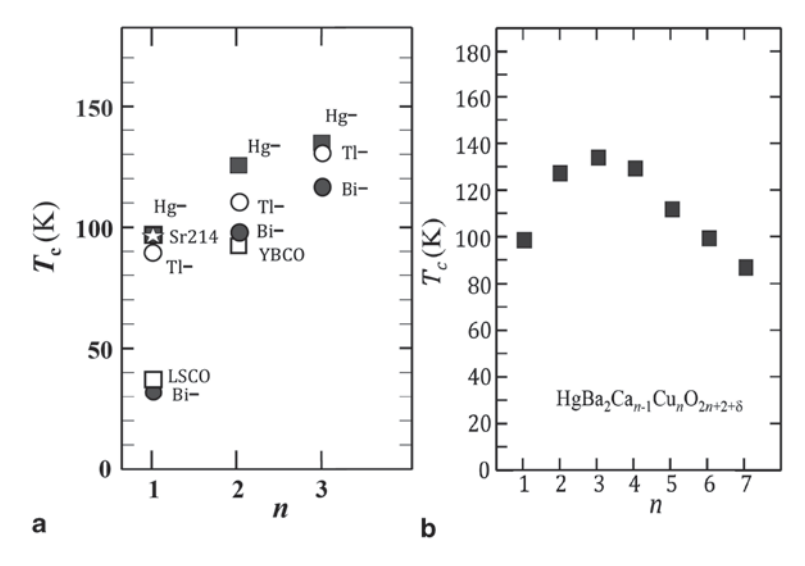


**Fig. 3.14** a Plot of the  $T_c^{\text{opt}}$  values for various single-, bi-, and tri-layer cuprates attained after reducing disorder. b  $T_c^{\text{opt}}$  vs number (n) of  $\text{CuO}_2$  planes in a unit cell for a multilayer homologous series Hg12(n-1)n [13, 14]

YBCO ( $T_{\rm c}^{\rm opt}=93~{\rm K}$ )). In this case, again, the suppression of  $T_{\rm c}$  appears to take place along with the reduction of  $\rho_{\rm s}$ . It remains open whether or not the  $T_{\rm c}$  reduction is explained by the Abrikosov–Gorkov pair-breaking mechanism due to 'normal' impurities in a d-wave superconductor [62].

As will be described in 3.6.1, reduction of disorder in the apical-O blocks actually leads to sizeable enhancement of  $T_c^{\rm opt}$  in some of the cuprate materials;  $T_c^{\rm opt}$  of the trilayer Tl1223, in which a major source of disorder is thought to be Tl-Ba intersite mixing, is enhanced to 133 K [63], close to the highest  $T_c$  record in Hg1223, and  $T_c^{\rm opt}$  of the bilayer Bi2212 is improved to 98 K [64]. In one of the single-layer cuprates,  ${\rm Sr_2CuO_{3+\delta}}$ , with the same "214" structure as that of LSCO,  $T_c^{\rm opt}$  reaches 98 K when dopant atoms get ordered [65], sharing the  $T_c$  record with Hg1201. These "optimized"  $T_c$  values are summarized in Fig. 3.14a for single-, bi-, and tri-layer cuprates.

## 3.5.3 Multilayer Effect

The number of  $\text{CuO}_2$  planes, n, in a unit cell is one of the old-known factors influencing  $T_c$  values as the history of high- $T_c$  indicates. Even after reducing disorder, the multilayer effect is surely seen in Fig. 3.14a,  $T_c$  values being significantly higher for bilayer and trilayer cuprates than for single-layer cuprates, As plotted in Fig. 3.14b for the multilayer homologous series [Hg12(n-1)n] [13, 14],  $T_c^{\text{opt}}$  rises with increasing n up to 3 but turns to decrease for  $n \ge 4$  [14]. A problem to be explained

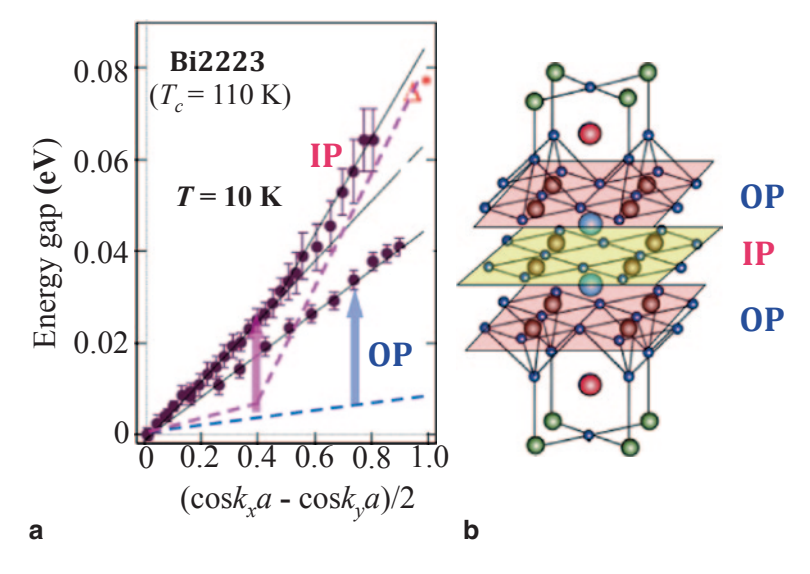


**Fig. 3.15** a Enhanced superconducting energy gaps in the trilayer  $Bi_2Sr_2Ca_2Cu_3O_{8+\delta}$  observed by ARPES [67]. The gap magnitudes in both inner (IP) and outer planes (OP) (shown in **b**) are plotted as a function of momentum starting from the nodes toward antinodes. They are enormously enhanced as compared to the values for the bilayer Bi2212 with nearly the same doping levels

is why  $T_{\rm c}$  decreases for n larger than 4. This certainly arises from the charge imbalance, difference in the hole density between outer  ${\rm CuO_2}$  planes (OP) and inner planes (IP) [66]. The hole density in IPs tends to be smaller as they have no apical-O atoms and are sandwiched on both sides by  ${\rm Ca^{2^+}}$  layers, making an electro-positive circumstance for holes to enter.

The ARPES measurement on the trilayer Bi2223 with  $T_c$ =110 K tells us what is going on in the multilayer system [67]. The ARPES confirms the result of the preceding NMR experiments in that two OPs are in fact overdoped, whereas IP is heavily underdoped. The hole density estimated from the Fermi surface (FS) area is  $p \sim 0.23$  in OP and  $p \sim 0.07$  in IP. When these values are mapped on the phase diagram of the bilayer Bi2212,  $T_c$ 's of OP and IP should be well below 50 K. To the contrary, the SC gap of OP follows the d-wave momentum dependence over the entire FS without showing PG feature near antinodes and the d-wave gap magnitude is  $\Delta_0$ =43 meV by a factor of 4 or more enhanced with respect to the estimated value for Bi2212 with p=0.23 (indicated in Fig. 3.15). The SC gap of IP shows a PG feature on approaching the antinodal region of FS, but the feature is considerably weakened as compared to that in Bi2212 with p ~0.07. The SC gap magnitude obtained by extrapolating to the antinode  $\Delta_0$ =60 meV is again much or even more enhanced. Certainly, a multilayer effect is at work in Bi2223 which simultaneously enhances the pairing interactions in both OP and IP via a coupling between them.

The c-axis optical spectrum gives a hint on this problem. The measurement of the c-axis optical response allows one to directly measure the interlayer Josephson coupling [68]. The coupling strength is proportional to the square of the frequency

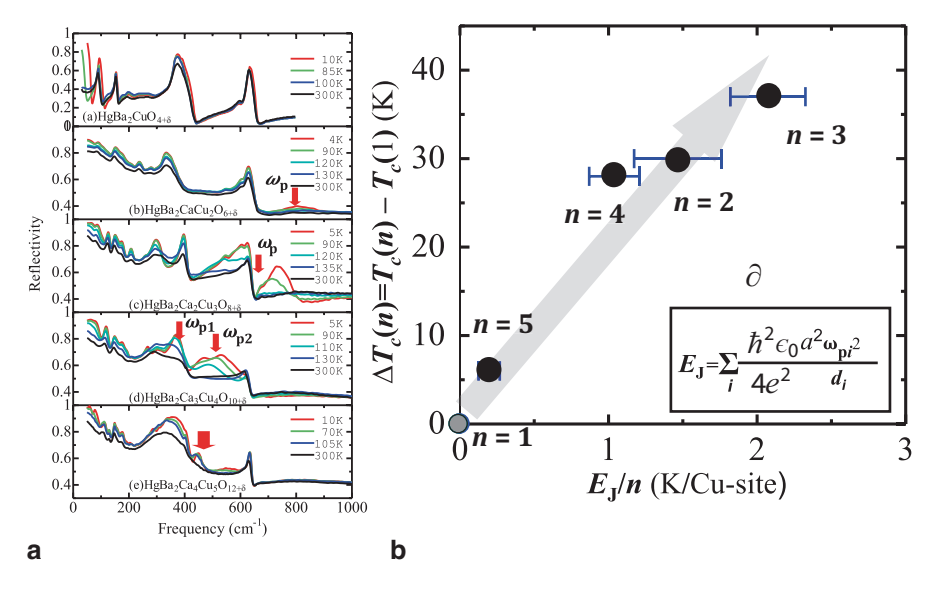


Fig 3.16 a Optical spectra of multilayer Hg12(n-1)n from n=1 to 5 measured at various temperatures [71]. The optical Josephson plasma modes (indicated by *arrows*) are seen to develop below  $T_c$ . **b** Enhancement of  $T_c$  in the multilayer with respect to  $T_c$  of single-layer,  $\Delta T_c = T_c(n) - T_c$  (1) plotted against the Josephson coupling energy per plane  $E_J/n$  estimated from the frequencies of the Josephson plasma modes observed for Hg12(n-1)n with n=2-5

of the Josephson plasma mode showing up below  $T_{\rm c}$  as a reflectivity edge in the c-axis polarized infrared optical spectrum. The multilayer cuprate which contains more than two  ${\rm CuO_2}$  planes in a unit cell is an alternating array of more than one kind of Josephson junctions—a bilayer cuprate is a stack of a stronger junction within a bilayer and and a weaker junction between bilayers. In such structure additional modes, called 'optical' Josephson plasma modes [69], appear like the optical phonon modes in a crystal with more than two inequivalent atoms in a unit cell. In a typical bilayer system YBCO this optical mode is observed at fairly high frequency, 400– $500~{\rm cm^{-1}}$  (50– $60~{\rm meV}$ ) [70], reflecting stronger coupling between closely spaced  ${\rm CuO_2}$  planes within a bilayer.

A systematic study of the Josephson plasma modes was carried out for the Hgbased multilayer system, Hg12(n-1)n [71]. The result, shown in Fig. 3.16a, revealed how the interlayer Josephson coupling strength within a multilayer varies with n. In Hg-based multilayer cuprates the frequency  $\omega$  of the optical Josephson plasma mode is distinctly high,  $\omega_0 \sim 800~{\rm cm}^{-1}$  for n=2, indicating a strong interlayer coupling within bilayer, strongest among the known bilayer cuprates. The highest frequency of this mode appears to correlate with the highest transition temperature  $T_c=127~{\rm K}$  for Hg1212. On the other hand, the frequencies of the optical plasma modes tend to decrease for n>2 which is apparently related to a slow down and a subsequent decrease in  $T_c$ 

Various scenarios have so far been proposed to account for the multilayer enhancement of the pairing interactions. The interlayer tunneling (ILT) theory [72] is

one of the proposals which try to explain the rise of  $T_{\rm c}$  with increasing n. The tunneling of Cooper pairs in a  ${\rm CuO}_2$  plane between the planes via Josephson coupling gains kinetic energy along the c-axis (perpendicular to the planes) which promotes the pair formation within the plane. In this model  $T_{\rm c}$  is an increasing function of n. However, a serious problem with this ILT model was found for single-layer cuprates in which the strength of interlayer Josephson coupling estimated from the Josephson-plasma frequency is too weak to account for the superconducting condensation energy [73]. However, the interlayer pair hopping within a multilayer (intra-multilayer tunneling) remains a possible scenario to explain the enhancement of  $T_{\rm c}^{\rm opt}$ . The systematic evolution of the optical Josephson plasma modes with n [71] appears to support the multilayer scenario [74]. In this scenario  $T_{\rm c}$  is an increasing function of n with C being a constant;

$$T_c(n) = T_c(1) + C(1-1/n).$$

A remarkable correlation is found between  $\Delta T_{\rm c}$  ( $T_{\rm c}(n)-T_{\rm c}(1)$ ) and intra-multilayer Josephson coupling energy  $E_{\rm J}$  which is estimated from the Josephson plasma frequencies observed for  ${\rm Hg}12(n-1)n$ . The correlation strongly suggests that the interlayer tunneling within a multilayer may be at work to contribute to the enhancement of  $T_{\rm c}$ , whatever the pairing mechanism, which determines  $T_{\rm c}(1)$ , is in a  ${\rm CuO}_2$  plane. As seen in Fig. 3.16a,  $E_{\rm J}$  and  $T_{\rm c}$  decrease for n greater than 3. The decrease appears to be related to the pronounced doping imbalance between IP and OP which weakens the Josephson coupling strength within a multilayer. This seems to happen even in the trilayer material as inferred from the lower frequency of the optical Josephson plasma mode in  ${\rm Hg}1223$  than that for the bilayer  ${\rm Hg}1212$  – the reason for the increase of  $E_{\rm J}$  for n=3 with respect to n=2 is that the trilayer structure has two near neighbor junctions.

An alternative scenario was proposed by considering nonlocal Coulomb interaction arising from poor screening along the c axis [75], and the same relation between  $T_c$  and n was derived. From a similar viewpoint, a possible contribution of phonon-mediated pairing in the multilayer cuprates is considered in [76]. In the case of, e.g., trilayer Bi2223, the OP has SrO on one side and  $Ca^{2+}$  on the other, and the IP is sandwiched by Ca on both sides. So, IP has mirror symmetry, whereas the symmetry is broken in OP (see Fig. 3.15b). The broken symmetry establishes a local electric field. The local field exists in the OP and does not in the IP. It enhances the electron-phonon coupling in the OP, specifically to the c-axis phonons. This phonon coupling may provide an additional pairing channel to the d-wave pairing in each  $CuO_2$  plane, and thereby enhances  $T_c$  with respect to the single-layer system.

## 3.5.4 Lattice Effect

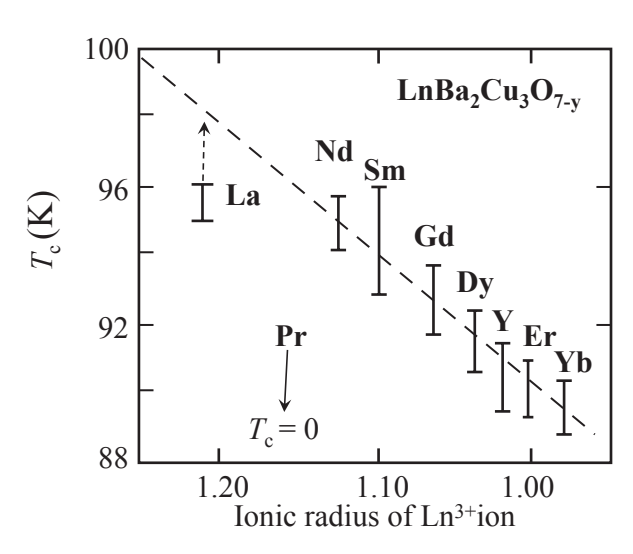
There are some known correlations between  $T_{\rm c}^{\rm opt}$  and lattice parameters. Well known is that  $T_{\rm c}^{\rm opt}$  is higher for the material with longer apical-oxygen distance from the neighboring  ${\rm CuO}_2$  plane or equivalently with flatter  ${\rm CuO}_2$  plane [77]. For single-layer systems the wide distribution of the values of  $T_{\rm c}^{\rm opt}$  arises from the disorder effect as was discussed in 3.5.2. On the other hand, among the bilayer cuprates, one notices that  $T_{\rm c}^{\rm opt}$  of the cleaner YBCO is relatively low as compared with  $T_{\rm c}^{\rm opt}$  (=98 K, see 3.6.1.1) of highly disordered Bi2212, and much lower than 110 K for Tl2212 and 127 K for Hg1212. The low  $T_{\rm c}^{\rm opt}$  for YBCO was ascribed to the warped (not flat)  ${\rm CuO}_2$  planes. A plausible parameter that gives rise to this difference in  $T_{\rm c}^{\rm opt}$  as well as to the flatness of the  ${\rm CuO}_2$  plane is the distance of apical oxygen (apical-O) from the  ${\rm CuO}_2$  plane. The apical-O distances (d) are d=2.30 Å for YBCO, 2.43 Å for Bi2212, 2.70 Å for Tl2212, and 2.80 Å for Hg1212, just in the order of increasing  $T_{\rm c}^{\rm opt}$ . Note that this is also in the order of increasing optical Josephson plasma frequency in the bilayer cuprates [71].

It is argued in [77] that the longer apical-O distance enhances the longer-range hopping of electrons which changes the Fermi surface with larger curvature unfavorable for the formation of competing orders such as CDW and SDW. A theoretical analysis based on the local (point charge) model of the cuprates find a correlation between  $T_{\rm c}$  and Madelung energy difference between in-plane and apical O sites [78]. It is argued that the longer apical-O distance results in a larger Madelung energy difference and hence favors higher  $T_{\rm c}$  by stabilizing local spin singlets.

The enhancement of  $T_{\rm c}$  under pressure [12] and the transient redistribution of interlayer coupling strength by short-pulsed light excitations [79] are thought to be intimately related to the change of lattice parameters. In the multilayer cuprates, the inner  ${\rm CuO}_2$  planes (IPs) are more apart from the apical-O atoms, which might explain the observed stronger pairing interaction in IPs. To understand the microscopic origin of this effect on  $T_{\rm c}^{\rm opt}$  theoretical investigations in the Migdal–Eliashberg framework appear helpful. One of the hints from such study is that contribution of out-of-plane orbitals,  ${\rm Cu}3d_{z^2}$  and  ${\rm Cu}4s$ , to the states on the Fermi surface may work to reduce the pairing interactions, so that longer apical-O distance would be favorable for higher  $T_{\rm c}$  [80].

It is also known empirically that in some families  $T_c^{\text{opt}}$  tends to be higher for materials consisting of cations with bigger ionic radius. For the  $\text{LnBa}_2\text{Cu}_3\text{O}_{7-y}$  system  $T_c^{\text{opt}}$  is lower for Ln with smaller ionic radius, *i.e.*, larger atomic number, known as "lanthanoid contraction" [81]. As plotted in Fig. 3.17,  $T_c^{\text{opt}}$ =96 K for Ln=Nd, and 89 K for Ln=Yb. The ionic radius of Y³+ is similar to that of  $\text{Dy}^3$ + or  $\text{Er}^3$ +, just on the relationship between  $T_c^{\text{opt}}$  and ionic radius of rare earth element. This trend may also be a consequence of the difference in the apical-O distance, since a larger ionic radius of Ln tends to make the apical-O distance longer in  $\text{LnBa}_2\text{Cu}_3\text{O}_{7-y}$ . However, the same trend is seen also in the electron doped cupartes,  $\text{Ln}_{2-x}\text{Ce}_x\text{CuO}_4$  without apical O atoms— $T_c^{\text{opt}}\sim 30$  K for Ln=Pr (La) and almost 0 K for Ln=Gd. The mechanism/reason of this  $T_c^{\text{opt}}$  degradation has never been addressed up to now.

Fig. 3.17  $T_{\rm c}^{\rm opt}$  of LnBa<sub>2</sub>Cu<sub>3</sub>O<sub>7</sub> (Ln123) for different rare-earth elements Ln in the order of increasing atomic number or decreasing radius of Ln<sup>3+</sup> ionic state. Pr123 is not a superconductor due to a circumstance arising from the special Pr ionic state, and  $T_{\rm c}^{\rm opt}$  of La123 is relatively low because of the disorder in the BaO block due to La-Ba intersite mixing



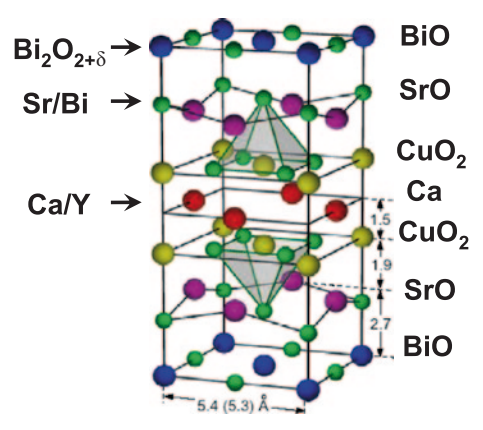
## 3.6 Possibility of Enhancing $T_c$

After the maximum value of  $T_{\rm c}$ =135 K was recorded in 1993,  $T_{\rm c}$  has stopped rising for more than 21 years. This does not imply that we should give up the effort to obtain higher  $T_{\rm c}$  values. There is a possibility or hope of enhancing the cuprate  $T_{\rm c}$  in view of the following observations; (i) the superconducting gap magnitude is typically 40–50 meV which corresponds to the mean-field  $T_{\rm c}^{\rm MF} \sim 200$  K or higher, (ii) the SC fluctuations or Cooper pair without phase coherence seem to exist at temperatures as high as 200 K, and (iii)  $T_{\rm c}$ =164 K was actually attained by applying high pressure to the Hg1223 cuprate [12]. To the best of the current understanding, major causes of the diverse  $T_{\rm c}^{\rm opt}$  are the number of CuO<sub>2</sub> planes n (multilayer effect), disorder in the charge reservoir blocks, and the apical oxygen position/distance. These, in turn, show the way to further increase  $T_{\rm c}$ .

## 3.6.1 Increasing $T_c$ by Reducing Disorder

In this sub-section two cases are shown that demonstrate  $T_c$  enhancement/improvement by reducing disorder outside the  $\text{CuO}_2$  plane. One is bilayer Bi-based cuprate,  $\text{Bi}_2\text{Sr}_2\text{CaCu}_2\text{O}_{8+\delta}$ , and the other is single-layer  $\text{Sr}_2\text{CuO}_{3+\delta}$  with the same  $\text{K}_2\text{NiF}_4$  crystal structure as that of the first high- $T_c$  cuprate  $\text{La}_2\text{CuO}_4$ . In both cases  $T_c$  is actually enhanced by reducing most harmful disorder in the former and by ordering dopant atoms in the latter.

**Fig. 3.18** Three disorder sites in the bilayer Bi2212



 $Bi_2Sr_2CaCu_2O_{8+\delta}(Bi2212)$ 

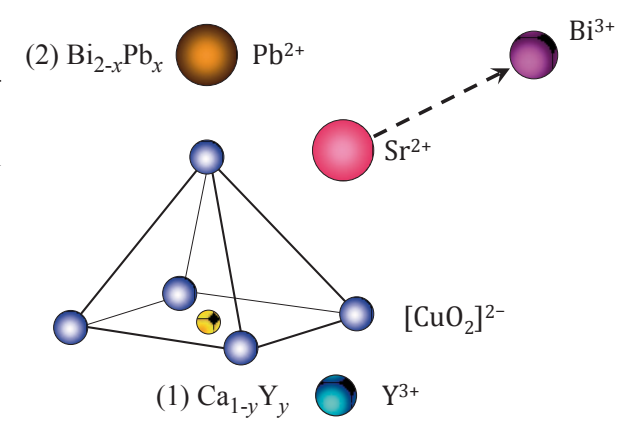
## 3.6.1.1 Reducing Disorder in Bi<sub>2</sub>Sr<sub>2</sub>CaCu<sub>2</sub>O<sub>8+δ</sub>

The effect of disorder is quantitatively examined [62], specifically in the single-layer Bi-based cuprate (Bi2201) in which disorder is intentionally introduced at the Sr site by partial substitution of various rare-earth elements (Ln),  $\text{Bi}_2\text{Sr}_{2-x}\text{Ln}_x$ .  $\text{CuO}_{6+\delta}$  (Ln-Bi2201). The result indicates that this type of disorder has a substantial influence on  $T_c$ , and hence that Bi-based cuprates with highly disordered crystal structures provide sufficient room for increasing  $T_c$ .

Bi<sub>2</sub>Sr<sub>2</sub>CaCu<sub>2</sub>O<sub>8+δ</sub> (Bi2212) is composed of three building blocks other than two CuO<sub>2</sub> planes: Bi<sub>2</sub>O<sub>2</sub> block, SrO block, and Ca block (see Fig. 3.18). These three blocks are charge reservoirs, and, at the same time, sources of disorder. Excess oxygen atoms ( $\delta$ ) are hole dopants and randomly distributed in the BiO block. The BiO blocks are also disturbed by the so-called structural supermodulations. The Ca<sup>2+</sup> ions are in the plane sandwiched by two CuO, planes forming a bilayer, and are easily substituted by rare-earth (Y or Ln) ions. In as-grown crystals of Bi2212 the SrO blocks are highly disordered due to Bi-Sr intersite mixing—Bi<sup>3+</sup> ions tend to invade the Sr sites. This is because (i) the CuO, bilayer is negatively charged, [CuO<sub>2</sub>-Ca-CuO<sub>2</sub>]<sup>2-</sup> and so more electro-positive Bi<sup>3+</sup> ions are allocated to occupy the neighboring Sr<sup>2+</sup> sites, and (ii) the SrO block composed of relatively small Sr<sup>2+</sup> ions as compared with Ba<sup>2+</sup> has smaller tolerance factor and hence is vulnerable to the intrusion of different cations to stabilize the structure. In fact, typical Bi2212 crystals contain a fairy large amount of Bi at the Sr sites, and the actual chemical formula is  $Bi_{2+x}Sr_{2-x}CaCu_2O_{8+\delta}$  with x=0.10-0.20. Usually, increasing/decreasing disorder in the charge reservoir block changes doping level and hence affecting  $T_c$ . However, in Bi2212 doping level can be controlled also by an operation to other building blocks. In this regard Bi2212 is a good playground for investigating the effect of disorder in each block on  $T_c$  and for the effort of increasing  $T_c$ .

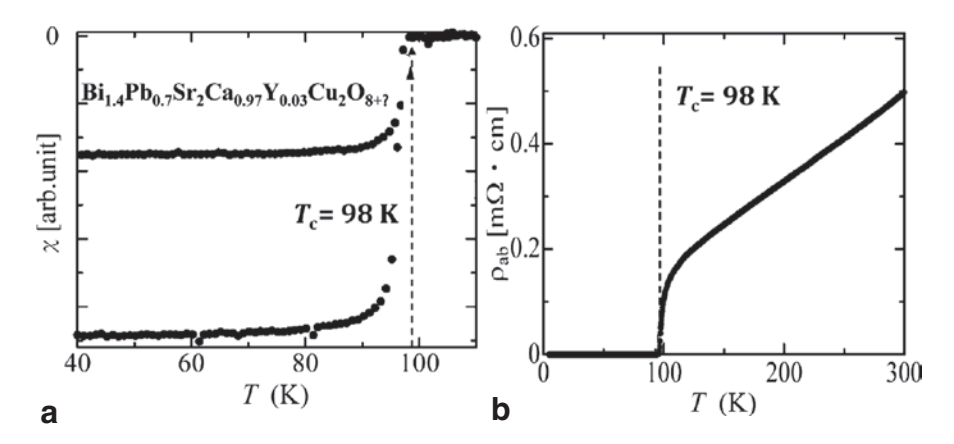
As pointed out in [60] in their paper in 2004, and also in view of the systematic investigation of disorder effect on Bi2201 [62] disorder in the SrO block is most

Fig. 3.19 Two steps for reducing the Bi-Sr intersite mixing; (1) partial Y substitution for Ca and (2) partial Pb substitution for Bi [64]. Both are expected to purge Bi atoms occupying the Sr sites



influential on  $T_c$ . Hence, the Bi/Sr site mixing (depicted in Fig. 3.19) is considered to be most detrimental for  $T_c$  in Bi2212, since Bi<sup>3+</sup> ion has different ionic charge from Sr<sup>2+</sup> and its ionic radius is considerably smaller than that of Sr<sup>2+</sup>. On the other hand, disorder in other two blocks, BiO and Ca, has very small effect. The small effect of disorder in the BiO block, due to both excess oxygen atoms and supermodulation, is conceivable, since it is well apart from the CuO<sub>2</sub> planes. In fact, it has been long known that YBCO is one of the cleanest systems, although there is rather strong disorder in the charge reservoir CuO chain layers where oxygen vacancies/defects exist.  $T_c$  is almost unchanged when disorder in the CuO chains is removed by ordering oxygen/oxygen-deficiency in the chains achieved by post-annealing at relatively low temperatures. Interestingly, though not widely anticipated, the disorder in the Ca block has negligible influence on  $T_c$ , even though the location of the Ca site is close to the CuO<sub>2</sub> planes. Residual resistivity is a measure of the scattering strength of charge carriers due to impurities and/or defects and hence a good measure of the strength of disorder. It is experimentally confirmed that for Bi2212 disorder in the Ca as well as BiO blocks does not produce appreciable residual resistivity, whereas disorder in the SrO block, either Ln or Bi partially substituted for Sr does small but finite residual resistivity [62]. Therefore, an effective way to increase  $T_a$  for Bi2212 is to reduce the disorder, specifically the Bi-Sr site mixing, in the SrO block.

The best way to reduce this type of disorder in Bi2212 would be replacement of Sr by Ba, but Ba tends to form impurity phases such as BaBiO<sub>3</sub>. Then, a practical way is to minimize the disorder in the SrO block at the expense disorder in other two blocks, Bi<sub>2</sub>O<sub>2</sub> and Ca layers, which has a minimal effect on  $T_c$ . This was actually done in [64] in two steps as sketched in Fig. 3.19. The first step is to partially substitute Y for Ca, Bi<sub>2+x</sub>Sr<sub>2-x</sub>Ca<sub>1-y</sub>Y<sub>y</sub>Cu<sub>2</sub>O<sub>8+δ(opt)</sub>. The Y<sup>3+</sup> substitution for Ca<sup>2+</sup> decreases the hole density p in the CuO<sub>2</sub> planes, so it should be compensated by increasing and adjusting the excess oxygen content  $\delta$  to yield maximum  $T_c$  (this, in turn, limits the amount of Y-substitution to y<0.10). The reason for why the Y-substitution reduces the Bi-Sr site mixing is supposed to be that introduction of Y<sup>3+</sup>



**Fig. 3.20** Temperature dependences of **a** the in-plane resistivity and **b** magnetic susceptibility for "optimized" Bi2212 (Bi<sub>1.4</sub>Pb<sub>0.7</sub>Sr<sub>2</sub>Ca<sub>0.97</sub>Y<sub>0.03</sub>Cu<sub>2</sub>O<sub>8+ $\delta$ </sub>) showing a superconducting transition at 98 K [64]

makes [CuO<sub>2</sub>-Ca-CuO<sub>2</sub>]<sup>2-</sup> bilayer more electropositive which would purge Bi<sup>3+</sup> ions from the SrO blocks.

The second step is to partially substitute Pb for Bi. The Pb substitution is known to relax the supermodulation of the BiO block, but this does not affect  $T_{\rm c}$  as described above. An expected effect of Pb substitution is to decrease the total amount of Bi which reduces the possibility of Bi intruding the SrO block. The ionic valence of Pb is expected to be Pb²+, so Pb substitution for Bi increases the hole density. This compensates, to some extent, the decrease of p due to the Y substitution for Ca, making the optimization of p by adjusting  $\delta$  easier. Some of Pb may also occupy the Sr site (Pb/Sr-site mixing). Fortunately, the ionic state of Pb (Pb²+) is identical to that of Sr, and the ionic radius of Pb²+ is nearly equal to that of Sr²+. Therefore, the Pb-Sr site mixing is harmless for  $T_{\rm c}$ . After this 'two-step optimization', the maximum  $T_{\rm c}$  =98 K was achieved for Bi<sub>2-w</sub>Pb<sub>w</sub>Sr<sub>2</sub>Ca<sub>1-y</sub>Y<sub>y</sub>Cu<sub>2</sub>O<sub>8+ $\delta$ </sub> (nominal) with w=0.60–0.65 and y=0.03–0.05 as shown in Fig. 3.20.

Note that the first process cannot apply to the single-layer Bi2201 without Ca block in its structure. In order to increase  $T_{\rm c}$  in Bi2201, the La substitution for Sr is usually adopted. La<sup>3+</sup> has least mismatch in the ionic radius with that of Sr<sup>2+</sup>, and may play a role in reducing the Bi/Sr-site mixing to some extent. However, disorder due to the charge mismatch remains between Sr<sup>2+</sup> and La<sup>3+</sup> which continues to produce relatively stronger disorder, which is the reason for its lowest  $T_{\rm c}$  (~30 K) even after optimization as compared with  $T_{\rm c}$ ~90 K realized in the isostructural Tl- ${}_2$ Ba<sub>2</sub>CuO<sub>6+8</sub> (Tl2201).

Although the maximum  $T_c$  of 98 K was achieved for Bi2212 which is comparable with (or a bit higher than) that of much cleaner YBCO, a question remains why it is lower by 10–30 K than the maximum  $T_c$  of its close relatives such as Tl2212 (~110 K) and Hg1212 (~127 K). It is possible that Bi atoms are not completely

removed from the SrO blocks. It is also inferable that other factors might be responsible for the  $T_c$  difference among these bilayer cuprates.

## 3.6.1.2 Dopant Oxygen Ordering in Sr<sub>2</sub>CuO<sub>3+δ</sub>

Single-layer cuprates comprise two groups in  $T_{\rm c}$ . Hg1201 and Tl2201 having  $T_{\rm c}^{\rm opt}$  exceeding 90 K, belong to a high  $T_{\rm c}$  group, while LSCO (LBCO), Bi2201 and Ca<sub>2-x</sub>Na<sub>x</sub>CuO<sub>2</sub>Cl<sub>2</sub> with  $T_{\rm c}^{\rm opt}$  at highest 40 K form a low  $T_{\rm c}$  group. Obviously, the difference between the two groups is in the location of dopant atoms and/or disordered block. For the low- $T_{\rm c}$  group disorder is in the block next to the CuO<sub>2</sub> plane, that is, in the block containing the apical-O atoms (apical-O block) which is highly disordered due to randomly distributed substituent/dopant atoms (e.g. Sr in the case of LSCO) with different ionic charges from those of host cations (e.g. La in LSCO). Since doping into this block is essential for inducing SC in these single-layer cuprates, there is no way to remarkably increase  $T_{\rm c}$  by reducing disorder. Ordering of randomly located doping cations is practically impossible, as these cations (Sr, Bi and Na) have very low diffusion constants in the crystals.

As was discussed in 3.5.2 and 3.6.1.1, the apical-O atom forming a  $\text{CuO}_5$  pyramid or a  $\text{CuO}_6$  octahedron is known to have an impact on the electronic structure. Hence, disorder in the apical-O sites is expected to have substantial effect on  $T_c$ . However, for almost all the hole-doped cuprates, apical-O sites are fully occupied. The stoichiometric  $\text{Sr}_2\text{CuO}_3$  (see Fig. 3.4) is a well-known cuprate with Cu-O chains aligning along the crystalline a-axis and is an insulator. Introduction of extra O atoms,  $\text{Sr}_2\text{CuO}_{3+\delta}$ , and application of high pressure ( $\sim$ 6 GPa) convert the structure to a layered  $\text{K}_2\text{NiF}_4$  structure. The  $\text{Sr}_2\text{CuO}_{3+\delta}$  compound can be synthesized only under high pressure or in the form of thin films grown on a certain substrate. It is a unique cuprate with the  $\text{K}_2\text{NiF}_4$  structure in that the apical sites are partially occupied;  $(1+\delta)$  apical sites are occupied and  $(1-\delta)$  sites are empty, and that the extra apical-O atoms  $(\delta)$  themselves play a role of hole dopants.

It was first synthesized by Hiroi et al. [82] and was found to show superconductivity at 70 K. After this discovery the quality of the  $\mathrm{Sr_2CuO_{3+\delta}}$  superconductors was improved and  $T_{\rm c}$  was enhanced to well above 90 K by post annealing (shown in Fig. 3.21) [65]. The annealing effect is dramatic as shown in the inset. When it is annealed at temperatures higher than 300 °C, superconductivity is completely destroyed. The 90 K class superconductivity is realized only by low-temperature (in the range between 200 and 250 °C) annealing.  $T_{\rm c}$  rises to 98 K after optimization [83] which highest among the known single-layer cuprates.

Although no direct evidence exists as yet because of difficulty in synthesizing a large amount of single-phase samples, it is highly probable that ordering of dopant apical-O atoms is essential in realizing high- $T_{\rm c}$  superconductivity in this cuprate, as the diffusion constant of O is large. Satellite spots observed by the electron diffraction experiment suggest that they correspond to some periodic distortions of Sr or Cu sublattices associated with an ordering of the apical-O atoms [65]. The annealing temperature below 250 °C is low enough not to cause a change of oxygen

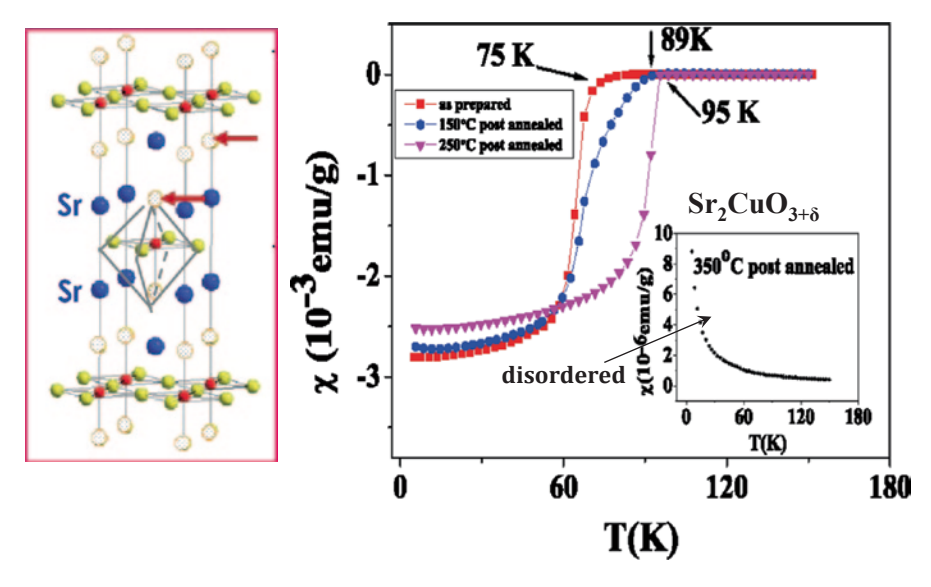


**Fig. 3.21** a The "214" structure of  $Sr_2CuO_{3+\delta}$  which is transformed at high pressures from the  $Sr_2CuO_3$  chain structure. In this structure the apical sites of  $CuO_6$  octahedra are not fully occupied by oxygen atoms. **b**  $Sr_2CuO_{3+\delta}$  becomes a superconductor with  $T_c$  exceeding 95 K after annealing at low temperatures which promotes ordering of apical-O atoms [65]

content. If apical-O atoms order, then the compound is regarded as a regular array of three different CuO<sub>4</sub> plaquettes with apical-O on both sides, on one side, and without apical-O.

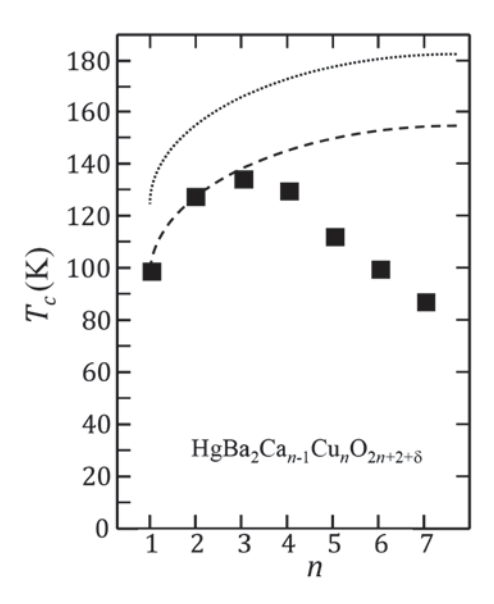
The reason for the high  $T_{\rm c}$  value comparable with that of Hg1201 is not clear yet. Geballe and Marezio [84] suggest a possibility that this compound might be a very heavily hole doped cuprate, presumably  $\delta \sim 0.2$  ( $p \sim 0.4$ ) and the highest  $T_{\rm c}$  may be realized in the second  $T_{\rm c}$  dome. The content of the extra apical-O atoms $\delta$ , i.e., the hole-doping level, is difficult to estimate even at present. Another possibility is that the average apical-O distance would be large, if one supposes an "infinite" apical-O distance for the  ${\rm CuO_4}$  plaquettes without apical-O. It is empirically suggested that the longer apical-O distance favors higher  $T_{\rm c}$  (see 3.5.4).

 $\mathrm{Sr_2CuO_{3+\delta}}$  is likely the first case demonstrating that the ordering of dopant atoms reduces disorder and thereby enhances  $T_{\rm c}$  to well above liquid nitrogen temperature. Dopant order, if applicable to other cuprate materials, is one of effective ways to increase the cuprate- $T_{\rm c}$ .

## 3.6.2 Optimizing Multilayer Structure

As was described in 3.5.3, the multilayer effect surely exists that enhances  $T_{\rm c}$  with respect to  $T_{\rm c}$  of single-layer cuprates. Also, considering the fact that the maximum  $T_{\rm c}$  (135 K at ambient pressure and 164 K at high pressure) is actually achieved in

**Fig. 3.22**  $T_c$  vs n plot (the same as that in Fig. 3.15b). The dashed curve indicates the interlayer-tunneling model for the situation of all equivalent CuO, planes assuming that the interlayer Josephson coupling strength within a multilayer recovers to the level in the bilayer material [74]. When the pairing interaction within a plane is strengthened by about  $\Delta T$ (n=1)=30 K, as might be the case under high pressure, further enhancement of  $T_a$  is like that shown by the dotted curve



trilayer Hg1223, it is natural to expect that higher  $T_{\rm c}$  in the cuprates would be realized in the multilayer structure. The ARPES experiment on Bi2223 unambiguously shows that the SC gap magnitude and therefore pairing interaction is enhanced in the trilayer with respect to single and bilayer materials. For further enhancement of  $T_{\rm c}$  in the multilayer cuprates, a challenging problem to be attacked is to improve the circumstances that degrade  $T_{\rm c}$  for n larger than 4. This is thought to arise from the charge imbalance, difference in the hole density between outer  ${\rm CuO_2}$  planes (OP) and inner planes (IP). The hole density in IPs tends to be smaller as they have no apical-O atoms and are sandwiched on both sides by  ${\rm Ca^{2+}}$  layers, making an electropositive circumstance for holes to enter. If the position of the apical-O atoms were far away from OP, then the circumstance of OP would be similar to that of IP and the charge imbalance would be diminished.

The correlation between  $\Delta T_{\rm c}$  and intra-multilayer Josephson coupling energy  $E_{\rm J}$  strongly suggests that the interlayer tunneling within a multilayer may contribute to the enhancement of  $T_{\rm c}$  in the multilayer. As was seen in Fig. 3.16b,  $E_{\rm J}$  (and hence  $T_{\rm c}$ ) decreases for n greater than 3. The decrease of  $\Delta T_{\rm c}$  appears to originate from the doping imbalance between IP and OP which weakens the Josephson coupling strength within a multilayer. Then, it could be guessed, if the Josephson coupling strength were recovered to the level of that in the (n=2) bilayer system by, for example, reducing the doping imbalance,  $T_{\rm c}$  would go up further. Quantitative estimate is possible, assuming that all the  ${\rm CuO_2}$  planes become equivalent, so that the Josephson coupling between the neighboring planes within a multilayer maintains the strength of the bilayer Hg1212. This corresponds to the assumption of the interlayer tunneling (ILT) model [74].  $T_{\rm c}$  is enhanced for  $n \ge 3$ , and the "optimized"  $T_{\rm c}$  increases with n following the equation,  $T_{\rm c}$  (n)= $T_{\rm c}$ (n)+ $T_{\rm c}$ (n)= $T_{\rm c}$ (n)+ $T_{\rm c}$ (n)= $T_{\rm c}$ (n)+ $T_{\rm c}$ (n)= $T_{\rm c}$ (n)+ $T_{\rm c}$ (n)= $T_{\rm c}$ (n)+ $T_{\rm c}$ (n)= $T_{\rm c}$ (n)+ $T_{\rm c}$ (n)= $T_{\rm c}$ (n)+ $T_{\rm c}$ (n)= $T_{\rm c}$ (n)+ $T_{\rm c}$ (n)= $T_{\rm c}$ (n)+ $T_{\rm c}$ (n)= $T_{\rm c}$ (n)+ $T_{\rm c}$ (n)= $T_{\rm c}$ (n)+ $T_{\rm c}$ (n)= $T_{\rm c}$ (n)+ $T_{\rm c}$ (n)= $T_{\rm c}$ (n)+ $T_{\rm c}$ (n)= $T_{\rm c}$ (n)+ $T_{\rm c}$ (n)+ $T_{\rm c}$ (n)+ $T_{\rm c}$ (n)= $T_{\rm c}$ (n)+ $T_{\rm c}$ (n)+ $T_{\rm c}$ (n)= $T_{\rm c}$ (n)+ $T_{\rm c}$ (n)+

References 55

 $T_{\rm c}^{\rm opt}$  values for n=1 and 2). Estimated  $T_{\rm c}$  values are  $\sim 150$  K for  $n \ge 5$ , but it is significantly lower than 164 K achieved in the real trilayer (n=3) cuprate at pressure of 30 GPa.

Suppose, for example, that pressure were to make the apical-O distance from outer-plane (OP) longer, and then it would reduce the circumstantial difference between IP and OP and thereby enhance Josephson coupling strength between planes involving IP. It should be noted that the high-pressure experiment on Hg12(n-1)nwith n=1 to 3 [12] actually shows that  $T_c$ 's of all the multilayers, even the single layer, increase by ~30 K in the high pressure limit. This is suggestive of an additional effect of pressure which enhances the pairing interaction in each plane or increases  $T_c(1)$  in the ILT model via, e.g., lattice effect discussed in 3.5.4. Alternatively, pressure might quench the superconducting fluctuations by increasing the phase stiffness  $\rho_s$  and/or by strengthening the interlayer Josephson coupling. When the value of  $T_c(1)$  is reset to 130 K, the ILT model yields the  $T_c(n)$  curve as indicated by the dotted line in Fig. 3.22. These two effects of pressure may explain the record high  $T_c = 164$  K at 30 GPa. From this perspective, an accessible way to achieve  $T_c > 150 \text{ K}$  at ambient pressure would be to quench the high-pressure structure either by applying chemical pressure or by fabricating thin films of the multilayer cuprate on a suitable substrate material.

#### References

- 1. Bednorz JG, Müller KA (1986) Possible high  $T_{\rm c}$  superconductivity in the Ba-La-Cu-O system. Z Phys B 64:189–193
- Takagi H, Uchida S, Kitazawa K, Tanaka S (1987) High-T<sub>c</sub> superconductivity in La-Ba-Cu-O II: specification of the superconducting phase. Jpn J Appl Phys 26:L123–L124
- 3. Kishio K et al (1987) New high temperature superconducting oxides:  $(La_{1-x}Sr_x)_2CuO_4$  and  $(La_{1-x}Ca_x)_2CuO_4$ . Chem Lett 2:429–432
- Cava RJ, van Dover RB, Batlogg B, Rietman EA (1987) Bulk Superconductivity at 36 K in La<sub>1.8</sub>Sr<sub>0.2</sub>CuO<sub>4</sub>. Phys Rev Lett 58:408–410
- Anderson PW (1987) The resonating valence bond state in La<sub>2</sub>CuO<sub>4</sub> and superconductivity. Science 235:1196–1198
- Shaplygin IS, Kakhan BG, Lazarev VB (1979) Preparation and properties of the compounds Ln<sub>2</sub>CuO<sub>4</sub> (Ln = La, Pr, Nd, Sm, Eu, Gd) and some of their solid solutions. Zhurnal Neorganicheskoi Khimii 24:1478–1485
- Wu MK et al. (1987) Superconductivity at 93 K in a new mixed phase Y-Ba-Cu-O compound system at ambient pressure. Phys Rev Lett 58:908–910
- Hazen RM et al (1987) Crystallographic description of phases in the Y-Ba-Cu-O superconductor. Phys Rev B 35:7238–7241
- Maeda H, Tanaka Y, Fukutomi M, Asano T (1988) A new high-T<sub>c</sub> oxide superconductors without a rare earth element. Jpn J Appl Phys 27:L209–L210. doi:10.1143/JJAP.27.L209
- Sheng ZZ, Hermann AM (1988) Superconductivity in the rare-earth-free Tl-Ba-Cu-O system above liquid nitrogen temperature. Nature 332:55–58. doi:10.1038/332055a0
- Schilling A, Cantoni M, Guo JD, Ott HR (1993) Superconductivity above 130 K in the Hg-Ba-Ca-Cu-O system. Nature 363:56–58. doi:10.1038/363056a0
- 12. Gao L et al (1994) Superconductivity up to 164 K in HgBa<sub>2</sub>Ca<sub>n-1</sub>Cu<sub>n</sub>O<sub>2m+2+ $\delta$ </sub> (m = 1, 2,and 3) under quasihydrostatic pressures. Phys Rev B 50:4260–4263

- Scott BA, Suard EY, Tsuei CC, Mitzi DB, MaGuire TR, Chen B-H, Walker D (1994) Layer dependence of the superconducting transition temperature of HgBa<sub>2</sub>Ca<sub>n-1</sub>Cu<sub>n</sub>O<sub>2n+2+δ</sub>. Physica C 230:239–245
- Iyo A, Tanaka Y, Kodama Y, Kito H, Tokiwa K, Watanabe T (2006) Synthesis and physical properties of multilayered cuprates. Physica C 445–448:17–22. doi:10.1016/j.physc.2006.03.067
- 15. Deslandes F, Nazzal AI, Torrance JB (1991) Search for superconductivity in analogues of La<sub>2</sub>  $_x$  Sr $_x$ CuO $_4$ : Sr $_2$ - $_x$ Ln $_x$ VO $_4$  (Ln = La, Ce, Pr, Nd, Eu). Physica C 179:85–90. doi:10.1016/0921-4534(91)90014-P
- Takada Y et al (1990) Crystal chemistry and physical properties of La<sub>2-x</sub>Sr<sub>x</sub>NiO<sub>4</sub> (0≤x≤1.6). Mater Res Bull 25:293–306
- Tsuei CC et al (1994) Pairing symmetry and flux quantization in a tricrystal superconducting ring of YBa<sub>2</sub>Cu<sub>2</sub>O<sub>7-8</sub>. Phys Rev Lett 73:593–596
- Uemura YJ et al (1989) Universal correlation between T<sub>c</sub> and n<sub>s</sub>/m\* in high-T<sub>c</sub> cuprate superconductors. Phys Rev Lett 62:2317–2320
- Alloul H, Bobroff J, Gabay M, Hirschfeld PJ (2009) Defects in correlated metals and superconductors. Rev Mod Phys 81:45. doi:10.1103/RevModPhys.81.45
- Bozovich I, Logvenov G, Verhoeven MAJ, Caputo P, Goldobn E, Geballe TH (2003) No mixing of superconductivity and antiferromagnetism in a high-temperature superconductor. Nature 422:873–875. doi:10.1038/nature01544
- 21. Haug D et al (2010) Neutron scattering study of the magnetic phase diagram of underdoped YBa<sub>2</sub>Cu<sub>3</sub>O<sub>6+x</sub>. New J Phys 12:105006. doi:10.1088/1367-2630/12/10/105006
- Tranquada JM, Sternlieb BJ, Axe J, Nakamura Y, Uchida S (1995) Evidence for stripe correlations of spins and holes in copper oxide superconductors. Nature 375:561–563
- Ghirighelli G et al (2012) Long-range incommensurate charge fluctuations in (Y, Nd)Ba<sub>2</sub>Cu<sub>3</sub>O<sub>6+x</sub>. Science 337:821–825. doi:10.1126/science.1223532
- Chang J et al (2012) Direct observation of competition between superconductivity and charge density wave order in YBa<sub>2</sub>Cu<sub>3</sub>O<sub>6.67</sub>. Nature Phys 8:871–876. doi:10.1038/nphys10345
- Comin R et al (2014) Charge order driven by Fermi-Arc instability in Bi<sub>2</sub>Sr<sub>2-x</sub>La<sub>x</sub>CuO<sub>6+8</sub>.
   Science 343:390–392. doi:10.1126/science.1242996
- da Silva Neto EH et al (2014) Ubiquitous interplay between charge ordering and high-temperature superconductivity in cuprates. Science 343:393–396. doi:10.1126/science.1243479
- Kohsaka Y et al (2007) An intrinsic bond-centered electronic glass with unidirectional domains in underdoped cuprates. Science 315:1380–1385. doi:10.1126/science.1138584
- Fujita K et al (2014) Direct phase-sensitive identification of a d-form factor density wave in underdoped cuprates. Proc Natl Acad Sci U S A 111:E3026–E3032. doi:10.1073/ pnas.1406297111
- 29. Hücker M et al (2014) Competing charge, spin, and superconducting orders in underdoped YBa<sub>2</sub>Cu<sub>3</sub>O<sub>2</sub>. Phys. Rev. B 90: 054514. doi:10.1103/PhysRevB.90.054514
- Blanco-Canosa S et al (2014) Resonant X-ray scattering study of charge density wave correlations in YBa<sub>2</sub>Cu<sub>3</sub>O<sub>6+x</sub>. Phys. Rev. B 90: 054513. doi: 10.1103/PhysRevB.90.054513
- Wu T, Julien M-H et al (2011) Magnetic-field-induced charge-stripe order in the high-temperature superconducting YBa<sub>2</sub>Cu<sub>3</sub>O<sub>v</sub>. Nature 477:191–194. doi:10.1038/nature10345
- LeBoeuf D et al (2011) Lifshitz critical point in the cuprate superconductor YBa<sub>2</sub>Cu<sub>3</sub>O<sub>y</sub> from high-field Hall effect measurements. Phys Rev B 83:054506. doi:10.1103/Phys-RevB.83.054506
- 33. Doiron-Leyraud N et al (2007) Quantum oscillations and the Fermi surface in an underdoped high-*T*<sub>c</sub> superconductor. Nature 447:565–568. doi:10.1038/nature15872
- Sebastian SE et al (2010) Metal-insulator quantum critical point beneath the high-T<sub>c</sub> superconducting dome. Proc Natl Acad Sci U S A 107:6175–6179. doi:10.1073/pnas.0913711107
- Ramshaw BJ et al (2014) A quantum critical point at the heart of high temperature superconductivity. Preprint at http://arXiv.org/abs/1409.3990. Accessed 13 Sept 2014

References 57

 Ito T, Takenaka K, Uchida S (1993) Systematic deviation from T-linear behavior in the in-plane resistivity of YBa<sub>2</sub>Cu<sub>3</sub>O<sub>7-y</sub>: evidence for dominant spin scattering. Phys Rev Lett 70:3995–3998

- Marshall DS et al (1996) Unconventional electronic structure evolution with hole doping in Bi<sub>2</sub>Sr<sub>2</sub>CaCu<sub>2</sub>O<sub>8+8</sub>. Phys Rev Lett 76:4841–4844
- Kohsaka Y et al (2008) How Cooper pairs vanish approaching the Mott insulator in Bi<sub>2</sub>Sr<sub>2</sub>Ca-Cu<sub>2</sub>O<sub>8+8</sub>. Nature 454:1072–1078. doi:10.1038/nature07243
- Wang YY, Li L, Naughton MJ, Gu GD, Uchida S, Ong NP (2005). Field-enhanced diamagnetism in the pseudogap state of the cuprate Bi<sub>2</sub>Sr<sub>2</sub>CaCu<sub>2</sub>O<sub>8+δ</sub> superconductor in an intense magnetic field. Phys Rev Lett 95:247002. doi:10.1103/PhysRevLett.95.247002
- Dubroka A et al (2011) Evidence of a precursor superconducting phase at temperatures as high as 180 K in RBa<sub>2</sub>Cu<sub>3</sub>O<sub>7-δ</sub> (R = Y, Gd, Eu) superconducting crystals from infrared spectroscopy. Phys Rev Lett 106:047006. doi:10.1103/PhysRevLett.106.047006
- 41. Fauque B, Sidis Y, Hinkov V, Pailhes S, Lin CT, Chaud X, Bourges P (2006) Magnetic order in the pseudogap phase of high- $T_{\rm c}$  superconductors. Phys Rev Lett 96:197001. doi:10.1103/PhysRevLett.96.197001
- Varma CM (1997) Non-Fermi-liquid states and pairing instability of a general model of copper oxide metals. Phys Rev B 55:14554–14580
- Lawler MJ et al (2010) Intra-unit-cell electronic nematicity of the high-T<sub>c</sub> copper oxide pseudogap states. Nature 466:347–351. doi:10.1038/nature09169
- 44. Shekhter A et al (2013) Bounding the pseudogap with a line of phase transitions in YBa<sub>2</sub>Cu<sub>3</sub>O<sub>6+8</sub>. Nature 498:75–77. doi:10.1038/nature12165
- Dai P, Mook HA, Hayden SM, Aeppli G, Perring TG, Hunt RD, Dogan F (1999) The magnetic excitation spectrum and thermodynamics of high-Tc superconductors. Science 284:1344– 1347. doi:10.1126/science.284.5418.1344
- Uemura YJ et al (1993) Magnetic penetration depth in Tl<sub>2</sub>Ba<sub>2</sub>CuO<sub>6+δ</sub> in the overdoped regime. Nature 364:605–607. doi:10.1038/364605a0
- Plate M et al (2005) Fermi surface and quasiparticle excitations of overdoped Tl<sub>2</sub>Ba<sub>2</sub>CuO<sub>6+δ</sub>.
   Phys Rev Lett 95:077001. doi:10.1103/PhysRevLett.95.077001
- Dean MPM et al (2013) Persistence of magnetic excitations in La<sub>2-x</sub>Sr<sub>x</sub>CuO<sub>4</sub> from the undoped insulator to the heavily overdoped non-superconducting metal. Nat Mater 12:1019– 1023. doi:10.1038/nmat3723
- Moodenbaugh AR, Xu Y, Suenaga M, Folkerts TJ, Shelton RN (1988) Superconducting properties of La, "Ba, CuO<sub>4</sub>. Phys Rev B 38:4596–4600
- Takagi H et al (1992) Systematic evolution of temperature-dependent resistivity in La<sub>2-x</sub>Sr<sub>x-</sub>CuO<sub>4</sub>. Phys Rev Lett 69:2975–2978
- Takenaka K et al (2002) Coherent-to-incoherent crossover in the optical conductivity of La<sub>2-x</sub>Sr<sub>x</sub>CuO<sub>4</sub>: charge dynamics of a bad metal. Phys Rev B 65:092405. doi:10.1103/Phys-RevB.65.092405
- Anderson PW (2002) In praise of unstable fixed points: the way things actually work. Physica B 318:28–32. doi:10.1016/S0921-4526(02)00770-6
- Tokura Y, Takagi H, Uchida S (1989) A superconducting copper oxide compound with electrons as the charge carriers. Nature 337:345–347. doi:10.1038/337345a0
- 54. Karimoto S, Naito M (2004). Electron-doped infinite-layer thin films with  $T_c$  over 40 K grown on DyScO<sub>3</sub> substrates. Appl Phys Lett 84:2136–2138. doi:10.1063/1.1688979
- Krockenberger Y et al (2013) Emerging superconductivity hidden beneath charge-transfer insulator. Sci Rep 3:2235. doi:10.1038/srep02235
- Tajima S, Noda T, Eisaki H, Uchida S (2001) c-Axis optical response in the static stripe ordered phase of the cuprates. Phys Rev Lett 86:500–503
- Li Q, Hücker M, Gu GD, Tsvelik AM, Tranquada JM (2007) Two-dimensional superconducting fluctuations in stripe-ordered La<sub>1.875</sub>Ba<sub>0.125</sub>Cu<sub>4</sub>. Phys Rev Lett 99:067001. doi:10.1103/PhysRevLett.99.067001

- Khasanov R et al (2004) Direct observation of the oxygen isotope effect on the in-plane magnetic penetration depth in optimally doped YBa<sub>2</sub>Cu<sub>3</sub>O<sub>7-δ</sub>. Phys Rev Lett 92:057602. doi:10.1103/PhysRevLett.92.057602
- 59. Sawa H et al (1989) Unusual simple crystal structure of an Nd-Ce-Sr-Cu-O superconductor. Nature 337:347–348. doi:10.1038/337347a0
- Eisaki H et al (2004) Effect of chemical inhomogeneity in bismuth-based copper oxide superconductors. Phys Rev B 69:064512. doi:10.1103/PhysRevB.69.064512
- 61. Mesaros A et al (2011) Topological defects coupling smectic modulations to intra-unit-cell nematicity in cuprates. Science 333:426–430. doi:10.1126/science.1201082
- 62. Fujita K, Noda T, Kojima KM, Eisaki H, Uchida S (2005) Effect of disorder outside the  ${\rm CuO_2}$  planes on  $T_{\rm c}$  of copper oxide superconductors. Phys Rev Lett 95:097006. doi:10.1103/PhysRevLett.95.097006
- Tanaka K et al (2001) Tl valence change and T<sub>c</sub> enhancement (>130 K) in (Cu, Tl)Ba<sub>2</sub>Ca<sub>2</sub>Cu<sub>3</sub>O<sub>v</sub> due to nitrogen annealing. Phys Rev B 63:064508. doi:10.1103/PhysRevB.63.064508
- Hobou H, Ishida S, Fujita K, Ishikado M, Eisaki H, Uchida S (2009) Enhancement of the superconducting critical temperature in Bi<sub>2</sub>Sr<sub>2</sub>CaCu<sub>2</sub>O<sub>8+δ</sub> by controlling disorder outside CuO<sub>2</sub> planes. Phys Rev B 79:064507. doi:10.1103/PhysRevB.79.064507
- 65. Gao WB, Liu QQ, Yang LX, Yu Y, Li FY, Jin CQ, Uchida S (2009) Out-of-plane effect on the superconductivity of Sr<sub>2-x</sub>Ba<sub>x</sub>CuO<sub>3+δ</sub> with T<sub>c</sub> up to 98 K. Phys Rev B 80:094523. doi:10.1103/PhysRevB.80.094523
- Kotegawa H et al. (2001) NMR study of carrier distribution and superconductivity in multilayered high-T cuprates. J Phys Chem Solids 62:171–175. doi:10.1016/S0022-3697(00)00122-0
- Ideta S et al (2010) Enhanced superconducting gaps in the trilayer high-temperature Bi<sub>2</sub>-Sr<sub>2</sub>Ca<sub>2</sub>Cu<sub>3</sub>O<sub>10+δ</sub> cuprate superconductor. Phys Rev Lett 104:227001. doi:10.1103/PhysRev-Lett.104.227001
- Tamasaku K, Nakamura Y, Uchida S (1992) Charge dynamics across the CuO<sub>2</sub> planes in La<sub>2-</sub> "Sr"CuO<sub>4</sub>. Phys Rev Lett 69:1455–1458
- van der Marel D, Tsvetkov AA (1996) Transverse optical plasmons in layered superconductors. Czech J Phys 46:3165–3168
- 70. Homes CC, Timusk T, Liang R, Bonn DA, Hardy WN (1993) Optical conductivity of c axis oriented YBa<sub>2</sub>Cu<sub>2</sub>O<sub>6.70</sub>: evidence for a pseudogap. Phys Rev Lett 71:1645–1648
- Hirata Y, Kojima KM, Ishikado M, Uchida S, Iyo A, Eisaki H, Tajima S (2012) Correlation between the interlayer Josephson coupling and an enhanced superconducting transition temperature of multilayer cuprate superconductors. Phys Rev B 85:054501. doi:10.1103/Phys-RevB.85.054501
- Anderson PW (1995) Interlayer tunneling mechanism for high-T<sub>c</sub> superconductivity: comparison with c-axis infrared experiment. Science 268:1154–1155. doi:10.1126/science.268.5214.1154
- Tsvetkov AA et al (1998) Global and local measures of the interlayer Josephson coupling in Tl<sub>2</sub>Ba<sub>2</sub>CuO<sub>6</sub> as a test of the interlayer tunneling model. Nature 395:360–362. doi:10.1038/26439
- 74. Chakraverty S et al (1998) Do electrons change their c-axis kinetic energy upon entering the superconducting state? Eur Phys J B 5:337–343. doi:10.1007/S100510050451
- Leggett AJ (1999) Cuprate superconductivity: dependence of T<sub>c</sub> on the c-axis layering structure. Phys Rev Lett 83:392–395. doi:10.1103/PhysRevLett.83.392
- Johnston S, Vernay F, Moritz B, Shen Z-X, Nagaosa N, Zaanen J, Devereaux TP (2010) Systematic study of electron-phonon coupling to oxygen modes across the cuprates. Phys Rev B 82:064513. doi:10.1103/PhysRevB.82.064513
- Pavarini E, Dasgupta I, Saha-Dasgupta T, Jepsen O, Andersen OK (2001) Band structure trend in hole-doped cuprates and correlation with T<sub>cmax</sub>. Phys Rev Lett 87:047003. doi:10.1103/ PhysRevLett.87.047003
- Ohta Y, Tohyama T, Maekawa S (1991) Apex oxygen and critical temperature in copper oxide superconductors: universal correlation with the stability of local singlets. Phys Rev B 43:2968–2982

References 59

 Hu W et al. (2014) Optically enhanced coherent transport in YBa2Cu3O6.5 by ultrafast redistribution of interlayer coupling, Nat Mater. 13: 705-711. doi: 10.1038/nmat3963

- Sakakibara H, Suzuki K, Usui H, Kuroki K, Arita R, Scalapino DJ, Aoki H (2012) Multiorbital analysis of the effects of uniaxial and hydrostatic pressure on T<sub>c</sub> in single-layered cuprate superconductors. Phys Rev B 86:134520. doi:10.1103/PhysRevB.86.134520
- 81. Mallett B et al. (2012)  $T_c$  is insensitive to magnetic interactions in high- $T_c$  superconductors. http://arXiv.org/abs/1202.3078. Accessed 23 Feb 2012
- 82. Hiroi Z, Takano M, Azuma M, Takeda Y (1993) A new family of copper oxide superconductors  $Sr_{n+1}Cu_nO_{2n+1+\delta}$  stabilized at high pressure. Nature 364:315–317. doi:10.1038/364315a0
- Liu QQ et al (2006) Enhancement of the superconducting critical temperature of Sr<sub>2</sub>CuO<sub>3+δ</sub> up to 95 K by ordering dopant atoms. Phys Rev B 74:100506(R). doi:10.1103/ PhysRevB.74.100506
- Geballe T, Marezio M (2010) Enhanced superconductivity in Sr<sub>2</sub>CuO<sub>4-y</sub>. http://arXiv.org/ abs/0904.2788. Accessed 18 April 2009

# **Chapter 4 Iron-Based Superconductors**

**Abstract** The iron-based superconductors (Fe-SCs) comprise a big family having the highest  $T_{\rm c}$ =55 K. In this family, an indispensable element is the typical magnetic element Fe, and except for the layer structure the characteristic electronic parameters are largely different from those in the cuprates. The discovery of this family, therefore, evidences that there are more than one route to finding high- $T_{\rm c}$  materials with  $T_{\rm c}$  higher than 50 K. The parent compounds are antiferromagnetic metals, and both chemical substitution (doping) and application of pressure induce superconductivity. Like the cuprates, Fe-SCs show unconventional pairing, suggesting that strong electronic correlations play a major role in the pair formation. The strong correlations and high  $T_{\rm c}$  have a root in the unique characteristics of the common building block composed of Fe and As (Se) layers in which an unusual antiferromagnetic state is also formed.  $T_{\rm c}$  is material dependent, but the maximum  $T_{\rm c}$  reaches around 50 K in most of sub-families after optimization, and never exceeds 55 K. For further enhancement of  $T_{\rm c}$ , it may be needed to prepare an additional pairing channel by fabricating a novel structure.

#### 4.1 Introduction

 $T_c$  = 26 K superconductivity in iron-based superconductors (Fe-SC) was discovered in 2008 [1] for LaFeAsO<sub>1-x</sub>F<sub>x</sub>.  $T_c$  values went up to 43 K by application of pressure to the same compound, and then as high as 55 K by replacement of La by other rare earth element, SmFeAsO<sub>1-x</sub>F<sub>x</sub> [2]. This was quite unexpected in that the superconductors contain, as an indispensable element, one of the typical magnetic elements Fe (the elemental Fe metal is known to be a superconductor under high pressure), and the maximum  $T_c$  value exceeding 50 K has never been achieved in materials other than the cuprates.

Except for the layered crystal structures, the electronic parameters of Fe-SCs are quite different from those of the cuprates; (i) spin quantum number associated with Fe is larger than 1/2, (ii) they are multi-band system with multiple Fermi surface pockets, both electrons and holes, and (iii) on-site Coulomb repulsive energy U

and the spin-superexchange energy J are considerably smaller. Therefore, Fe-SCs opened a new avenue of quest for higher  $T_{\rm c}$  superconductors. Like the cuprates, superconductivity (SC) emerges upon "doping" into the parent compounds which are antiferromagnetic (AF) metals at low temperatures. SC can also be induced by applying pressure to the parent compounds, unlike the cuprates. The phase diagram with AF and SC as two major phases is generic and resembles those in other superconducting materials with strongly correlated electrons, such as the cuprates and the heavy fermion compounds. Strong correlations are tied to superconductivity having unconventional pairing symmetry with sign-changing SC order parameter. In fact, unconventional pairing symmetries have been confirmed for Fe-SCs.

The strong correlations and high  $T_{\rm c}$  have a root in the unique characteristics of the common building block composed of Fe and As (Se) layers. Like the cuprates  $T_{\rm c}$  is material dependent, but the maximum  $T_{\rm c}$  reaches around 50 K in most of subfamilies after optimization, and never exceeds 55 K. For further enhancement of  $T_{\rm c}$ , it may be needed to prepare an additional pairing channel by fabricating a novel structure.

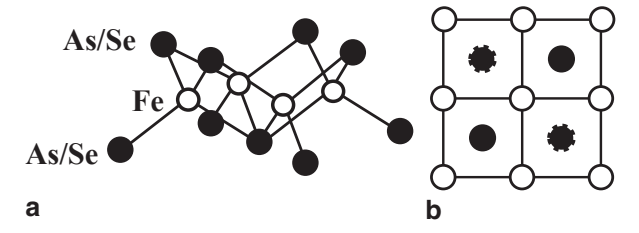
In this chapter, in parallel to that for the cuprates, the  $T_{\rm c}$ -physics of Fe-SCs is extended in the following sequence, (1) material dependence of  $T_{\rm c}$  and parameters that influence  $T_{\rm c}$ , (2) uniqueness of Fe-As or Fe-Se combination, (3) phase diagram with unusual AF and unconventional SC phases, (4) roles of doping and electronic correlations in SC, and (5) possibility of enhancing  $T_{\rm c}$ .

## 4.2 Material Dependence of $T_c$ and Parameters that Influence $T_c$

## 4.2.1 Material Dependence of T<sub>c</sub>

It turned out that, like the high- $T_{\rm c}$  cuprates, the iron-based superconductors comprise a large families of iron arsenides (FeAs) and iron selenides (FeSe) having a common structural unit, FeAs or FeSe block in which a Fe atom is coordinated by As/Se distorted tetrahedron, shown in Fig. 4.1. In this unit Fe atoms form a tetragonal lattice layer sandwiched by a layer of As (Se) atoms above and below it. Fe and As/Se atoms are bonded with strong covalent bond. The structure of

**Fig. 4.1 a** Common structural unit of iron arsenide and selenide high- $T_c$  superconductors. **b** Its top view



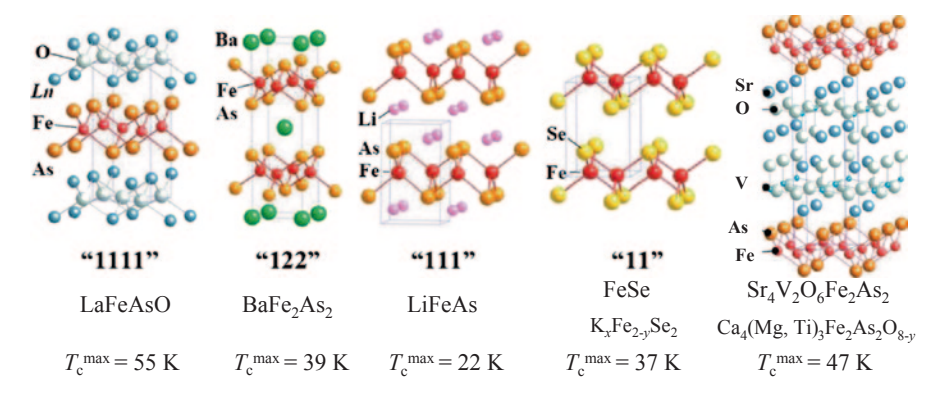


Fig. 4.2 Crystal structures of five representative sub-families of iron-based superconductors. The maximum  $T_c$  value so far achieved for a member of each sub-family is indicated

this FeAs/FeSe block is a familiar one already seen in the  $T_c$  = 23 K borocarbide, YPd<sub>2</sub>B<sub>2</sub>C, as well as the first discovered heavy fermion superconductor Ce- $Cu_2Si_2$ , and provides a playground of superconductivity with second highest  $T_2$ among the known superconductors. Again, like the cuprates, several families of Fe-SCs have been discovered, showing strong material dependence of  $T_a$ . Representative sub-families are (1) LnFeAsO (abbreviated by 1111), (2) BaFe<sub>2</sub>As<sub>2</sub> (122) [3], (3) LiFeAs (111) [4], (4) Fe(Se, Te) (11) [5] and K<sub>x</sub>Fe<sub>2-y</sub>Se<sub>2</sub> [6], and (5)  $Sr_4V_2O_6Fe_2As_2$  (42622) [7]. The crystal structure and its maximum  $T_c$  value for each sub-family are shown in Fig. 4.2. The first two compounds, LnFeAsO and BaFe<sub>2</sub>As<sub>2</sub>, and FeTe are not superconductors but metals showing an antiferromagnetic order below a temperature  $T_N$ , accompanied  $(T_N = T_s)$  or preceded  $(T_{\rm N} < T_{\rm s})$  by a tetragonal-orthorhombic structural phase transition at  $T_{\rm s}$ . Hereafter the low-temperature phase is called as antiferromagnetic-orthorhombic (AFO) phase with respect to the high-temperature paramagnetic-tetragonal (PT) phase. T<sub>c</sub> range between 60 and 200 K. They are called as "parent" compounds, in analogy to that in the cuprates, and are made superconductors by chemical substitution or oxygen reduction (in the case of 1111)—"doping" and by external pressure (in the case of 122). The other two, 111 and 42622, are "self-doped" superconductors. The normal state (above  $T_c$ ) of the SC region is in most cases paramagnetic and tetragonal in structure. The  $\alpha$ -PbO type FeSe is a superconductor in its own with low  $T_c = 8$  K, but  $T_c$  is enhanced to ~35 K by alkaline atom (K or Rb) doping into a modified Fe-deficient compound,  $K_x Fe_{2-\nu} Se_2$ . The maximum  $T_c$  value,  $T_c^{max}$ ranges from 8 K (for 11), 22 K (for 111), 39 K (for 122) to 55 K (for 1111) across the Fe-SC family. Also, in each family  $T_c^{\text{max}}$  significantly varies, e.g., between 26 K (LaFeAsO<sub>1-x</sub>F<sub>x</sub>) and 55 K (SmFeAsO<sub>1-x</sub>F<sub>x</sub>) for 1111, depending on the constituent elements other than Fe and As (Se) and degree of disorder.

## 4.2.2 Parameters that Influence $T_c$

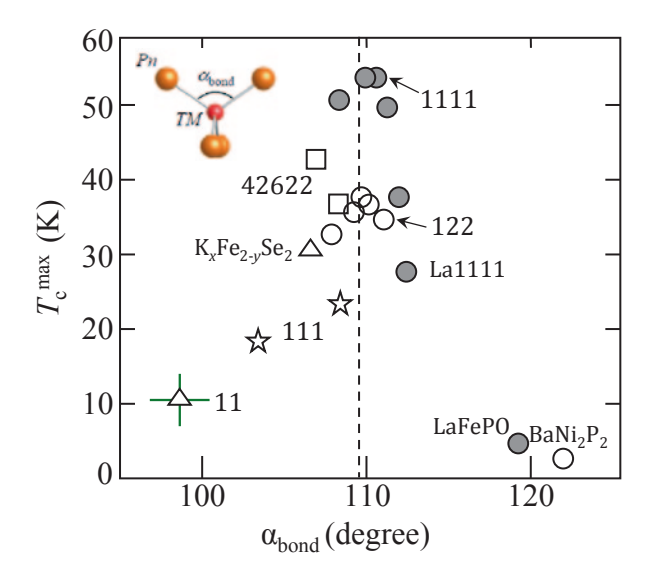
The key parameter is again *doping* that induces SC and hence controls  $T_c$ , but somewhat in a different ways from that in the cuprates. As in the case of the cuprates, the major doping process is chemical substitution for constituent cations or oxygen reduction. For 1111, e.g., LaFeAsO, the electron doping is made by various processes, (i) F-substitution for O, LaFeAsO $_{1-x}F_x$ , (ii) O-reduction, LaFeAsO $_{1-y}$ , and (iii) hydrogen (H<sup>-</sup>) substitution for O, LaFeAsO<sub>1-x</sub>H<sub>x</sub>. For 112, BaFe<sub>2</sub>As<sub>2</sub>, both electron and hole dopings are possible, e.g., Ba(Fe<sub>1-x</sub>Co<sub>x</sub>)<sub>2</sub>As<sub>2</sub> for the former and Ba<sub>1-x</sub>K<sub>x</sub>Fe<sub>2</sub>As<sub>2</sub> for the latter. In this case, even "isovalent" doping, either BaFe<sub>2</sub>( $As_{1-r}P_r$ ), or Ba(Fe<sub>1-x</sub>Ru<sub>x</sub>)<sub>2</sub>As<sub>2</sub>, induces superconductivity. As will be discussed in 4.5, a major effect of doping is not necessarily changing the carrier density. Doping tunes the lattice parameters and, the strength of electronic correlations as well. Differences from the cuprates are also (i) the parent compounds, e.g., BaFe2As2, are metals, and (ii) even doping, chemical substitution, into the active Fe-As (Se) layer induces SC. The parent compounds of the cuprates are Mott (or charge-transfer) insulators, and only one type of carriers can be doped to induce superconductivity. Moreover, direct chemical substitution, such as Zn or Ni for Cu, in the CuO, plane can never drive SC but easily destroys SC.

**Disorder**, to some but lesser extent than in the cuprates, affects  $T_{\rm c}$ . The maximum  $T_{\rm c}$  value,  $T_{\rm c}^{\rm max}$ , is significantly lower for materials doped into the active FeAs blocks than  $T_{\rm c}^{\rm max}$  achieved by doping into layers outside the FeAs block. For BaFe<sub>2</sub>As<sub>2</sub>,  $T_{\rm c}^{\rm max}$  decreases in the order of Ba<sub>1-x</sub>K<sub>x</sub>Fe<sub>2</sub>As<sub>2</sub> ( $T_{\rm c}^{\rm max}$ =39 K), BaFe<sub>2</sub>(As<sub>1-x</sub>P<sub>x</sub>)<sub>2</sub> ( $T_{\rm c}^{\rm max}$ =32 K), and Ba(Fe<sub>1-x</sub>Co<sub>x</sub>)<sub>2</sub>As<sub>2</sub> ( $T_{\rm c}^{\rm max}$ =25 K). This site-dependent disorder effect is similar to that in the cuprates, but a crucial difference is that even a substitution of other transition-metal element for Fe is not so destructive of SC. The low  $T_{\rm c}^{\rm max}$ =18–22 K for 111 materials, LiFeAs and NaFeAs, are ascribed to disorder in the layers of alkali-metal ions (Li or Na) which are incidentally located close to the As planes, while the disorder site located far away from the FeAs block is one of the reasons for the highest  $T_{\rm c}$  in 1111.

**Competing order**, which is widely agreed on, is the AFO order alone. It competes with SC in that SC emerges when AFO is suppressed both by doping and by applying pressure. However, in some materials, the AFO phase is sharply separated from the SC phase, and both coexist in others. Notably,  $T_{\rm c}$  is always maximal near the boundary of AFO and SC phases, and tends to decrease as one moves away from the AFO phase. Role of the AF order is apparently different from that in the cuprates.

The crystal structure seems more influential on  $T_c$  than doping, and there are actually correlations between  $T_c$  and some structural parameters. Just after the discovery, a correlation was found between  $T_c$  and the **Pn-TM-Pn bond angle**  $\alpha_{bond}$  (Pn and TM stand for pnictogen and transition-metal element, respectively) [8]. They found that  $T_c$  as a function of  $\alpha_{bond}$  is peaked at 109.5° which corresponds to the ideal (undistorted) TM-Pn<sub>4</sub> tetrahedron (see Fig. 4.3). This is particularly the case with the iron arsenides with highest  $T_c$  such as  $T_c = 50$  K-class 1111 and Ba<sub>1-x</sub>K<sub>x</sub>Fe<sub>2</sub>As<sub>2</sub>.

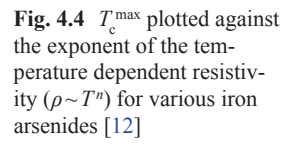
Fig. 4.3  $T_c$  vs Pn-TM-Pn bond angle (defined in the inset) plotted for various TM pnictides (simplified from that in Ref. [8]). The angle,  $109.5^{\circ}$ , of the ideal tetrahedron is indicated by the dashed line

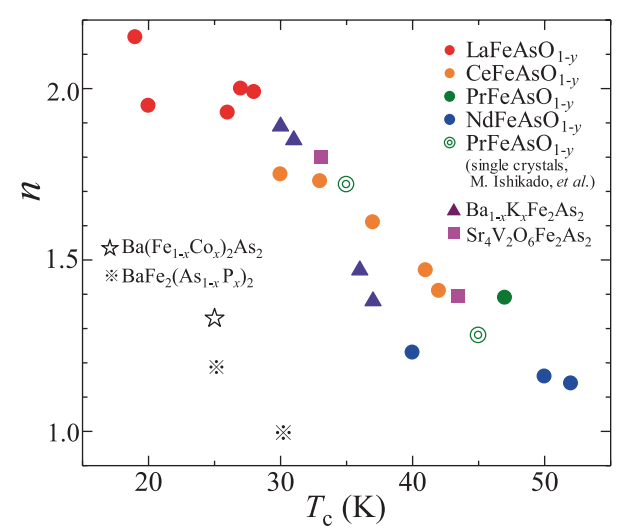


The lower  $T_{\rm c}$  (=26 K) for LaFeAsO<sub>1-x</sub>F<sub>x</sub> than that (55 K) for SmFeAsO<sub>1-x</sub>F<sub>x</sub> is ascribable to the larger bond angle. However, no unique correlation is found across the sub-families—CsFe<sub>2</sub>As<sub>2</sub> with  $T_{\rm c}$ =2.6 K is a known exception having  $\alpha_{\rm bond}$  close to 109.5°. It is theoretically an open question why the ideal tetrahedral configuration favors higher  $T_{\rm c}$ .

A closely related but alternative structure parameter is the distance of pnictogen (chalcogen) atom from the adjacent Fe layer (so called *pnictogen height* or anion height  $h_p$ ).  $T_c$  was found to have a peak around  $h_p \sim 1.38$  Å [9]. The theoretical calculations based on the spin-fluctuation-mediated pairing scenario show that the FS nesting condition and the appearance of an extra hole pocket are sensitively affected by a change of the pnictogen height [10]. They argue that large  $h_p$  favors nodeless sign reversing  $(s_+)$  pairing rather than nodal (e.g. d-wave) pairing and thereby favors high  $T_c$  owing to the robustness of SC against impurities. The pnictogen height is reminiscent of the apical-O distance of the cuprates. However, the former would have more direct relevance to the electronic state (affecting the nearest neighbor hopping t) of iron pnictides as the FePn block is an active layer, while the apical-O is outside the active  $\text{CuO}_2$  plane (affecting the long distance hopping, t'). Again, at present it is not clear whether the above theoretical explanation is generically applicable across different TM pnictides and Fe selenides sub-families.

In conventional superconductors  $T_{\rm c}$  is more or less correlated with the magnitude of resistivity in the normal state, since the electron-phonon interaction is responsible for both SC and scattering of carriers. By contrast, the optimally doped cuprates show universal **T-linear resistivity** in the normal state irrespective of the  $T_{\rm c}^{\rm opt}$  values. Fe-SCs show both features. Like the cuprates, the resistivity for the compound that is "optimally doped", tends to be dominated by a linear-in-T term regardless of its  $T_{\rm c}$  value [11]. On the other hand, as plotted in Fig. 4.4 mainly for





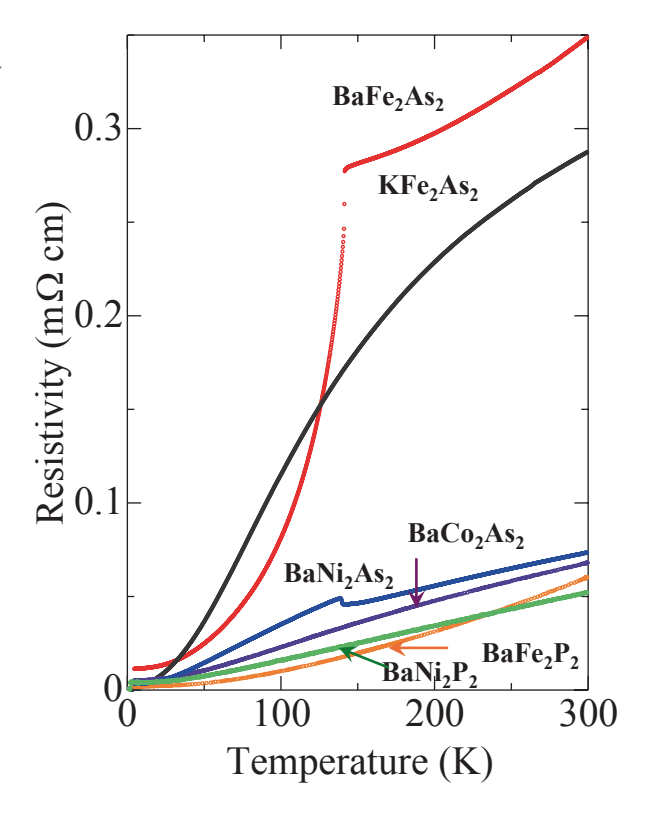
the 1111 family, the compounds with 50 K-class, e.g., NdFeAsO $_{1-x}F_x$ , show T-linear resistivity, whereas the low- $T_c$  members, e.g., LaFeAsO $_{1-x}F_x$ , show  $T^2$  dependence, typical of a Fermi liquid, indicating that stronger electron scattering favors higher  $T_c$  [12]. The correlation between electron scattering strength and  $T_c^{max}$  suggests that scattering from some (bosonic) excitations which gives rise to the T-linear resistivity is relevant to stronger pairing interaction in Fe-SCs. This is similar to conventional superconductors of the electron-phonon mechanism, but is in contrast to the cuprates in which the T-linear resistivity is generic for optimally doped materials irrespective their  $T_c$  values.

## 4.3 Uniqueness of Iron Arsenides/Selenides

#### 4.3.1 Unique Fe-As(Se) Combination

So far hundreds of transition-metal (TM) pnictide and chalcogenide compounds with similar structures have been synthesized. To date, only iron-arsenides and selenides show superconductivity with  $T_{\rm c}$  well above 20 K. One of the unique features of the iron arsenides/selenides is that they show the AFO order in their "undoped" and sometimes in the "heavily doped" regimes, indicating that the electrons in the Fe 3d orbitals or a part of them are on the verge of localization. Another unique feature is that the normal-state resistivity is distinctly high (typically 200–400  $\mu\Omega$  cm at room temperature) among other metallic TM pnictides, as displayed in Fig. 4.5 for various TM pnictides with the same 122 structure. The high resistivity is indicative of either low carrier density or strong carrier scattering or both.

Fig. 4.5 Temperature dependent in-plane resistivity measured for various transition-metal pnictides with the same "122" structure



Fe-SCs are, in common with the cuprates, combinations between 3d-TM and anions with filled s/p orbitals. The basic physics is, however, is entirely different. The main electronic bands around the Fermi level are basically Fe 3d-derived bands with all five 3d orbitals involved. Every Fe atom is tetragonally coordinated by As (Se) atoms, and the Fe layer in which the Fe atoms form a simple square lattice is sandwiched between two As slabs. Because of this, the hybridization between Fe and As is not strong and also the electronegativity of As ion (As<sup>3-</sup>) is much smaller than that for  $O^{2-}$ . However, this does not mean that As (Se) atoms are irrelevant. The heavy As (Se) 4p orbitals are much spread in space as compared with the O2p orbitals and highly polarizable which are affected sensitively by extra charges in their vicinity. The unique electronic properties, the fragile AF spin order, itinerant electrons, superconductivity, are probably, in part, ascribable to the large As (Se) polarizability [13].

## 4.3.2 Unique Electronic State

The electronic structure of Fe-SC (specifically iron arsenides) in the normal state, i.e., in the paramagnetic-tetragonal (PT) phase, is well described by the band structure derived from Fe 3*d*- orbitals. Fermi surface (FS) consists of two or three

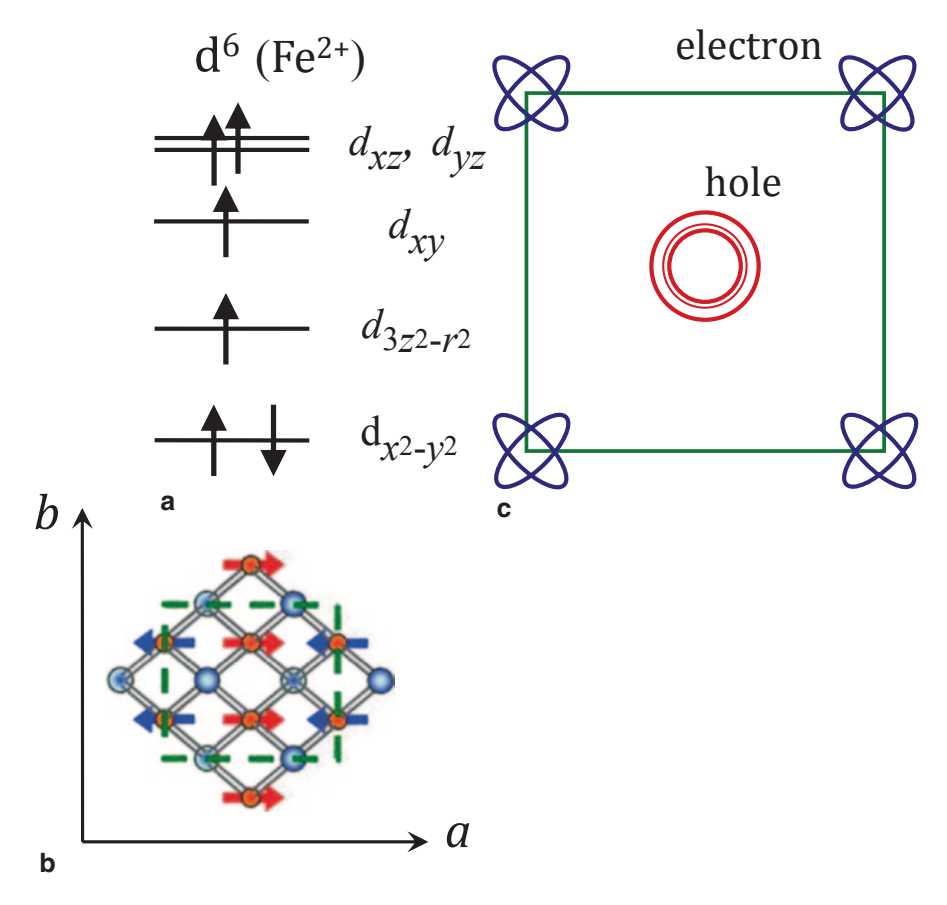


Fig. 4.6 a Electron filling of the 3d orbitals in the  $Fe^{2+}$  state. **b** Magneto-structural ordered state with collinear AF spin order and orthorhombic lattice distortions. **c** Schematic picture of Fermi surface typical of iron arsenides in the high-temperature tetragonal phase

hole pockets around the Brillouin zone (BZ) center and two electron pockets centered at  $(0, \pm \pi)$  and  $(\pm \pi, 0)$  zone boundary [14] (schematic sketch of FS is shown in Fig. 4.6). To be strict, the presence of two inequivalent As sites (above and below the Fe lattice layer, sketched in Fig. 4.1b) makes the BZ folded to contain two Fe atoms in a unit cell and put the electron FS pockets at the BZ corners  $(\pm \pi, \pm \pi)$ . These FS pockets have quasi-2D cylindrical shapes. Some of them are warped along the c axis (cylindrical direction), so that the electronic properties are not two-dimensional but anisotropic 3D metallic. The calculated band structures, mainly by LDA, qualitatively agree with the experiments such as ARPES and quantum oscillations.

#### 4.4 Phase Diagram and Competing Order

#### 4.4.1 Temperature-Doping Phase Diagram

There are two classes of materials showing distinct temperature (T)-doping (x) phase diagram. As schematically shown in Figs. 4.7a and b, in one class, LnFeAsO $_{1-x}F_x$  (Ln=La and Nd) and Sr(Ca)Fe<sub>2</sub>As<sub>2</sub>, the AFO and SC phases are sharply separated by a first-order like phase transition and do not overlap [15]. SmFeAsO $_{1-x}F_x$  [16] and the doped BaFe<sub>2</sub>As<sub>2</sub> systems belong to the second class in which both phases overlap and coexist over a range of doping. Whether AFO and SC are phase-separated or uniformly coexist is still a matter of debate. Also material dependent are the two transition temperatures that characterize the AFO phase, the tetragonal-orthorhombic structural transition at  $T_s$  and the paramagnetic-antiferromagnetic transition at  $T_N$ .  $T_s$  coinsides with  $T_N$  in 122 compounds, whereas  $T_s$  is higher than

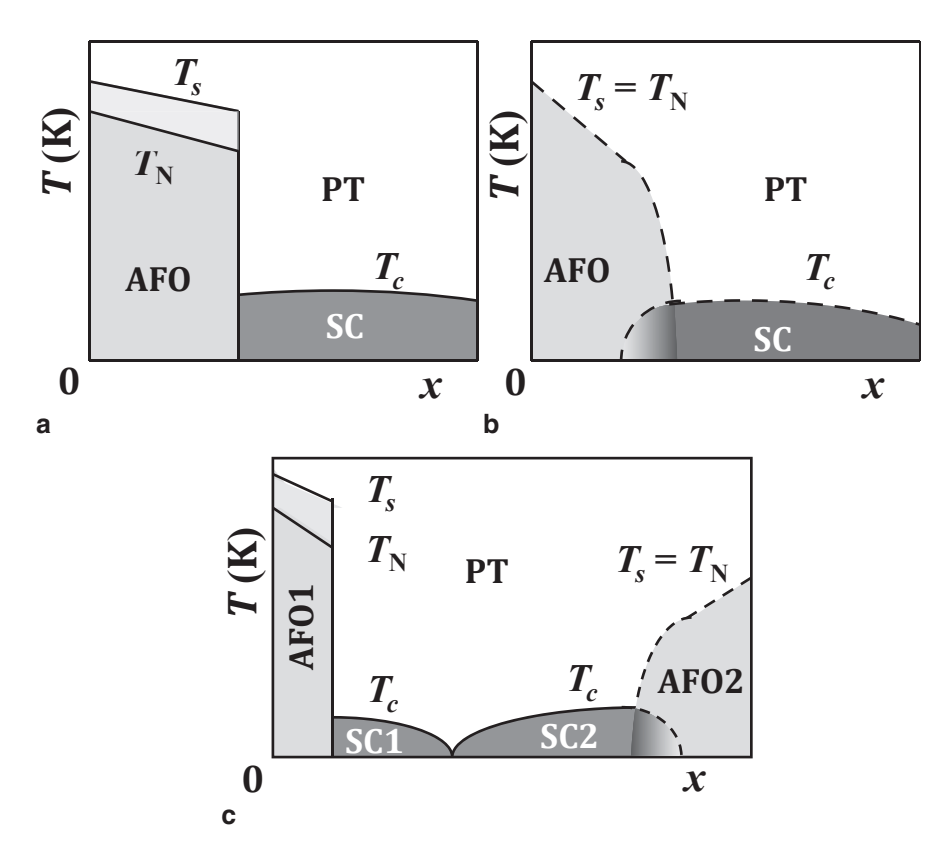


Fig. 4.7 a, b Two types of the temperature (T)—doping (x) phase diagram, schematically drawn. c A new type of phase diagram has been reported with double  $T_c$  domes and bipartite antiferromagnetic phases [19, 21]

 $T_{\rm N}$  in 1111 compounds. The material parameters that make such difference are not known yet.

A hotly debated issue concerning the T-x phase diagram is on the presence or otherwise of a quantum critical point (QCP) near the AFO-SC phase boundary and 'nematic' fluctuations in the PT phase. The latter is conceivably associated with this putative QCP and with the electronic anisotropy seen in the AFO phase. The experimental results supportive for nematicity are the resistivity anisotropy persisting to well above  $T_s$  in the AFO phase of the Co underdoped Ba(Fe<sub>1-x</sub>Co<sub>x</sub>)<sub>2</sub>As<sub>2</sub> [17] and the weak magnetic anisotropy in the PT phase detected by magnetic torque measurements on BaFe<sub>2</sub>(As<sub>1-x</sub>P<sub>x</sub>)<sub>2</sub> [18]. It is not clear yet If the nematic state/phase and/or QCP are generic to Fe-SCs, considering that such anisotropy has ever been observed for the doped SrFe<sub>2</sub>As<sub>2</sub> (CaFe<sub>2</sub>As<sub>2</sub>) system which not only shows a sharp first-order phase transition at  $T_s$  from AFO to PT but also a sharp (first-order transition like) change from AFO to SC (PT) as a function of doping concentration.

 $T_{\rm c}$  is always maximal near the boundary of AFO and SC phases including the coexisting region. As  $T_{\rm c}$  tends to decrease at higher doping levels or as one moves away from the AFO phase, the  $T_{\rm c}$  vs doping or pressure characteristics forms a flattop half-dome shape. For one of the electron-doped systems, LaFeAsO<sub>1-x</sub>H<sub>x</sub>, two-dome structure is observed [19] (two domes are also observed for K<sub>x</sub>Fe<sub>2-y</sub>Se<sub>2</sub> and related compounds as a function of pressure [20]). In the former case, the second dome ends up when the second antiferromagnetic phase shows up at  $x \sim 0.5$  [21]. Interestingly, in both cases  $T_{\rm c}^{\rm max}$  is higher for the second dome, 36 K in comparison with 26 K for the first dome (32 K for the first and 48 K for the second dome in the case of pressure-tuned K<sub>x</sub>Fe<sub>2-y</sub>Se<sub>2</sub>). It remains to be seen if the two-dome structure in the phase diagram is a generic feature of Fe-SCs.

## 4.4.2 Nature of the Competing Order

#### 4.4.2.1 Origin of Magnetism

It was hotly debated whether the magnetic order in the AFO phase is due to spins localized on Fe atoms or whether it originates from itinerant magnetism more properly described by a spin-density-wave (SDW) order due to (nesting) instability of the FS. Nominal Fe valence is Fe<sup>2+</sup> with  $3d^6$  electron filling which takes either highspin state with spin quantum number S=2, shown in Fig. 4.6a or non-magnetic lowspin state with S=0, depending on the strength of the Hund's rule coupling. Finite Fe magnetic moments are observed, though the magnitude is smaller  $(0.5-2.1 \mu_B)$ . than that expected from the S=2 local spins which indicates that a localized spin picture appears more appropriate. Real-space spin arrangement consists of spins aligned antiferromagnetically along the tetragonal a-axis and ferromagnetically along the b axis, so-called "collinear" AF spin order (shown in Fig. 4.6b). A lot of efforts have been devoted to elucidate that a localized spin model has any validity for an obviously metallic system [22]. Regardless of the exact description of spins,

it is clear that magneto structural coupling between electrons, both spin and orbital degrees of freedom, and lattice is important in Fe-SC in the AFO phase and perhaps in the SC phase. In fact, the magnetic transition (at  $T_{\rm N}$ ) is always accompanied by a structural phase transition (at  $T_{\rm S}$ )—from tetragonal to orthorhombic, and  $T_{\rm S}$  is equal to or higher than  $T_{\rm N}$ .

An antiferromagnetically ordered phase in proximity to the SC phase is universally observed in superconductors with strongly correlated electrons. The AF long-range order in the undoped and dilutely doped cuprates, which are insulating, is realized by an arrangement of Cu spins on a square lattice. On the other hand, the collinear (bi-collinear in FeTe) AF order in Fe-SCs, a stripy spin arrangement in the Fe layer, preserves a metallic state. Despite the high spin quantum number S=2 of Fe<sup>2+</sup>, the AFO order is easily suppressed by chemical substitution (doping) and pressure, giving a way to SC. No doubt, the partner anion, As or Se, with high polarizability conspires to form this unique AFO order. It is the only known order that competes with SC in Fe-SCs in contrast to the cuprates with a variety of competing phases, SDW, CDW, stripe order, and in particular the pseudogap (PG) phase. As will be discussed below, its peculiar electronic state and close connection to SC are reminiscent of PG in the underdoped cuprates.

#### 4.4.2.2 Electronic Anisotropy

BaFe<sub>2</sub>As<sub>2</sub> is a representative parent compound and undergoes a tetragonal-orthorhombic structural phase transition at temperature  $T_{\rm s}$  (= 143 K) with a shorter b axis and a longer a axis in the orthorhombic phase [23]. At the same temperature (or slightly lower temperature  $T_{\rm N}$  in some other parent compounds) the collinear AF order takes place. Reflecting the tetragonal (4-fold rotation) symmetry breaking, the AFO phase shows various anisotropic electronic properties such as anisotropic spin and charge excitations detected by the neutron scattering [24] and by optical measurement [25], respectively. Among them probably the most unusual is the inplane resistivity. The resistivity anisotropy measured on a BaFe<sub>2</sub>As<sub>2</sub> single crystal detwinned by uniaxial pressure is vanishingly small at low temperatures (see Fig. 4.8a), but the anisotropy emerges upon doping Co.

The almost isotropic resistivity for the undoped compound contrasts the robust and pronounced anisotropy seen in the optical conductivity spectrum [25] shown in Fig. 4.8b. In the AFO phase below  $T_s$ , the optical conductivity measured on a detwinned crystal of BaFe<sub>2</sub>As<sub>2</sub> is higher for light polarization along the a axis ( $\sigma_a(\omega)$ ) than that for b-axis polarization ( $\sigma_b(\omega)$ ) in the energy region below 1350 cm<sup>-1</sup> ( $\sim$ 0.15 eV). The anisotropy is reversed above this energy, and the anisotropy persists up to energy  $\sim$ 2 eV. Upon lowering T below  $T_s$ , the spectra for both polarizations exhibit a gap feature—the low-energy conductivity is suppressed and transferred to the higher energy region as the AFO order develops. The anisotropy arises from a difference in the gap energy scales for different polarization. As displayed in Fig. 4.8c, the b-axis gaps are larger in energy the a-axis ones which make  $\sigma_b$  lower than  $\sigma_a$  in the low energy region. One of the origins of the gap anisotropy is

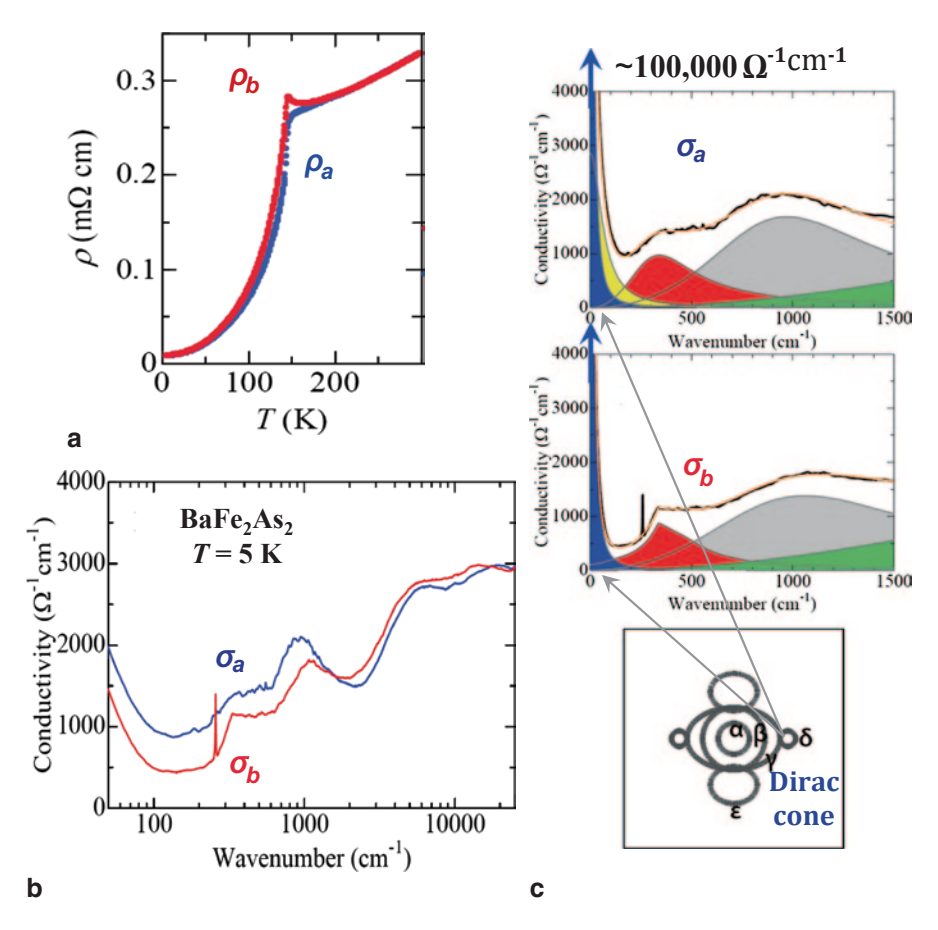


**Fig. 4.8** a In-plane resistivity along two orthorhombic axes (a and b, defined in Fig. 4.6b) measured for a detwinned single crystal of BaFe<sub>2</sub>As<sub>2</sub> with improved quality [25]. **b** Optical conductivity spectra of BaFe<sub>2</sub>As<sub>2</sub> for light polarization along the a- and b-axis direction, measured at T=5 K deep inside the AFO phase [25]. **c** Decomposition of the low-energy optical conductivity spectra for a-axis and b-axis polarization shown on a logarithmic frequency (wavenumber) scale. The pronounced sharp Drude peak observed in both spectra originates from the small Fermi surface pockets of Dirac electrons inherent to the AFO phase [27] as shown in the attached sketch below

the energy splitting between  $d_{xz}$ -orbital derived and  $d_{yz}$ -orbital derived bands [26], which are degenerate in energy in the PT phase, due to the (tetragonal) symmetry breaking in the AFO phase.

In the lowest energy region both spectra are dominated by a sharp Drude conductivity peak. The width of this peak becomes extremely narrow and its peak height becomes extremely large (exceeding 30,000  $\Omega^{-1}$  cm<sup>-1</sup> at T=5 K). The almost isotropic resistivity at low temperature stems from this gigantic Drude peak present in both spectra. This peak originates from small electron-FS pockets associated with the energy bands showing Dirac-cone-shaped dispersions (see the sketch in Fig. 4.8c). The presence of the "Dirac" bands is not accidental but is created by the

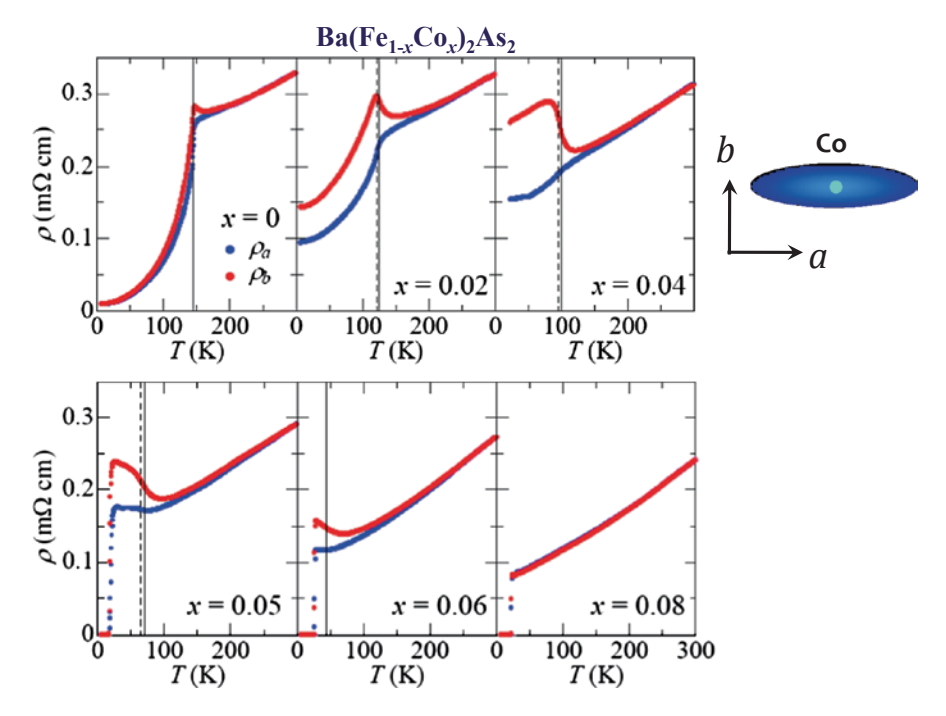


Fig. 4.9 Evolution of anisotropic resistivity with Co doping into BaFe<sub>2</sub>As<sub>2</sub> [28]. An impurity state formed around a Co impurity is schematically sketched

special electronic situation in the AFO phase [27]. Unique topological nature of the band structure inhibits the backscattering of electrons from impurities, making the electron mobility very high. The Dirac electrons are robustly present in the Co doped compounds as long as the AFO order is established, as they are protected the unique topology (parity) of the relevant bands in the AFO phase.

Upon Co doping into BaFe<sub>2</sub>As<sub>2</sub>, the resistivity becomes highly anisotropic, and to the contrary, the anisotropy in optical conductivity is diminished [28]. Co impurities induce a resistivity anisotropy on one hand, but suppress the anisotropic AFO order parameter on the other. As a consequence of this competition, the magnitude of the resistivity anisotropy, as a function of Co content, initially increases, eventually levels off, and then decreases as doping proceeds in the AFO phase, as shown in Fig. 4.9. The resistivity along the *b* axis ( $\rho_b$ , in the direction of shorter lattice constant and ferromagnetic spin alignment) is found always higher than that along the *a* axis ( $\rho_a$ , in the direction of longer axis and AF spin alignment). This is counter-intuitive to conventional wisdom, e.g., the double-exchange mechanism. The analysis of the optical conductivity spectrum indicates that anisotropy in resistivity arises from the anisotropic scattering cross-section of a Co impurity for the isotropic Dirac electrons. With Co doping, the peak in  $\sigma_b$  ( $\omega$ ) is more rapidly broadened and hence the peak height is more rapidly lowered with Co doping, resulting in the dc resistivity anisotropy  $\rho_b > \rho_a$ .

In the high-temperature PT phase, the Co atom substituted for Fe is not a strong impurity and only supplies one extra electron carrier. It dramatically changes its nature in the AFO phase. A Co atom introduced into the FeAs blocks is supposed to polarize its electronic and lattice surroundings anisotropically and thereby forms an anomalous impurity state with an anisotropic scattering cross section for charge carriers. The speculation is supported by the direct STM observation [29] of an anisotropic impurity state around a doped Co atom with electron cloud more extended along the *a* axis. It may be that an extra electron around a Co atom modulates the collinear AF spin arrangement locally and/or that it induces a local orbital order by distorting the underlying orthorhombic lattice. The same but weaker dopant induced anisotropy is observed in the AFO phase of P-Ba122, but almost no anisotropy is observed for K-Ba122 [30]. The dopant-site dependence indicates that the magnitude of resistivity anisotropy depends on the strength of dopant impurity potential.

The striking anisotropy in the phonon intensity is also seen in the optical conductivity spectrum [25, 28]. An optical phonon seen at 257 cm<sup>-1</sup> in the spectrum in the PT phase (presumably the phonon mode corresponding to the relative displacements of Fe and As atoms) enhances its intensity in  $\sigma_b$  ( $\omega$ ) and entirely looses the intensity in  $\sigma_a$  ( $\omega$ ) (see Figs. 4.8b and c). It is not a new phonon mode appearing in the AFO ordered state, but its polarization-selective intensity appears to require the presence of an anisotropic polarization field induced by the dynamical lattice distortion. The induced polarization cancels the dipole field associated with the optical phonon mode in the a direction, whereas it reinforces the dipole field along the b direction. Both charge and orbital degrees of freedom would be involved to form this dynamical polarization field.

The AFO phase is thus an unusual metal showing strongly anisotropic response to static impurities and to a dynamical lattice distortion. This phase is unique to the compounds of Fe with  $3d^6$  electronic configuration in combination with heavy As (Se) anions with high polarizability, and may be regarded as an ordered state of spin-charge-orbital-lattice complex. The fact that  $T_c$  attains maximum values near the AFO-SC phase boundary suggests that the fluctuations of this complex order might play a relevant role in the formation of Cooper pairs in Fe-SCs.

## 4.4.3 Unconventional Superconductivity

Superconductivity in Fe-SCs is almost certainly unconventional with sign-changing order parameter ( $\Delta$ ) [31]. In Fig. 4.10 are shown possible gap symmetries in Fe-SCs proposed so far. It turns out that, unlike the d-wave gap in the cuprates, the positions of the gap nodes are both material and doping dependent. In some cases no gap nodes are observed on FS and in others the nodes are located on FS [32]. In the former case, typically for Ba<sub>1-x</sub>K<sub>x</sub>Fe<sub>2</sub>As<sub>2</sub> in the x region lower than 0.8 and Fe(Se, Te), gap on the electron-FS pockets around the BZ corner has an opposite sign to that on the hole-FS pockets around the zone center which are well separated in the BZ, so that, each FS is fully gapped like s-wave gap. The gap nodes should lie at

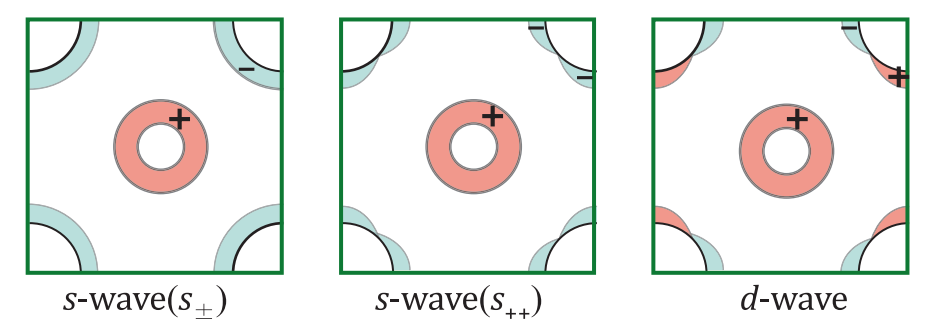


**Fig. 4.10** Superconducting gap and its sign for three types of pairing symmetry,  $s_+$ ,  $s_+$ , and d, mapped on the Fermi surface of a typical iron-based superconductor. For simplicity, only one hole and one electron Fermi surface pockets are shown

some positions in between both types of FS which are not necessarily high symmetry points. This gap symmetry corresponds to that so-called  $s_{+-}$  wave. The interband electron-hole interaction presumably linked to the spin (orbital) fluctuations was thought to give rise to electron pairing. When the K-content further increases close to x=1 and the electron-FS pockets completely disappear, nodes appear on the hole-FS around the BZ center. This was interpreted as a change of the gap symmetry from  $s_{+-}$  to d, But the recent thermal conductivity and magnetic penetration depth measurements have suggested that the gap nodes shift to the positions between hole-FS pockets around the zone center with basically s-wave symmetry gap ( $s_{++}$  gap with accidental nodes). The shift of the nodes with change of doping and/or disorder indicates that the gap nodes are not symmetry protected due to multiband FS structure of Fe-SCs in stark contrast to the robust (symmetry protected) d-wave gap nodes in the cuprites.

Considering that the high- $T_c$  superconductivity ( $T_c^{max} = 32 \text{ K}$ ) emerges in highly electron doped  $K_x Fe_{2-y}Se_2$  with no hole-FS pocket and possibly with unconventional pairing, electron-electron interaction, not specific to the electron-hole interaction or nesting between electron- and hole-FS, is generically important for superconductivity of Fe-SCs with multiband FS structure. Basically *s*-wave symmetry of the gap explains the robustness of SC against disorder/impurity even if their location is in the FeAs (FeSe) block. Also, similar to the cuprates, the superfluid density is small in most of Fe-SCs [33].

## 4.5 Role of Doping and Electronic Correlations

As was stated in the previous section, doping in Fe-SC is not simply changing charge (electron/hole) density or electron filling. Both electron and hole doping and even doping by substitution of isovalent atoms are possible to transform non-SC parent compound to superconductors. Also, modulation of local structure, FePn<sub>4</sub>

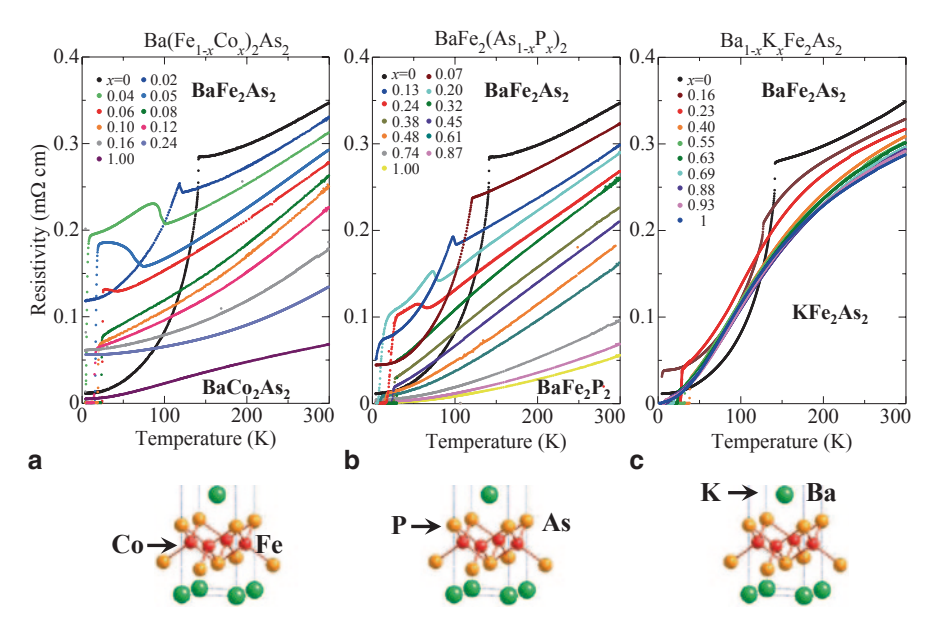


Fig. 4.11 Doping evolution of the temperature dependent in-plane resistivity for three types of doping into BaFe<sub>2</sub>As<sub>5</sub>; a electron (Co) doping, b isovalent P doping, and c hole (K) doping [40]

tetrahedron, significantly affects the electronic state and hence superconductivity, SC gap symmetry and/or  $T_{\rm c}$ . The systematic and comparative study of various doping processes in the parent compound BaFe<sub>2</sub>As<sub>2</sub> has given an important insight into the physical implication of the doping in Fe-SC. Doping, atomic substitution, is possible into all the three different lattice sites: Ba<sub>1-x</sub>K<sub>x</sub>Fe<sub>2</sub>As<sub>2</sub> (K-Ba122), BaFe<sub>2</sub>(As<sub>1-x</sub>P<sub>x</sub>)<sub>2</sub> (P-Ba122), and Ba(Fe<sub>1-x</sub>Co<sub>x</sub>)<sub>2</sub>As<sub>2</sub> (Co-Ba122) corresponding to hole, isovalent, and electron doping, respectively. Doping evolutions of the temperature-dependent resistivity are shown in Figs. 4.11a–c measured for the three types of doping into BaFe<sub>2</sub>As<sub>2</sub>.

## 4.5.1 Role of Doping

The resistivity of the parent BaFe<sub>2</sub>As<sub>2</sub> rapidly decreases below  $T_s$ =143 K, following  $T^2$  dependence, to very low values at lowest temperature [25]. It is, on the other hand, high above  $T_s$ ,  $\rho_{ab} \sim 300~\mu\Omega$  cm, comparable with that for optimally doped cuprates and shows only a weak T dependence. The optical conductivity spectrum of BaFe<sub>2</sub>As<sub>2</sub> in the PT phase shows a small peak at  $\omega$ =0 and a long tail merging into a peak of interband transitions at higher energies, similar to that of the high- $T_c$  cuprates in the normal state. The spectrum in the low energy region is better described by two Drude components with distinct character; one is narrow in width and having much smaller spectral weight (SW) and the other is broad with much bigger SW.

Hereafter, focus is on the PT phase. Upon Co substitution, *electron doping*, the resistivity gradually decreases toward x=1 (BaCo<sub>2</sub>As<sub>2</sub>). This is in contrast to that in the AFO phase, where major role of Co dopant is to produce an anisotropic impurity potential which electrons more strongly in one direction. Certainly, Co with one extra electron with respect to Fe supply electron carriers in the PT phase, as is also confirmed by a decrease in the Hall coefficient with negative sign [34] as well as by the ARPES study of FS with electron-FS pockets expanding and hole-FS shrinking with doping [35].

The *isovalent P doping* makes resistivity to gradually decrease as in the case of the Co doping which is rather surprising, since the isovalent P substitution for As does not supply either electron or hole. The ARPES-FS does not show an appreciable change with doping to explain a similar evolution of resistivity to that with Co doping [36]. What is actually going on is that the P doping increases the spectral weight (SW,  $\sim n/m^*$ ) of the narrow (coherent) Drude component [37] which is most likely associated with the electron-FS. The effect of P doping on the lattice is also appreciable. The substitution of P with smaller ionic radius results in a shrink of the unit-cell volume which leads to an increase of the bond angle  $\alpha_{\rm bond}$  (or decrease in the pnictogen height). So, a possible mechanism of P doping is to apply chemical pressure, making the electron mobility larger (more coherent) by widening the bandwidth or decreasing  $m^*$  which explain the increase of the coherent spectral weight.

Similarity of electron and isovalent doping effect is suggestive of striking electron-hole asymmetry in the PT phase of Fe-SCs. This corroborates the contrasting doping dependence of resistivity for *hole-doped K-Ba122*. The K substitution for Ba, hole doping, increases the hole density, as evidenced by ARPES-FS measurement—the hole FSs expand while the electron FSs shrink and eventually disappear [38, 39]. Nevertheless, the change of resistivity is modest, and the T dependence in the high T region remains weak. To reconcile the doping evolution of resistivity with that of ARPES-FS it is necessary to suppose that quasiparticles (QPs) on the hole-FS are incoherent, comprising a broad Drude component in the optical spectrum. In fact, the mean-free-path  $I_h = v_F \tau$ , estimated from the Drude width  $(1/\tau)$  and the Fermi velocity  $(v_F)$  determined by the ARPES measurement, is shorter than the lattice spacing a [40].

It is thus inferable that the doping evolution of resistivity, the  $\omega=0$  conductivity, is predominated by the electron-FS, forming the coherent Drude component, while the hole-FS contributes to conductivity as a nearly constant, incoherent, term. The contribution of the holes becomes apparent at high temperatures as a tendency for resistivity saturation, in particular, for K-Ba122, when the peak of the narrow, coherent, Drude is suppressed by its *T*-broadening. This indicates that the hole carriers are always subject to strong scattering. As plotted in Fig. 4.12, the coherent Drude spectral weight (SW)  $N_{\rm D}$ , or the fraction of  $N_{\rm D}$  in the low-energy SW, increases with Co (P) doping by increasing the density of electrons (or by decreasing the effective mass), whereas it does not, even decreases with K-doping. The decrease of  $N_{\rm D}$  in the case of K doping might be due to an increase of the effective mass, as the

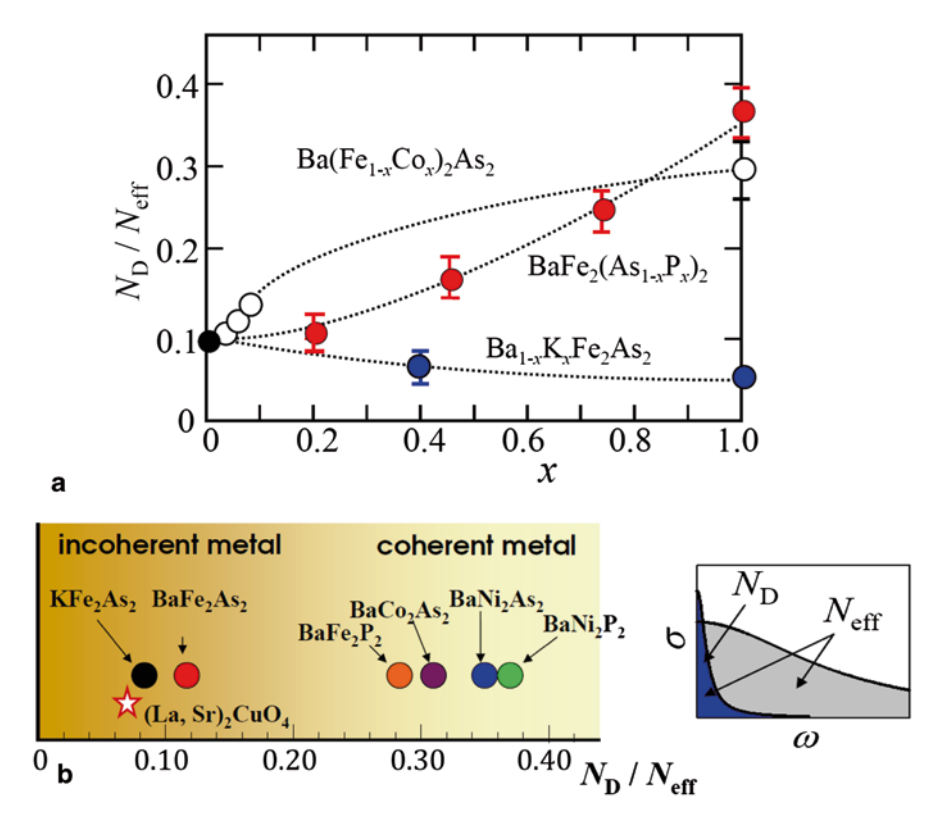


**Fig. 4.12** a Doping dependence of the fraction of the coherent Drude spectral weight  $N_{\rm D}/N_{\rm eff}$  in the low-energy optical conductivity spectrum for Co-, P-, and K-doped BaFe<sub>2</sub>As<sub>2</sub>. **b** Diagram showing the values of  $N_{\rm D}/N_{\rm eff}$  for various transition-metal pnictides with the same "122" crystal structure and one typical cuprate

measurement of quantum oscillations for KFe<sub>2</sub>As<sub>2</sub> reported an enhancement of the hole-carrier effective mass by a factor of 4–5 with respect to that for BaFe<sub>2</sub>As<sub>2</sub> [41].

As regards the SC phase induced by doping, it is surprising that either of three different types of doping leads to the emergence of SC. The critical doping level above which SC appears more or less depends on the suppression rate of the AFO ordering temperature  $T_{\rm s}$ . The same factors that influence  $T_{\rm c}$  value, disorder, electron filling, and local structure, would also affect  $T_{\rm s}$ , but it is still open why AFO and SC phases are sharply separated in some classes of materials, while they coexist in others.

Two important features emerge from these systematic studies. One is that, on looking at the change of the T-dependence of resistivity with doping, it is found that in the SC doping region the normal-state resistivity shows a sizable T-linear term and its coefficient is particularly large at dopings near the AFO-SC boundary or coexisting region where  $T_{\rm c}$  is highest. This tendency is often seen for SC in strongly correlated electron systems [42], such as the cuprates, heavy fermions, and

organic compounds. SC in these systems is argued in the context of quantum critical fluctuations near a QCP. The presence of a QCP at  $x \sim 0.3$  near the end point of the AFO-SC coexisting region is suggested for P-Ba122 [18]. At present, the quantum critical behavior does not seem a generic to Fe-SCs. No signatures suggestive of QCP are observed for Co-Ba122 and K-Ba122. For LnFeAsO<sub>1-x</sub>F<sub>x</sub> (Ln: La and Nd), the AFO and SC phases are sharply separated by a first-order like phase transition, and  $T_c$  is high over a wide range of doping, even two  $T_c$  domes are observed for LaFeAsO<sub>1-x</sub>H<sub>x</sub>. Apparently, a simple QCP scenario does not apply to Fe-SC as in the case of high- $T_c$  cuprates. Nevertheless, considering the fact that  $T_c$  attains large values near the AFO phase, it is likely that the fluctuations associated with the AFO phase play a crucial role in superconductivity.

#### 4.5.2 Electronic Correlations

Now there is wide consensus on the unconventional nature of the Cooper pairs with sign-changing SC gap (order parameter) in the momentum space. The phase diagram, T vs doping x and/or pressure P, is also quite similar to the cuprate phase diagram. The "parent" compound is an antiferromagnet with localized magnetic moment, and the AFO and SC phases are always next to each other. These facts are strongly suggestive of electronic correlations playing a dominant role in Fe-SCs as in the cuprates.

The origin of striking electron-hole asymmetry or incoherence/strong scattering of hole carriers deserves to explore to understand a role of electronic correlations in the emergence of superconductivity and unconventional pairing in Fe-SC. The parent compounds are metals, albeit not good metals, and are not close to a Mott insulating state, so the Fe arsenides and selenides are usually thought to be in the intermediate correlation regime. Nevertheless, they show features of strong correlations such as frozen spin magnetic moments and T-linear resistivity characteristic of a non-Fermi liquid. There exist theoretical attempts to solve this controversy by incorporating the effect of the Hund's rule coupling ( $J_{\rm H}$ ) in addition to the on-site Coulomb interaction (U) [43]. It is suggested that, even when  $J_{\rm H}$  and U are not large enough, both may cooperate to strengthen the correlation effect on particular 3d orbitals in multi-orbital metals.

Optical spectroscopy is used to probe the dynamical response of electrons to an external electromagnetic field and can provide information on the electronic correlations which impede the electronic motion. Figure 4.5 displays the in-plane resistivity for BaFe<sub>2</sub>As<sub>2</sub> and related isostructural compounds with various TM and Pn atoms. In the high T region, these are clearly separated into two groups. The iron arsenides, BaFe<sub>2</sub>As<sub>2</sub> and KFe<sub>2</sub>As<sub>2</sub>, have distinctly high resistivity from others. High resistivity in iron arsenides arises from the small SW,  $N_D$  ( $\sim n/m^*$ ), of the marrow (coherent) Drude component in the optical conductivity spectrum. The lowenergy spectrum is also dominated by another Drude component with extremely broad width (incoherent Drude). This is more the case with FeTe and K<sub>x</sub>Fe<sub>2-y</sub>Se<sub>2</sub>

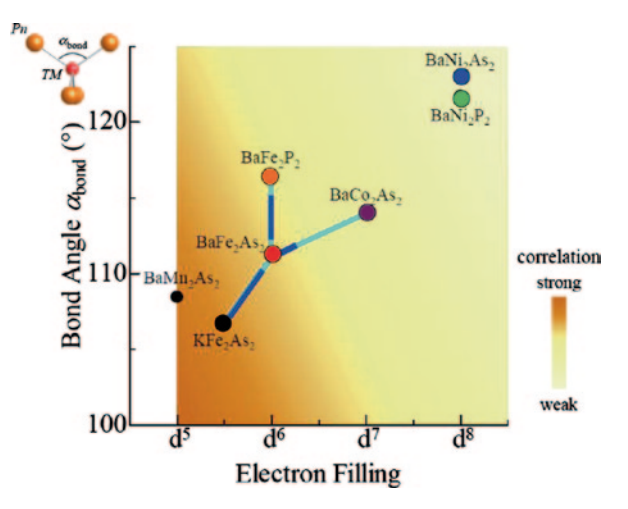
which have even higher resistivity and a tiny  $N_{\rm D}$  in the optical conductivity. The low-energy spectra of other TM pnictides are also roughly decomposed into two, but the distinction between the two is much less clear and  $N_{\rm D}$  occupies a substantial fraction of the low-energy SW. A fraction of  $N_{\rm D}$ ,  $N_{\rm D}/N_{\rm eff}$ , in the low-energy SW,  $N_{\rm eff}$ , which is approximated by the sum of dominant two Drude components, is a measure of the degree of coherence of carriers. If the incoherence arises from the electronic correlations, as, for instance in the cuprates, then,  $N_{\rm D}/N_{\rm eff}$  is a good indicator of the strength of correlations. The values of  $N_{\rm D}$  for iron arsenides are indeed small as compared with those for other TM pnictides, as displayed in Fig. 4.12b. They are comparable with the similarly estimated vales for the hole underdoped cuprates, e.g.,  $La_{2-x}{\rm Sr}_x{\rm CuO}_4$  with x=0.10 [44]. The incoherent charge dynamics in the cuprates certainly originates from strong U (or superexchange J) that frustrates coherent hole motion. Although U is not so large in FeAs, it is conceivable that the electronic correlations stem also from the Hund's coupling  $J_{\rm H}$  reflecting the multiorbital nature of the Fe-based compounds.

The two iron arsenides are found to have smaller Pn-TM-Pn bond angles than others.  $\alpha_{\rm bond}$  is nearly equal or somewhat smaller than 109.5° ( $\alpha_{\rm bond}$ =111.1 and 106.7° for BaFe<sub>2</sub>As<sub>2</sub> and KFe<sub>2</sub>As<sub>2</sub>, respectively), the bond angle for an ideal tetrahedron, whereas  $\alpha_{\rm bond}$ 's for other pnictides are significantly larger than 109.5° ( $\alpha_{\rm bond}$ =116.4° for BaFe<sub>2</sub>P<sub>2</sub> and 114.0° for BaCo<sub>2</sub>As<sub>2</sub>). In view of the trend that the width (W) of the relevant electronic bands (TM-3d and Pn-p orbitals derived bands) becomes larger for larger bond angles, an increase of  $\alpha_{\rm bond}$  works to weaken the electronic correlations by decreasing U/W and  $J_{\rm H}/W$ . In this regard, the major effect of P substitution for As in BaFe<sub>2</sub>As<sub>2</sub> is an application of chemical pressure, leading Ba122 toward weaker correlations. The Co doping works similarly, but the K doping goes the other direction, applying negative chemical pressure.

In the plot of  $N_D/N_{\text{eff}}$  as a function of x for three types of doping into BaFe<sub>2</sub>As<sub>2</sub> (Fig. 4.12), a remarkable difference is seen even between Co-Ba122 and P-Ba122. For Co-Ba122  $N_{\rm D}/N_{\rm eff}$  steeply increases upon Co doping, while the increase is gradual for P-Ba122 in contrast to the larger chemical pressure effect of P doping. This is suggestive of presence of additional effect of doping that probably originates from a change of the electron (hole) density with doping. The K substitution for Ba reduces the Fe3d orbital filling from  $d^6$  to  $d^{5.5}$ , whereas the Co substitution increases it toward  $d^7$ . Note that  $d^5$  is special, all the five 3d orbitals are singly occupied—just half filling, at which the electronic correlation is maximally strong [45]. In fact, BaMn, As, with d<sup>5</sup> is probably a Mott insulator and has a robust magnetic order [46]. In this regard, the hole (electron) doping, the decrease (increase) in the electron filling from  $d^6$  points toward stronger (weaker) correlation, explaining the striking electron-hole asymmetry in the doping effect. As was discussed in 4.5.1, even in a compound where both electron and hole carriers coexist, there is a remarkable asymmetry in the dynamics (scattering strength) between electrons and holes. So, it is likely that the asymmetry between quasiparticles on electron and hole FS is conceived to have an intimate connection to the above doping asymmetry.

Microscopically, the asymmetry would arise from the "orbital differentiation" or orbital-selective correlation effect [43]. Theoretically the electronic correlations

**Fig. 4.13** Various transition-metal pnictides mapped on the diagram of Pn-TM-Pn bond angle vs 3*d* electron filling of TM in the TM<sup>2+</sup> state. The dotted lines are trajectories of three types of doping into BaFe<sub>2</sub>As<sub>2</sub>. Superconductivity is observed on the trajectories indicated by solid lines. Variation of the strength of electronic correlations on the map is roughly shown in a gray scale



are considerably stronger on the  $3d_{xy}$  orbital as compared to those on  $3d_{yz}$  and  $3d_{xz}$  orbitals, so that electrons/holes on the  $3d_{xy}$  orbital are almost Mott localized [47]. The ARPES study has indeed confirmed that the states on the hole-FS in FeAs are predominantly of  $3d_{xy}$  character, while the states on the electron FS have relatively large  $3d_{yz}/3d_{xz}$  character [48]. The strong correlation, in particular the strong Hund's correlation tends to inhibit mixing of the orbitals, which would highly frustrate the hole motion. As the hole and electron FS pockets are located at different places in the momentum space, the orbital differentiation is at the same time the momentum differentiation which also characterizes the normal state of the high- $T_c$  cuprates, particularly in the underdoped region.

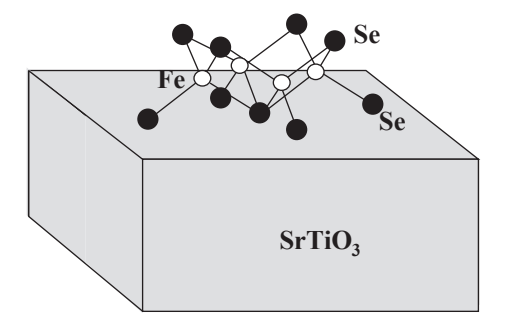
Putting the structural parameter  $(a_{bond})$  together with the electron filling (n) of the 3d orbitals, the diagram of  $\alpha_{bond}$  vs n, shown in Fig. 4.13, maps the strength of electronic correlations for various TM pnictides [49]. Both small  $\alpha_{bond}$  and low electron filling locate KFe<sub>2</sub>As<sub>2</sub> at the strongest correlations among various TM pnictides investigated here, and the Ni pnictides with larger  $a_{\rm bond}$  and higher filling are the weakest counterparts. This map just corroborates the result of  $N_{\rm D}/N_{\rm eff}$  shown in Fig. 4.12a. The diagram clearly indicates that a major role of doping into BaFe<sub>2</sub>As<sub>2</sub> is to tune the correlation strength, to weaker (stronger) correlations by Co and P doping (K doping). The diagram also suggests that superconductivity in the TM pnictides emerges in the doping region where fairly strong electronic correlations are sustained, and that either too strong or too weak correlations are not favorable for superconductivity with high  $T_c$  values. From the diagram high  $T_c$  turns out to be realized when the electron filling is near  $d^6$ , in between  $d^5$  (BaMn<sub>2</sub>As<sub>2</sub>) and  $d^7$ (BaCo<sub>2</sub>As<sub>2</sub>) and when the bond angle is around 109.5°, the angle for an ideal tetrahedron. The "optimal" bond angle is consistent with the empirical relationship between  $T_c$  and  $\alpha_{bond}$  shown in Fig. 4.3, and the 1111 members with 50 K-class  $T_c$ are also located in the vicinity of d6 filling and  $\alpha_{bond} = 109.5^{\circ}$ . The parent BaFe<sub>2</sub>As<sub>2</sub> itself is near this "optimal" point. Its ground state is the AFO ordered state, but it is readily converted to SC upon doping and by application of pressure.

## 4.6 Possibility of Enhancing T<sub>c</sub>

 $T_{\rm c}^{\rm max}$  = 55 K recorded for 1111 in 2008 remains to be highest among so-far known Fe-SCs, although  $T_{\rm c}^{\rm max}$  of other classes has been gradually improved. For 122  $T_{\rm c}^{\rm max}$  = 45–49 K was reported in  ${\rm Ca_{1-x}Ln_xFe_2As_2}$  [50] albeit small SC volume fraction (a new structure,  ${\rm Ca_{1-x}Ln_xFeAs_2}$  (112), was proposed which might be a superconductor with  $T_{\rm c}^{\rm max}$  higher than 40 K [51]). The iron arsenide with big building block,  ${\rm Sr_4V_2O_6Fe_2As_2}$ , has  $T_{\rm c}$  = 37 K at ambient pressure, but one of its relatives,  ${\rm Ca_4(Mg,Ti)_3Fe_2As_2O_{8-y}}$  shows SC at  $T_{\rm c}$  = 47 K [52]. The potassium-doped iron-deficient selenides,  ${\rm K_xFe_{2-y}Se_2}$  and (Tl, Rb) $_{\rm x}{\rm Fe_{2-y}Se_2}$ , also shows higher  $T_{\rm c}^{\rm max}$  = 48–49 K in its second  $T_{\rm c}$  dome realized under high pressure. Even for the 11-FeSe,  $T_{\rm c}$  goes up to 37 K upon application of pressure [53].

At the present stage, it seems that every family of Fe-SCs has a potential  $T_c^{\text{max}}$ of  $\sim 50$  K when optimized in structure and/or doping or disorder. This, in turn, suggests that there might be a ceiling of  $T_c^{\text{max}}$  in Fe-SCs. Unlike the cuprates which apparently have a room for  $T_c$  to be enhanced over the maximum value of 135 K at ambient pressure, there is no indication of a rise of  $T_c$  for the 1111 system with  $T_c$  = 55 K. However, a monolayer FeSe film grown on a SrTiO<sub>3</sub> (STO) substrate, schematically sketched in Fig. 4.14, was found to show a big magnitude of SC gap corresponding to a mean-field  $T_c^{\text{MF}}$  = 65 K [54]. The ARPES measurement on the same system observed a gap opening at 60-65 K [55], although zeroresistivity is observed only below ~30 K (recently one group has reported the film resistance drops to zero at  $T \sim 100 \text{ K}$  [56]). The recent ARPES measurement has suggested the coupling to the high-frequency (~1000 cm<sup>-1</sup>) phonon in the STO substrate might enhance  $T_c$  of FeSe with respect to the value that is sustainable for FeSe alone [57]. The  $T_c$  enhancement with a help from phonons in SCs is also one of the proposed scenario explaining the  $T_c$  enhancement in the cuprates with multilayer structure [58]. Fabrication of such a hetero-structure might a promising route toward higher  $T_c$ .

**Fig. 4.14** Schematic picture of monolayer FeSe deposited on a SrTiO<sub>3</sub> substrate



References 83

#### References

 Kamihara Y, Watanebe T, Hirano M, Hosono H (2008) Iron-based layered superconductor La[O<sub>1</sub>, F<sub>2</sub>]FeAs with T<sub>2</sub>=26 K. J Am Chem Soc 130:3296–3297. doi:10.1021/ja800073m

- Ren ZA et al (2008) Superconductivity at 55 K in iron-based F-doped layered quaternary compound Sm[O<sub>1.</sub>F]FeAs. Chin Phys Lett 25:2215–2216. doi:10.1088/0256-307X/25/6/080
- 3. Rotter M, Panger IM, Tegel M, Johrendt D (2008) Superconductivity and crystal structure of  $(Ba_{1-x}K_y)Fe_2As_2$  (x=0-1). Angew Chem Int Ed 47:7949–7952. doi:10.1002/anie.200803641
- 4. Wang XC et al (2008) The superconductivity at 18 K in LiFeAs system. Solid State Commun 148:538–540. doi:10.1016/j.ssc.2008.09.057
- Hsu FC et al (2008) Superconductivity in the PbO type structure α-FeSe. Proc Natl Acad Sci U S A 105:14262–14264. doi:10.1073/pnas.0807325105
- Guo JG et al (2010) Superconductivity in the iron selenide K<sub>x</sub>Fe<sub>2</sub>Se<sub>2</sub> (0≤x≤1.0). Phys Rev B 82:180520. doi:10.1103/PhysRevB.82.180520
- Zhu XY, Han F, Mu G, Cheng P, Shen B, Zeng B, Wen HH (2009) Transition of stoichiometric Sr<sub>2</sub>VO<sub>3</sub>FeAs to a superconducting state at 37.2 K. Phys Rev B 79:220512(R). doi:10.1103/ PhysRevB.79.220512
- Lee CH et al (2008) Effect of structural parameters on superconductivity in fluorine-free LnFeAsO<sub>1-v</sub> (Ln=La, Nd). J Phys Soc Jpn 77:083704. doi:10.1143/JPSJ.77.083704
- 9. Kuroki K, Úsui H, Onari S, Arita R, Aoki H (2009) Pnictogen height as a possible switch between high- $T_{\rm c}$  nodeless and low- $T_{\rm c}$  nodal pairings in the iron-based superconductors. Phys Rev B 79:224511. doi:10.1103/PhysRevB.79.224511
- Johnston DC (2010) The puzzle of high temperature superconductivity in layered iron pnictides and chalcogenides. Adv Phys 59:803–1061. doi:10.1080/00018732.2010.513480.1
- Kasahara S et al (2010) Evolution from non-Fermi-to-Fermi-liquid transport via isovalent doping in BaFe<sub>2</sub>(As<sub>1-x</sub>P<sub>x</sub>)<sub>2</sub> superconductors. Phys Rev B 81:184519. doi:10.1103/Phys-RevB.81.184519
- 12. Ishida S et al (2010) Strong carrier scattering in iron pnictide superconductors LnFeAsO<sub>1-y</sub> (Ln = La and Nd) obtained from charge transport experiments. Phys Rev B 81:094515. doi:10.1103/PhysRevB.81.094515
- Berciu M, Elfimov I, Sawatzky GA (2009) Electronic polarons and bipolarons in ironbased superconductors: the role of anions. Phys Rev B 79:214507. doi:10.1103/Phys-RevB.79.214507
- 14. Singh DJ (2009) Electronic structure of Fe-based superconductors. Physica C 469:418–424
- Luetkens H et al (2009) The electronic phase diagram of the LaO<sub>1-x</sub>F<sub>x</sub>FeAs superconductor. Nature Mater 8:305–309. doi:10.1038/nmat2397
- Drew AJ et al (2009) Coexistence of static magnetism and superconductivity in SmFeAsO<sub>1-x</sub>F<sub>x</sub> a revealed by moon spin rotation. Nature Mater 8:310–314. doi:10.1038/nmat2396
- Chu J-H et al (2010) In-plane resistivity anisotropy in an underdoped iron pnictide superconductor. Science 329:824

  –826. doi:10.1126/science.1190482
- Kasahara S et al (2012) Electronic nematicity above the structural and superconducting transition in BaFe<sub>2</sub>(As<sub>1-x</sub>P<sub>x</sub>)<sub>2</sub>. Nature 486:382–385. doi:10.1038/nature11178
- 19. Iimura S et al (2014) Two-dome structure in electron-doped iron arsenide superconductors. Nature Commun 3:943. doi:10.1038/ncomms1913
- Sun LL et al (2012) Re-emerging superconductivity at 48 kelvin in iron chalcogenides. Nature 483:67–69. doi:10.1038/nature10813
- Hiraishi M et al (2014) Bipartite magnetic parent phases in the iron oxypnictide superconductor. Nature Phys 10:300–303. doi:10.1038/nphys52906
- Yildirim T (2009) Strong coupling of the Fe-spin state and the As-As hybridization in ironprinciple superconductors from first-principle calculations. Phys Rev Lett 102:037003. doi:10.1103/PhysRevLett.102.037003

- Nandi S et al (2010) Anomalous suppression of the orthorhombic distortions in superconducting Ba(Fe<sub>1-x</sub>Co<sub>x</sub>)<sub>2</sub>As<sub>2</sub> single crystals. Phys Rev Lett 104:057006. doi:10.1103/PhysRev-Lett.104.057006
- Zhao J et al (2009) Spin waves and magnetic exchange interactions in CaFe<sub>2</sub>As<sub>2</sub>, Nature Phys 5:555–560. doi:10.1038/nphys1336.
- Nakajima M et al (2011) Unprecedented anisotropic metallic state in undoped iron arsenide BaFe<sub>2</sub>As<sub>2</sub> revealed by optical spectroscopy. Proc Nat Acad Sci U S A 108:12238–12242. doi:10.1073/pnas.1100102108
- Yin ZP, Haule K, Kotliar G (2011) Magnetism and charge dynamics in iron pnictides. Nature Phys 7:294–297. doi:10.1038/nphys1923
- Ran Y, Wang F, Vishwanath A, Lee D-H (2009) Nodal spin density wave and band topology of the FeAs-based materials. Phys Rev B 79:014505. doi:10.1103/PhysRevB.79.014505
- Nakajima M et al (2012) Effect of co doping on the in-plane anisotropy in the optical spectrum of underdoped Ba(Fe<sub>1-x</sub>Co<sub>x</sub>)<sub>2</sub>As<sub>2</sub>. Phys Rev Lett 109:217003. doi:10.1103/PhysRev-Lett.109.217003
- 29. Allan MP et al (2013) Anisotropic impurity state, quasiparticle scattering, and nematic transport in underdoped Ca(Fe<sub>1-v</sub>Co<sub>v</sub>)<sub>2</sub>As<sub>2</sub>. Nature Phys 9:220–224. doi:10.1038/nphys2544
- Ying JJ et al (2011) Measurement of the in-plane anisotropic resistivity of underdoped FeAs-based pnictide superconductors. Phys Rev Lett 107:067001. doi:10.1103/PhysRev-Lett.107.067001
- 31. Hanaguri T, Niitaka S, Kuroki K, Takagi H (2010) Unconventional s-wave superconductivity in Fe(Se, Te). Science 328:474–476. doi:10.1126/science.1187399
- Watanabe D et al (2014) Superconducting gap with sign reversal between hole pockets in heavily overdoped Ba, "K,Fe,As., Phys Rev B 89:115112, doi:10.1103/PhysRevB.89.115112
- Uemura YJ (2009) Commonalities in phase and mode. Nature Mater 8:253–255. doi:10.1038/ nmat2415
- 34. Rullier-Albenque F, Colson D, Forget A, Alloul H (2009) Hall effect and resistivity study of the magnetic transition, carrier content, and fermi-liquid behavior in Ba(Fe<sub>1-x</sub>Co<sub>x</sub>)<sub>2</sub>As<sub>2</sub>. Phys Rev Lett 103:057001. doi:10.1103/PhysRevLett.103.057001
- Sekiba Y et al (2009) Electronic structure of heavily electron-doped BaFe<sub>1.7</sub>Co<sub>0.3</sub>As<sub>2</sub> studied by angle-resolved-photoemission. New J Phys 11:025020. doi:10.1088/1367-2630/11/2/025020
- Shishido et al (2010). Evolution of the fermi surface of BaFe<sub>2</sub>(As<sub>1-x</sub>P<sub>x</sub>)<sub>2</sub> on entering the superconducting dome. Phys Rev Lett 104:057008. doi:10.1103/PhysRevLett.104.057008
- 37. Nakajima M et al (2013) Crossover from bad to good metal in BaFe<sub>2</sub>(As<sub>1-x</sub>P<sub>x</sub>)<sub>2</sub> induced by isovalent P substitution. Phys Rev B 88:094501. doi:10.1103/PhysRevB.88.094501
- 38. Liu C et al (2008) K-doping dependence of the fermi surface of the iron-arsenic Ba<sub>1-x</sub>K<sub>x</sub>Fe<sub>2</sub>As<sub>2</sub> superconductor using angle-resolved photoemission spectroscopy. Phys Rev 101:179005. doi:10.1103/PhysRevLett.101.179005
- 39. Malaeb W et al (2012) Abrupt change in the energy gap of superconducting Ba<sub>1-x</sub>K<sub>x</sub>Fe<sub>2</sub>As<sub>2</sub> single crystals with hole doping. Phys Rev B 86:165117. doi:10.1103/PhysRevB.86.165117
- 40. Nakajima M et al (2014) Normal state charge dynamics in doped BaFe<sub>2</sub>As<sub>2</sub>: role doping and necessary ingredients for superconductivity. Sci Rep 4:5873. doi:10.1038/srep05873
- 41. Terashima T et al (2010) Fermi surface and mass enhancement in  $KFe_2As_2$  from de Haas-van Alphen effect measurements. J Phys Soc Jpn 79:053702. doi:10.1143/JPSJ.79.053702
- 42. Norman MR (2011) The challenge of unconventional superconductivity. Science 332:196–200. doi:10.1126/science.1200181
- 43. Georges A, de'Medici L, Mravlje J (2013) Strong correlations from Hund's coupling. Annu Rev Condens Matter Phys 4:137–178. doi:10.1146/annurev-conmatphys-020911-125045
- 44. Uchida S, Ido T, Takagi H, Arima T, Tokura Y, Tajima S (1991) Optical spectra of La<sub>2-x</sub>Sr<sub>x</sub>CuO<sub>4</sub>: effect of carrier doping on the electronic structure of the CuO<sub>2</sub> plane. Phys Rev B 43:7942–7954
- Misawa T, Nakamura K, Imada M (2012) Ab initio evidence for strong correlation associated with mott proximity in iron-based superconductors. Phys Rev Lett 108:177007. doi:10.1103/ PhysRevLett.108.177007

References 85

Singh Y, Green MA, Huang Q, Kreyssig A, McQueeney RJ, Johnston DC, Goldman AI (2009) Magnetic order in BaMn<sub>2</sub>As<sub>2</sub> from neutron diffraction measurements. Phys Rev B 80:100403 (R). doi:10.1103/PhysRevB.80.100403

- de'Medici L, Giovannetti G, Capone M (2014) Selective mottness as a key to iron superconductors. Phys Rev Lett 112:177001. doi:10.1103/PhysRevLett.112.177001
- 48. Yi M et al (2013) Observation of temperature-induced crossover to an orbital-selective mott phase in A<sub>x</sub>Fe<sub>2-y</sub>Se<sub>2</sub> (A = K, Rb) superconductors. Phys Rev Lett 110:067003. doi:10.1103/PhysRevLett.110.067003
- Nakajima M et al (2014) Strong electronic correlations in iron pnictides: comparison of the optical spectra for BaFe<sub>2</sub>As<sub>2</sub>-related compounds. J. Phys. Soc. Jpn. 83: 104703. doi: 10.7566/ JPSJ.83.104703
- Wei FY, Lv B, Deng LZ, Meen JK, Xue YY, Chu CW (2013) Why is the superconducting T<sub>c</sub> so high in rare-earth-doped CaFe, As,? http://arXiv.org/abs/1309.0034. Accessed 6 Sept 2013
- 51. Kudo K et al (2014) Enhanced superconductivity to 43 K by P/Sb doping of Ca<sub>1-x</sub>La<sub>x</sub>FeAs<sub>2</sub>. J Phys Soc Jpn 83:025001. doi:10.1143/JPSJ.83.025001
- Ogino H, Shimizu Y, Ushiyama K, Kawaguchi N, Kishio K, Shimoyama J (2010) Appl Phys Express 3:063103. doi:10.1143/apex.3.063103
- Miyoshi K et al (2014) Enhanced superconductivity on the tetragonal lattice in FeSe under hydrostatic pressure. J Phys Soc Jpn 83:013702. doi:10.7566/JPSJ.83.013702
- 54. Wang QY et al (2012) Interface-induced high-temperature superconductivity in single unit-cell FeSe films on SrTiO<sub>3</sub>. Chin Phys Lett 29:037402. doi:10.1088/0256-307X/29/3/037402
- He S et al (2013) Phase diagram and electronic indication of high-temperature superconductivity at 65 K in single-layer FeSe films. Nature Mater 12:605–610. doi:10.1038/nmat3648
- 56. Ge JF, Xue QK, Jin JF (2014) Superconductivity in single-layer film of FeSe with a transition temperature above 100 K. http://arXiv.org/abs/1406.3435. Accessed 13 June 2014
- Lee JJ et al (2013) Evidence for pairing enhancement in single unit cell FeSe an SrTiO<sub>3</sub> due to cross-interfacial electron-phonon coupling. http://arXiv.org/abs/1312.2633. Accessed 10 Dec 2013
- Johnston S, Vernay F, Moritz B, Shen Z-X, Nagaosa N, Zaanen J, Devereaux TP (2010) Systematic study of electron-phonon coupling to oxygen modes across the cuprates. Phys Rev B 82:064513. doi:10.1103/PhysRevB.82.064513

# **Chapter 5 Summary and Perspectives**

**Abstract** One of the lessons learned from the study of the diverse families of high- $T_{\rm c}$  superconductors is that there are common ingredients for high  $T_{\rm c}$ . They are (i) layer structure, (ii) low carrier density in the normal state, (iii) low superfluid density in the superconducting state, (iv) light element and strong chemical bond giving rise to high phonon frequency. These lead to poor screening of electron-electron interaction which acts to enhance electron-phonon coupling in some families and to prepare a purely electronic channel for pairing in others. Instead of the old Matthias rules, these ingredients are a guiding principle for searching new high- $T_{\rm c}$  material families. In the two distinct highest  $T_{\rm c}$  families, the cuprates and the iron arsenides/selenides, 3d transition-metal elements, Cu and Fe, play an indispensable role. What makes them unique is the electron filling of the 3d orbitals, one electron less than the complete filling in the former and one electron more than half-filling in the latter. Based on this a candidate high- $T_{\rm c}$  material is discussed that is expected to have  $T_{\rm c}$  comparable with or hopefully higher than these two.

## 5.1 What Have We Learned from the Known High- $T_c$ Materials?

One of the lessons that we have learned from the history of HTSCs is that every epoch-making jump in  $T_{\rm c}$  does not result from a theoretical deduction nor from any empirical guide but simply from serendipity. The cuprates, fullerides, borocarbides,  $\beta$ -HfNCl, MgB<sub>2</sub>, and Fe-SCs were actually discovered by serendipity. There were no systems from which the amazing high  $T_{\rm c}$ 's of these 6 materials were foreseen. Ba<sub>1-x</sub>K<sub>x</sub>BiO<sub>3</sub> (BKBO) had a precedent, BaPb<sub>1-x</sub>Bi<sub>x</sub>O<sub>3</sub> with  $T_{\rm c}$ =12 K, and the realization of  $T_{\rm c}$  ~ 30 K in BKBO was a outcome of systematic research scheme. This is more or less the case with Ca at high pressures and possibly in a class of organic compounds, PAH.

The Matthias rules [1] which were a guiding principle for finding new superconducting materials with high  $T_{\rm c}$  before the discovery of the cuprates are; #1: find high-symmetry cubic crystals, #2, 3: find d-electron metals with the average

number of valence electrons, preferably odd numbers 3, 5, and 7, #4, 5: stay away from metals showing or in close vicinity of magnetism and from metals near a metal-insulator transition. These rules were based on the notion that higher electron density,  $n_{\rm e}$ , or higher electron density of state at the Fermi level,  $N(E_{\rm F})$ , is favorable for higher  $T_{\rm c}$  in the framework of the (BCS) Migdal-Eliashberg theory. Generally, high (atomic) density solids take the cubic structure, face-centered cubic (fcc) or body-centered-cubic (bcc), and d-electron metals have narrow d-bands, both making  $n_{\rm e}$  and/or  $N(E_{\rm F})$  larger. It was empirically known that  $N(E_{\rm F})$  tends to show maximum (minimum) for d-band metals with odd (even) number of valence electrons. A metal in the vicinity of insulating phase tends to have low carrier density, and magnetism is an enemy of s-wave BCS superconductors.

As described in the preceding chapters, the new high- $T_c$  materials are completely outside the Matthias rules. Many of them have *layer* structures, the cuprates, borocarbides,  $\beta$ -HfNCl, MgB<sub>2</sub>, Fe-SCs, and polycyclic aromatic hydrocarbons (PAHs). They, except for borocarbides and MgB<sub>2</sub>, are in close vicinity of metal-insulator phase transition boundary or in close contact with the AF ordered phase, and become superconductors by *doping* into insulating or AF parent compounds. As a consequence, most of them are metals with *low carrier density* in the normal state, pointing toward poor screening of electron-electron. Related to this, superconductivity is characterized by *low superfluid density (phase stiffness)*. In addition, most of them contain *light elements* (B, C, N, or O) which take part in *strong chemical bond*.

Notably, *strong electronic correlations* [2] play a dominant role in the formation of Cooper pairs in the cuprates and the iron-based compounds with the highest  $T_{\rm c}$ 's among all—correlations are actually strong enough to favor the *unconventional Cooper pairs* and to sustain the *spin magnetic moment* of substantial fraction of the moment in the AF ordered phase. *Electronic correlations* are perceived also to play a role in enhancing electron-phonon interaction and hence  $T_{\rm c}$  in most of the families,  ${\rm Ba_{1-x}K_xBiO_3}$  (BKBO), doped  ${\rm C_{60}}$ , doped  ${\rm \beta\text{-HfNCl}}$ , and possibly doped PAHs (Chap. 2). These features are in remarkable contrast to the Matthias rules for conventional superconductors. High  $N(E_{\rm F})$  do not necessarily favor SC with high  $T_{\rm c}$ , and instead poor screening of electron-electron interactions arising from e.g., low-carrier density and layered structure, appears to be a necessary ingredient for HTSCs. Enhanced Coulomb repulsive interaction is harmful for conventional pairing, but it provides a ground favorable for superconductivity with high  $T_{\rm c}$  either by enhancing electron-phonon coupling or by creating a new channel, purely electronic, for pairing.

In addition to them, a possible new scheme for enhancing  $T_{\rm c}$  is to fabricate some structure which enhances pairing interactions and/or provides an additional pairing channel like multilayer structure in the cuprates (Chap. 3) or FeSe monolayer on  ${\rm SrTiO_3}$  substrate (Chap. 4).

(\*) Footnote: High- $T_{\rm c}$  superconductors suitable for application If a high- $T_{\rm c}$  superconductor with  $T_{\rm c}$  near room-temperature could be realized, it would be an important issue to discuss about what is the constraint on the practical application.

Researchers agree that s-wave superconductors are more suitable for device application because enormous quasiparticles are excited in superconductors with gap nodes (unconventional pairing) and the inelastic scattering between quasiparticles is more at work with increasing temperature. From the viewpoint of critical current  $(J_c)$ , anisotropy and low superfluid density will be troublesome factors. With increasing anisotropy,  $J_c$  in high- $T_c$  superconductors is expected to sharply decrease [3]. From this, one of the future challenges in application will be to discover isotropic room-temperature superconductors with s-wave Cooper pairs. BKBO and doped  $C_{60}$  are *isotropic* and possibly s-wave superconductors, but isotropic HTSC with high superfluid density is difficult to foresee at present.

## 5.2 What is a Candidate for Next High- $T_c$ Superconductors?

The cuprates and the iron-based superconductors are distinct in their outstandingly high  $T_{\rm c}$  values,  $T_{\rm c}^{\rm max}$  = 135 and 55 K, respectively. An obvious commonality is that Cu and Fe are the elements in the 3*d*-transition-metal <sup>TM</sup> series. Common with these two systems is superconductivity with unconventional pairing symmetry with sign-changing order parameter and emergent by doping into parent compounds showing an antiferromagnetic order. Both evidence an important role of strong electronic correlation in the formation of Cooper pairs.

As was discussed in Chap. 4, the origin of striking electron-hole asymmetry in Fe-SCs is most likely the electronic correlations which are also deeply involved in the emergence of superconductivity and unconventional pairing in Fe-SCs. Incorporation of the effect of the Hund's rule coupling  $(J_{\rm H})$  in addition to the on-site Coulomb interaction (U) is conceived to cooperatively strengthen the correlation effect on particular 3d orbitals in multi-orbital metals, even when  $J_{\rm H}$  and U are not large enough. The hole doping into the parent compound reduces the Fe3d orbital filling from  $d^6$  toward  $d^5$ . The filling  $d^5$  is special with all the five 3d orbitals are singly occupied—just half filling—due to the effect of the Hund's coupling and on-site Coulomb. At the  $d^5$  filling realized in BaMn<sub>2</sub>As<sub>2</sub> the electronic correlation is maximally strong, making BaMn<sub>2</sub>As<sub>2</sub> a Mott insulator. On the other hand, the electron doping increases the filling toward  $d^7$  moving away from  $d^5$ . Thus, the hole (electron) doping points toward stronger (weaker) correlation (see the periodic table shown in Fig. 5.1).

The cuprates also show asymmetry with respect to electron and hole doping. Although it is difficult to dope both electrons and holes into one parent compound, various properties, including charge and spin dynamics and pseudogap phenomena, are quite different between hole-doped and electron-doped cuprates. One reason for the asymmetry is that doped holes enter the O2p orbitals, while doped electrons enter the Cu3d orbital. It is also ascribable to the "effective" filling in the 3d orbitals. The filling of 3d orbitals is  $d^9$  for the parent compound, e.g.,  $La_2CuO_4$ . Hole doping changes the formal filling from  $d^9$  toward  $d^8$  (as in, e.g.,  $La_2NiO_4$  for which

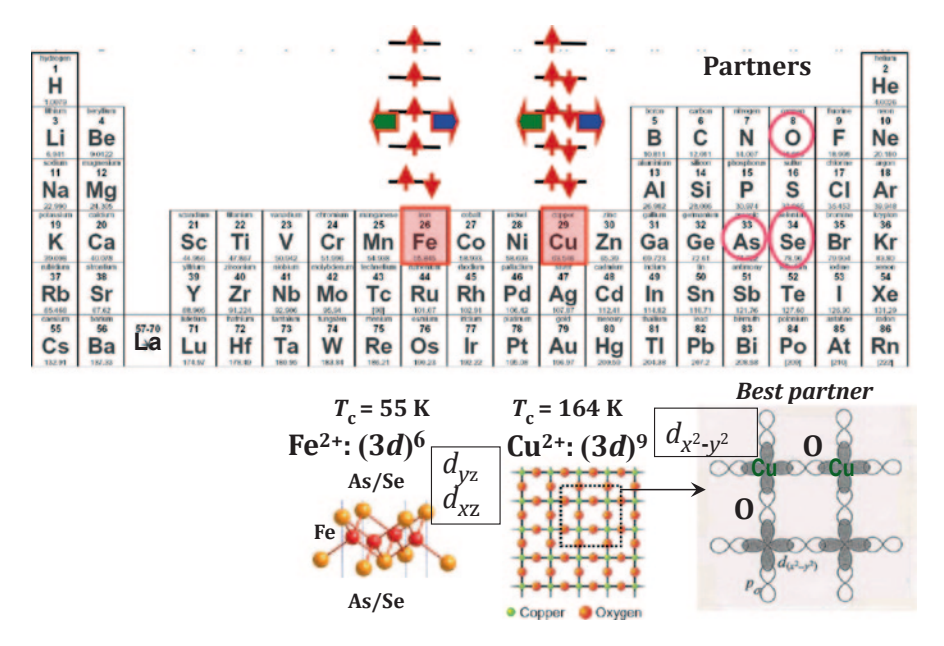


Fig. 5.1 Part of the periodic table emphasizing 3d-transition-metal elements and showing the effective electron filling of the 3d orbitals for  $Cu^{2+}$  and  $Fe^{2+}$  and the common structural units for the cuprate and iron-based high- $T_c$  superconductors. The effect of electron and hole doping is indicated by the *arrows* directing *right* and *left*, respectively

the Mott/CT insulating state is robust), whereas electron doping changes the filling toward  $d^{10}$  (Zn) in which the electronic correlation is weakest. Similar to the doping in the case of Fe-SCs, different type of doping changes the correlation strength in a different way.

From this and also from the discussions in Chaps. 3 and 4, we realize a common circumstance that makes the cuprates and the Fe-SCs special and distinct from others. That is, the 3d orbital filling  $d^9$  of  $Cu^{2+}$  is one electron less than the complete filling  $d^{10}$  and the filling  $d^6$  of  $Fe^{2+}$  is one electron more than the half filling  $d^5$ . If there were the third HTSC with high  $T_c$  values comparable with or hopefully higher than  $T_c$  of cuprates or Fe-SC, it might be discovered in 3d transition-metal (TM) compounds with 3d orbital filling one electron less or more than the special filling. There are three special fillings, complete filling  $d^{10}$ , half filling  $d^5$ , and empty  $d^0$ . Therefore, candidate HTSCs would have 3d TM element with fillings either  $d^9$ ,  $d^6$ ,  $d^4$ , or  $d^1$ . In addition to the search for 3d-TM element with these special fillings, one has to find a partner anion with which 3d-TM forms a layered structure and which make the AF order of 3d-TM spins fragile, as oxygen or arsenic/selenium does in the cuprates or Fe-SCs.

Typical  $d^4$  is Mn<sup>3+</sup> or Cr<sup>2+</sup> ionic state. However, Mn and Cr compounds tend to have high-spin states due to strong Hund's rule coupling, and thereby have robust magnetic ground states in which the AF order is difficult to collapse by doping. Thus, a possibility for HTS exists in  $d^1$  compounds with Ti<sup>3+</sup> or V<sup>4+</sup> valence (see the

hydropen 1 H 1.0379 Bhum	en	<b>Ti</b> <sup>4</sup>	·+: (3	3 <i>d</i> ) <sup>0</sup>	h	<b>M</b> n alf- ıll	n <sup>2+</sup> : (3 <i>d</i> ) <sup>5</sup>			<b>Zn</b> <sup>2+</sup> : (3			3 <i>d</i> ) <sup>1</sup>	.0	, .	categories	fazno	helian 2 He 4/000
Li 6561 sodken 11	Be 9:0122 (8339-93678 12			7		<del>1</del> 7					P			C 12.001 silicon 14	N 14.007 phosphone 15	8 O 15 000 sultur 16	F 10-1000 chostno 17	Ne 20.180 07.934 18
Policial National Nat	Mg		Sc Sc	Ti	Varioties V	Cr	Mn	Fe	Co	28 Ni	Cu	Zn	Al 20.002 301 Ga 09.724	Si 20.000 permaraan 32 Ge 77.41	P 30.074 33 As 74.007	Se 75.50	tromino 35 Br	Ar 39.948 krystm 36 Kr 83.80
Rb st.eds constant 55	Sr Sr er.ez		ylbitati 39 Y 50.005 kilcipen	Zr St. St. St. St. St. St. St. St. St. St.	Nb	Mo 95.94 Engelen 74	TC [96] streetum 75	Ru 101.07 Incomes 101.07	Rh	Pd 106.62 platemen	Ag	Cd	In 114.82 Bullett	50 Sn 116.71 1003 82	Sb 121.26 beenuth	Te	53   	Xe Xe 131.29
55 Cs	Ba 117.13	La	71 Lu 174.97	72 <b>Hf</b> 178,49	73 Ta	74 W 183,94	75 Re	76 Os 100.23	177  r 190.22	78 Pt	79 Au	Hg	81 TI 204.38	Pb	Bi 201.50	Po pox	At pro	86 Rn
$T_{\rm c} = 14 \text{ K}$						$T_{\rm c} = 55 \mathrm{K}$				$T_{\rm c} = 164 {\rm K}$								
$Ti^{3+}: (3d)^1$						Fe <sup>2+</sup> : $(3d)^6$ As/Te				$Cu^{2+}: (3d)^9$								
面面						Fe												
		LiTi	$_{2}0_{4}$			As/Te												

Special electron-filling

## **Fig 5.2** The same periodic table as that shown in Fig. 5.1 with a particular note to the $3d^1$ electron filling in the $\text{Ti}^{3+}$ state. The structure of $\text{LiTi}_2\text{O}_4$ with $T_c$ =14 K is shown as an example of superconducting Ti compounds

periodic table in Fig. 5.2) in which the minimal spin quantum number S=1/2 is a source of strong quantum fluctuations as in the case of the cuprates with  $d^1$  "hole" filling. A vanadium oxide, electron-doped  $Sr_{2-x}La_xVO_4$  [4], has many features in common with the high- $T_c$  cuprates, but is never be a superconductor probably due to the large energy difference in V3d and O2p levels and degeneracy of the lowest  $d_{xz}$  and  $d_{yz}$  orbitals, as was mentioned in Chap. 3. On the other hand, Ti compounds are promising, since the electron-doped  $SrTiO_3$  ( $T_c^{max} < 1$  K) [5] is an old known oxide superconductor and LiTi<sub>2</sub>O<sub>4</sub> is a superconductor with fairly high  $T_c = 14$  K [6]. These two Ti compounds are oxides with three-dimensional crystal structures, perovskite and spinel, respectively. Oxygen is probably not a best partner of titanium, since the Ti3d levels are well separated from the O2p levels as in the case of the above-mentioned vanadium oxide. Sulphur or selenium might be a better partner to Ti, but in the well known hexagonal TiS, and TiSe, [7] with layer structure, the electronic correlations are too weak to favor unconventional pairing and to sustain localized magnetic moment. Therefore, a route to finding a next HTSC is to search for best partner of Ti that forms layer structure with Ti and preserve strong electronic correlations.

This book ends up by listing new rules for searching high- $T_c$  superconductors:

- 1. #1: Search materials with layer structure.
- 2. #2: Search materials near the boundary of metal-insulator transition or in proximity to antiferromagnetically ordered phase, thereby having low carrier density.
- 3. #3: Search materials preferably composed of light elements and strong chemical bond.
- 4. #4: For extremely high  $T_{\rm c}$ , search materials with strong electronic correlations in which magnetic order is fragile due to strong fluctuations and/or frustrations.

#### References

- 1. Matthias BT (1955) Empirical relation between superconductivity and the number of valence electrons per atom. Phys Rev 97:74–76
- Scalapino DJ (2012) A common thread: the pairing interaction for unconventional superconductors. Rev Mod Phys 84:1383–1418. doi:10.1103/RevModPhys.84.1383
- Larbalestier D, Gurevich A, Feldmann M, Polyanskii (2001) High transition temperature superconducting materials for electric power applications. Nature 414:368–377. doi:10.1038/35104654
- Deslandes F, Nazzal AI, Torrance JB (1991) Search for superconductivity in analogues of La<sub>2-x</sub> Sr<sub>x</sub>CuO<sub>4</sub>: Sr<sub>2-x</sub>Ln<sub>x</sub>VO<sub>4</sub> (Ln = La, Ce, Pr, Nd, Eu). Physica C 179:85–90. doi:10.1016/0921-4534(91)90014-P
- Schooley JF, Hosler WR, Cohen ML (1964) Superconductivity in semiconducting SrTiO<sub>3</sub>. Phys Rev Lett 12:474–475
- Johnston DC, Prakash H, Zachariasen WH, Viswanathan R (1973) High temperature superconductivity in the Li-Ti-O ternary system. Mater Res Bull 8:777–784
- Morosan E, Zandbergen HW, Cava RJ (2006) Superconductivity in Cu<sub>x</sub>TiSe<sub>2</sub>. Nat Phys 2:544– 550. doi:10.1038/nphysS360